

Generation of novel animal models of amyotrophic lateral sclerosis

A thesis submitted for the partial fulfillment of the requirements for the degree of
Master of Research, Australian School of Advanced Medicine,

Macquarie University, October 2014



Alison Hogan

43162525

Supervisors: Associate Professor Dr Ian Blair¹

Dr Kelly Williams¹

¹Motor Neuron Disease Research Centre, Australian School of Advanced Medicine,
Faculty of Human Sciences, Macquarie University, Sydney, NSW, Australia

Keywords: amyotrophic lateral sclerosis, animal models, *CCNF*, *C.elegans*, zebrafish

Main text word count: 16,618

Abstract character count: 249

Number of figures: 36

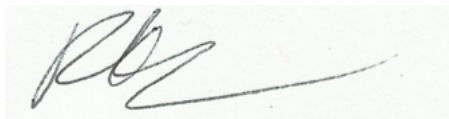
This thesis has not been submitted for a higher degree to any other university or
institution.

Declaration

Except where acknowledged in the customary manner, the material presented in this thesis is, to the best of my knowledge, original and has not been submitted in whole or part for a degree in any university.

The research presented in this thesis was conducted in the absence of any commercial or financial relationships that could be construed as a potential conflict of interest.

The research presented in this thesis was performed with the approval of the Macquarie University Animal Ethics Committee and the Macquarie University Human Research Ethics Committee. All experiments performed conformed to the relevant regulatory standards.

A handwritten signature in black ink, appearing to read 'ALISON HOGAN', written on a light-colored rectangular background.

Alison Louise Hogan

Acknowledgements

Foremost, I would like to thank my supervisor Ian Blair and his wonderful genetics team of Kelly Williams, Shu Yang, Sadaf Warraich, Jenn Fifita, Katherine Zhang and Emily McCann. They are an amazing group of people who have been incredibly helpful, patient and supportive throughout this project.

I would specifically like to acknowledge the work done by others that was used in this project:

- Ian Blair designed the β -actin primers used to validate the z*CCNF* cDNA library.
- Kelly Williams designed the primers for the *VCP* PCRs, the primers for the Q5 site-directed mutagenesis of h*CCNF* and the primers used for restriction enzyme cloning of h*CCNF*. I would also like to thank Kelly enormously for introducing a complete novice to genetics, cloning techniques and troubleshooting procedures.
- Emily McCann validated both mutations identified within the *VCP* gene of the patient tissue screened as part of this project.
- Emily Don provided advice on the zebrafish cloning techniques, support when they failed, and performed the zebrafish microinjections.

I am deeply grateful to each and every one of the genetics team and additionally to Emily Don. I look forward to many years of working with these inspiring people.

Abstract

Amyotrophic lateral sclerosis (ALS) is an invariably fatal neurodegenerative disease that is characterised by rapidly progressive motor neuron death. The pathological mechanisms responsible for the disease remain elusive and effective therapeutics are yet to be identified. Given the inherent difficulties of studying neurodegenerative conditions, animal models that reflect disease characteristics are essential to investigate the aetiology of the condition. By furthering our understanding of the cellular mechanisms involved, potential biomarkers and therapeutic targets can be identified for diagnostic, monitoring and treatment purposes.

Current animal models have provided limited insights into ALS pathogenesis and it is widely considered that no existing model of ALS adequately reflects the disease phenotype. Furthermore, therapeutics found to be beneficial in these models have so far failed to translate to human clinical trials. Therefore, there remains a need for novel animal models of ALS that better reflect human disease characteristics.

This project sought to develop novel zebrafish and nematode worm models of ALS using a variety of strategies, based upon recently identified disease-linked mutations in the *CCNF* gene. These models will be the first to allow examination of the phenotypic effect of motor neuron, compared to ubiquitous expression of a human ALS-linked transgene and its zebrafish homologue, and a determination of the effect of a fluorescent tag on protein behaviour *in vivo*. Comparison of these models will allow selection of the optimal model for immediate functional studies and provide information that may be used to inform the design of future animal models of the disease.

Manuscript arising from this candidature

K.L. Williams, S. Yang, X. Hu, J.A. Fifita, S.T. Warraich, K.Y. Zhang, N. Farrawell, B. Smith, S. Topp, C. Vance, A. Chesi, C.S. Leblond, V. Sundaramoorthy, C. Dobson-Stone, A. Lee, S. L. Rayner, M. P. Molloy, M. van Blitterswijk, D. W. Dickson, R. C. Petersen, N.R. Graff-Radford, B. F. Boeve, M. E. Murray, C. Pottier, E. Don, C. Winnick, A.P. Badrock, E. McCann, **A. Hogan**, H. Daoud, A. Levert, P. A. Dion, J. Mitsui, H. Ishiura, Y. Takahashi, Jun Goto, Jason Kost, Cinzia Gellera, Athina Soragia Gkazi, Jack Miller, Joanne Stockton, W.S. Brooks, K. Boundy, M. Polak, J. Muoz-Blanco, J. Esteban-Prez, A. Rbano, O. Hardiman, K. E. Morrison, N. Ticozzi, V. Silani, J. D. Glass, J. B. J. Kwok, G.J. Guillemin, R. S. Chung, S. Tsuji, R.H. Brown Jr, A. Garca-Redondo, R. Rademakers, J. E. Landers, A. D. Gitler, G.A. Rouleau, N. J. Cole, J. J. Yerbury, J. D. Atkin, C. E. Shaw, G. A. Nicholson, and I. P. Blair. *CCNF* mutations in amyotrophic lateral sclerosis and frontotemporal dementia. Manuscript submitted to *Nature Genetics*.

Contents

Acknowledgements	iii
Manuscript arising from this canditure	vii
List of Figures	xiii
List of Tables	xv
Abbreviations	xvii
1 Introduction	1
2 Methods	13
2.1 <i>VCP</i> gene mutation analysis	13
2.1.1 PCR	13
2.1.2 Imaging of PCR products	17
2.1.3 DNA sequencing and analysis	17
2.2 Developing expression constructs for <i>in vivo</i> ALS models	18
2.2.1 Overview	18
2.2.2 Alignment of zebrafish and human <i>CCNF</i> cDNA orthologues . .	19
2.2.3 Designing primers	20
2.2.4 RNA extraction from zebrafish	23
2.2.5 Generation of a zebrafish cDNA library	23
2.2.6 <i>CCNF</i> PCR for subcloning	24
2.2.7 Generating an adenine overhang on a PCR product for TA cloning	25
2.2.8 Purification of PCR products	26
2.2.9 Q5 site-directed mutagenesis	26

2.2.10	Restriction enzyme digestion	27
2.2.11	Ligation	27
2.2.12	BP recombination	28
2.2.13	LR recombination	29
2.2.14	Transformation of constructs into <i>E.coli</i>	30
2.2.15	PCR validation of constructs prior to sequencing	31
2.2.16	Purification of plasmids	32
2.2.17	Validation of final constructs	32
2.3	Microinjection of pmCherry-C1- <i>CCNF</i> constructs into zebrafish embryos	
	35	
2.3.1	Zebrafish ethics	35
2.3.2	Collection of embryos	35
2.3.3	Microinjection	35
2.3.4	Imaging of embryos	36
3	Results	39
3.1	<i>VCP</i> mutation analysis	39
3.2	Developing expression constructs for <i>in vivo</i> ALS models	44
3.2.1	Overview	44
3.2.2	Site-directed mutagenesis	44
Q5	site directed mutagenesis	44
3.2.3	Generation of Punc-25 expression constructs	47
	Generation of Punc-25 constructs	47
3.2.4	Alignment of zebrafish and human <i>CCNF</i> orthologues	53
3.2.5	RNA extraction from zebrafish embryos	53
3.2.6	Subcloning into pmCherry-C1 vector	54
3.2.7	Expression of pmCherry-C1 constructs	59
3.2.8	Generation of <i>CCNF</i> Tol2 constructs	60
	Generation of Tol2 Entry clones	62
4	Discussion	67
4.1	ALS gene discovery	67
4.1.1	Mutation screening of <i>VCP</i>	69
4.1.2	PCR optimisation for screening of <i>VCP</i>	71
4.2	Animal models of ALS	73
4.3	<i>C.elegans</i> models generated in this project	75

4.3.1	Nematode strain	75
4.3.2	Features of the <i>C.elegans</i> expression vectors	75
4.3.3	Transgenic techniques in <i>C.elegans</i>	76
4.3.4	Caveats of the <i>C.elegans</i> models	77
4.3.5	Characterisation of the <i>C.elegans</i> models	78
4.4	Zebrafish models generated in this project	78
4.4.1	Zebrafish strains	78
4.4.2	Zebrafish models	79
4.4.3	Features of the Tol2 constructs	81
4.4.4	Troubleshooting	82
4.4.5	Future completion of the Tol2 constructs	86
4.4.6	Transgenic techniques in the zebrafish	87
4.4.7	Establishing stable zebrafish transgenic lines	89
4.4.8	Caveats of the zebrafish models	92
4.4.9	Characterisation of the zebrafish models	92
4.5	Future applications of the <i>CCNF</i> models	93
4.5.1	Determination of effect of mutant <i>CCNF</i> on protein behaviour .	94
4.5.2	Functional studies in <i>C. elegans</i> models	95
4.5.3	Functional studies in zebrafish models	96
4.5.4	Therapeutic trials	96
4.6	Summary	99
	References	101

List of Figures

1.1	Schematic of the ubiquitin proteasome system (UPS).	10
2.1	Principles of the Tol2 cloning system.	19
2.2	pGEM-T vector map	25
2.3	pDONR:221 and pDONR:P2R-P3 vector maps.	28
2.4	Overlapping sequencing primers used to validate h <i>CCNF</i> constructs.	33
2.5	Overlapping sequencing primers used to validate z <i>CCNF</i> constructs.	33
2.6	Microinjection into zebrafish embryos	36
3.1	PCR optimisation for <i>VCP</i> exon amplification	40
3.2	PCR optimisation for amplification of <i>VCP</i> exons 1 and 15	40
3.3	Amplification of <i>VCP</i> exons	41
3.4	<i>VCP</i> missense mutation in exon 5	43
3.5	<i>VCP</i> deletion mutation in exon 14	43
3.6	Generation of mutant h <i>CCNF</i> constructs 1	45
3.7	Generation of mutant h <i>CCNF</i> constructs 2	46
3.8	Generation of mutant z <i>CCNF</i> constructs	47
3.9	Generation of Punc-25 expression constructs.	48
3.10	PCR amplification of h <i>CCNF</i> from pmCherry-C1 vector	50
3.11	Validation of recombinant clones.	50
3.12	Expression of Punc-25- <i>CCNF</i> _wt in <i>C.elegans</i>	52
3.13	Clustal Omega alignment of zebrafish and human <i>CCNF</i> orthologues.	53
3.14	RNA extracted from zebrafish embryos	53
3.15	RT-PCR amplification of β -actin from zebrafish cDNA library	54
3.16	Subcloning of h <i>CCNF</i> into pmCherry-C1 vector	56
3.17	Digested pGEM-T-z <i>CCNF</i> clones.	57
3.18	Subcloning of z <i>CCNF</i> into pmCherry-C1 vector.	58

3.19	Expression of pmCherry- <i>CCNF</i> constructs in zebrafish embryos	59
3.20	PCR amplification of h <i>CCNF</i> and z <i>CCNF</i> fusion sequences	63
3.21	BP recombination reaction	63
3.22	Restriction enzyme digests of Tol2 expression clones	65
4.1	Evolutionary conservation of amino acid 159 in <i>VCP</i>	69
4.2	Digestion of pmCherry-C1.	84
4.3	Digestion of pGEM-T-z <i>CCNF</i> vector	84
4.4	Contamination of pmCherry-C1 vector.	85
4.5	att site sequences	86
4.6	Construct maps of final Tol2 expression vectors	87
4.7	Establishing stable lines of zebrafish	91

List of Tables

1.1	ALS-associated genes and their related animal models	3
1.2	<i>C.elegans</i> and zebrafish as models of human neurodegenerative disease	6
1.3	Mutations in <i>VCP</i> identified in ALS and IBMPFD patients	8
1.4	<i>CCNF</i> mutations identified in ALS/FTD patients and control populations	9
2.1	PCR primers for amplification of <i>VCP</i> coding exons.	14
2.2	PCR conditions for amplification of <i>VCP</i> -coding exons.	15
2.3	Annealing temperature gradient for optimisation of <i>VCP</i> PCR conditions	15
2.4	PCR conditions for amplification of <i>VCP</i> -coding exons that failed to optimise under standard conditions.	15
2.5	Narrowed annealing temperature gradients used to optimise exons 1 and 15	16
2.6	PCR reactions for exons 2–14 and 16-17	16
2.7	PCR reactions for exons 1 and 15	17
2.8	Primers designed to generate each of the <i>CCNF</i> mutant constructs through Q5 site-directed mutagenesis	21
2.9	Primers used to amplify <i>CCNF</i> with the addition of restriction enzyme sites	22
2.10	Primers used to generate PCR products for BP reactions	22
2.11	Conditions for the generation of a cDNA library	23
2.12	β -actin primer sequences used to confirm the integrity of the zebrafish cDNA library	24
2.13	PCR conditions with Accuzyme DNA polymerase	24
2.14	PCR conditions with MyFi DNA polymerase	24
2.15	PCR conditions with Phusion DNA polymerase	25
2.16	Q5 site-directed mutagenesis PCR conditions	26

2.17	Ligation reaction composition	28
2.18	Composition of the BP reaction	29
2.19	Composition of the LR reaction	29
2.20	Entry clones used in LR recombination reactions	30
2.21	Antibioitic resistance of each vector	31
2.22	PCR conditions for validation of constructs	31
2.23	Internal <i>CCNF</i> primers for validation of colonies	31
2.24	Primers used to sequence h <i>CCNF</i> constructs	32
2.25	Primers used to sequence z <i>CCNF</i> constructs	33
2.26	Restriction enzymes used in digestion reactions for preliminary validation of correct insert in Tol2 expression clones	34
2.27	Digestion reactions to validate LR reaction products	34
3.1	Optimised PCR conditions for each <i>VCP</i> exon using MyTaq DNA polymerase	41
3.2	Anlaysis results of <i>VCP</i> gene screening	42
3.3	<i>CCNF</i> constructs to generate novel animal models of ALS	44
3.4	h <i>CCNF</i> cDNA PCR products.	49
3.5	PCR products and Punc-25 constructs generated	51
3.6	Tol2 clones used to generate zebrafish constructs	61
3.7	Tol2 entry clones generated through BP reactions	64
4.1	Tol2 expression constructs	80
4.2	Established zebrafish models of ALS.	80
4.3	Comparison of transgenic techniques in the Zebrafish.	88

Abbreviations

ALS	Amyotrophic lateral sclerosis
bp	Base pair
CNS	Central nervous system
CRISPR	Clustered regularly interspaced short palindromic repeats
dbSNP	Database of known SNPs
DNA	Deoxyribonucleic acid
dNTPs	Deoxynucleotide triphosphate
dpf	Days post fertilisation
ENU	N-ethyl-N-nitrosourea
FALS	Familial ALS
FTD	Frontotemporal dementia
GFP	Green fluorescent protein
h <i>CCNF</i>	Human <i>CCNF</i> sequence
IBMPFD	Inclusion body myopathy associated with Paget disease of bone and frontotemporal dementia
IVF	<i>In vitro</i> fertilisation
LB	Luria Broth
Mg	Magnesium

MN Motor neuron

NMJ Neuro-muscular junction

PCR Polymerase chain reaction

PolyA Polyadenylation

qRT-PCR Quantitative reverse transcriptase PCR

RNA Ribonucleic acid

RT-PCR Reverse transcriptase PCR

SALS Sporadic ALS

SNP Single nucleotide polymorphism

SVA Sequence Variant Analyzer

T_A Annealing temperature

TBE 90 mM tris base, 90 mM boric acid and 3 mM Na₄EDTA

TALENS Transcription activator-like effector nucleases

UPS Ubiquitin-proteasome system

zCCNF Zebrafish *CCNF* sequence

ZFN Zinc finger nucleases

1

Introduction

Amyotrophic lateral sclerosis (ALS) is a devastating neurodegenerative disease characterised by the progressive death of motor neurons in the motor cortex, brainstem and spinal cord. Clinically, this results in rapidly advancing muscle spasticity, atrophy and paralysis, typically progressing to patient death from respiratory complications within 3–5 years of symptom onset (**Rowland and Shneider, 2001**). Pathologically, the condition is characterised by the degeneration of both upper and lower motor neurons, cytoplasmic aggregation of ubiquitinated proteins within surviving neurons (**Lansbury and Lashuel, 2006**), eosinophilic intraneuronal inclusions (Bunina bodies) (**Okamoto et al., 2008**), and a neural inflammatory response with microglial activation (**Turner et al., 2004**). The majority of patients also demonstrate cytoplasmic mislocalisation of the TAR-DNA binding protein, TDP-43, which becomes a component of the characteristic cytoplasmic aggregates (**Barmada et al., 2010**).

Cytoplasmic aggregation of ubiquitinated proteins positive for TDP-43 is also seen in the neurons of the majority of patients with frontotemporal dementia (FTD), a neurodegenerative disease that develops as a result of neuronal loss in the frontal and temporal cortices (**Ling et al., 2013**). This neuronal loss leads to progressive and severe personality changes, as well as loss of language skills. Up to 50% of ALS

patients develop some degree of cognitive impairment (Ringholz et al., 2005) and approximately 15% meet the criteria for diagnosis of ALS-FTD. Conversely, approximately 15% of FTD patients develop the clinical signs of ALS. Therefore, the two conditions are linked both pathologically and clinically and so have come to be regarded as different ends of a neurodegenerative disease spectrum (Ringholz et al., 2005). The etiology underlying the characteristic pathology of both conditions remains poorly understood and reliable biomarkers and effective treatments are yet to be identified.

Investigating the underlying pathological mechanisms of ALS and FTD is challenging. This is due to the astounding complexity of the human central nervous system (CNS), compounded by the current lack of methods to access and study pathophysiological changes within the CNS *in situ* as the disease progresses. Such studies therefore, rely heavily on disease models generated to reflect pathological characteristics of the condition. These models are also essential for initial testing of the safety and efficacy of potential therapeutics.

The identification of ALS-linked mutations in the *superoxide dismutase 1* gene (*SOD1*) in 1993 represented a significant breakthrough in ALS research, as it allowed, for the first time, generation of cellular and animal models of the disease. Several additional genes that harbour ALS-linked mutations have since been identified (reviewed by Robberecht and Philips (2013); Ling et al. (2013)). This has led to the development of a variety of animal models based on ALS-linked mutations in a range of genes (Table 1.1). Approximately 10% of ALS cases are considered familial (FALS) as they demonstrate genetic inheritance of the disease, while the remaining 90% have no known family history and are considered to be sporadic (SALS). The majority of familial and sporadic cases are clinically and pathologically indistinguishable, therefore animal models based on FALS-linked mutations should reflect the pathological changes seen in both forms of the disease (Iguchi et al., 2013).

Multiple ALS-linked genes encode proteins that are involved in one of two overlapping pathways: RNA processing and protein homeostasis (Ling et al., 2013). Therefore, disturbances in these highly regulated pathways are strongly implicated in disease pathogenesis. No models have yet been developed based on mutations in ALS-linked genes known to function in protein homeostasis, however multiple models have been developed based on mutations in two ALS-linked genes involved in RNA processing,

TABLE 1.1: ALS-associated genes and their related animal models

Gene	Protein function	Model	Animal models	
<i>SOD1</i>	Cu/Zn binding enzyme	KO	<i>Drosophila melanogaster</i> (fly) (Phillips et al., 1989), <i>Mus musculus</i> (mouse) (Reaume et al., 1996)	
		Transgenic	<i>Caenorhabditis elegans</i> (Worm) (Oeda et al., 2001; Wang et al., 2009; Gidalevitz et al., 2009), Fly (Mockett et al., 2003; Parkes et al., 1998; Watson et al., 2008), <i>Danio rerio</i> (zebrafish) (Lemmens et al., 2007; Ramesh et al., 2010), Mouse (Gurney et al., 1994; Bruijn et al., 1998; Gong et al., 2000; Pramatarova et al., 2001; Jonsson et al., 2004; Rippes et al., 1995; Tu et al., 1996; Dal Canto and Gurney, 1995; Wang et al., 2003; Dal Canto and Gurney, 1997; Jonsson et al., 2006; Watanabe et al., 2005; Zang and Cheema, 2002; Jaarsma et al., 2008), <i>Ratus norvegicus</i> (Rat) (Aoki et al., 2005; Howland et al., 2002; Nagai et al., 2001), <i>Sus domestica</i> (Pig) (Yang et al., 2014)	
<i>TARDBP</i>	RNA binding protein	KO	Fly (Wang et al., 2011; Feiguin et al., 2009; Lin et al., 2011; Lu et al., 2009; Diaper et al., 2013), Zebrafish (Schmid et al., 2013; Kabashi et al., 2010), Mouse (Kraemer et al., 2010; Septon et al., 2010; Wu et al., 2010, 2012)	
		Transgenic	Worms (Vaccaro et al., 2012; Ash et al., 2010; Liachko et al., 2010), Fly (Estes et al., 2011; Hanson et al., 2010; Li et al., 2010; Miguel et al., 2011; Voigt et al., 2010; Li et al., 2010; Diaper et al., 2013), zebrafish (Kabashi et al., 2010), Mouse (Stallings et al., 2010; Wegorzewska et al., 2009; Wils et al., 2010; Xu et al., 2010; Swarup et al., 2011; Shan et al., 2010; Tsai et al., 2010; Igaz et al., 2011; Janssens et al., 2013), Rat (Zhou et al., 2010), Non-human primate (Uchida et al., 2012)	
<i>FUS</i>	RNA binding protein	KO	Fly (Wang et al., 2011; Sasayama et al., 2012), Zebrafish (Kabashi et al., 2011a)	
		Transgenic	Worms (Vaccaro et al., 2012), Fly (Lanson et al., 2011; Xia et al., 2012; Miguel et al., 2012; Chen et al., 2011; Sasayama et al., 2012), Zebrafish (Kabashi et al., 2011a), Rat (Huang et al., 2011)	
<i>C9orf72</i>	Unknown	KO	Zebrafish Ciura et al. (2013), Mouse (Lagier-Tourenne et al., 2013)	
<i>UBQLN2</i>	Linkage role in the UPS	Transgenic	Fly (Xu et al., 2013), Zebrafish (Lee et al., 2013)	
	None	None		
<i>OPTN</i>	Multifunctional, inc	None		
	RNA metabolism			
<i>ALS2</i>	Multifunctional, role in cell division	KO	Mouse (Cai et al., 2005; Deng et al., 2007; Hadano et al., 2006; Yamanaka et al., 2006; Devon et al., 2006), Zebrafish (Gros-Louis et al., 2008)	
<i>VCP</i>	Role in the UPS system	Transgenic	Mouse (Badadani et al., 2010; Custer et al., 2010)	
<i>SQSTM1</i>	Ubiquiting binding protein in the UPS	None		
<i>VAPB</i>	Unknown, associated with ER membrane	KO	Zebrafish (Kabashi et al., 2013)	
	Promotes angiogenesis	Transgenic	Fly (Sanhueza et al., 2014)	
<i>ANG</i>	Degradation of cell surface receptors	None		
<i>CHMP2B</i>	Formation of filaments	None		
<i>PFN1</i>	tous actin	None		
<i>SETX</i>	DNA repair, RNA production	None		

KO = knock out or known down of gene expression

TARDBP and *FUS*. These models demonstrate a motor neuron disease-like phenotype and reflect some of the pathological features of the disease. These and other animal models (Table 1.1) have indicated multiple cellular processes are involved in disease pathogenesis, including RNA dysregulation, protein misfolding, protein degradation, oxidative stress, excitotoxicity, defective axonal transport and mitochondrial dysfunction (Turner et al., 2013; Ling et al., 2013).

While genetic studies and animal models have been the principal tools in advancing our understanding of ALS, the pathological mechanisms responsible for the disease remain elusive. Novel, improved models are desperately required, as no model yet exists that adequately reflects the ALS phenotype (Turner et al., 2013). For example, some mouse models based on *TARDBP* mutations develop the hallmark ALS features of motor neuron death and subsequent muscle atrophy (Wegorzewska et al., 2009). However, they fail to reproduce other characteristic pathology, most notably a progression of paralysis over time, Bunina bodies and cytoplasmic mislocalisation of TDP-43. Moreover, death in these animals results from a loss of function of intestinal smooth muscle, leading to bowel obstruction, not as a consequence of motor neuron loss (Hatzipetros et al., 2013).

The greatest concern with current models is the failure thus far, of any potential therapeutic that has shown promise in animal trials to translate to successful human clinical trials (Benatar, 2007). To date, there have been over 50 publications describing therapeutic agents that extend the lifespan of the *SOD1* mouse, but none of these drugs have shown significant benefits in human patients. One drug that showed efficacy in the mouse model, minocycline, was actually found to be detrimental in a phase III clinical trial, with patients showing a more rapid decline and higher mortality rates (Gordon et al., 2007).

The majority of the current animal models of ALS have been developed in rodents, however the use of both *Caenorhabditis elegans* (nematode worm) and *Danio rerio* (zebrafish) as models of neurodegenerative disease are increasing in popularity. Both species have a comparatively simple nervous system, which is readily visualised *in vivo*, due to the transparency of the animal at the embryonic stage (zebrafish), or throughout life (*C. elegans*). Furthermore, their small size equates to low-cost housing and maintenance, while their external fertilisation, high fertility and fecundity, and rapid development allow for efficient disease model development (Teschendorf and

[Link, 2009](#); [Kabashi et al., 2011b](#)). This efficiency permits the cost-effective and rapid assessment of various transgenic strategies. Comparison of the phenotype that results from each technique allows the identification of the optimal model design within a short time period. Not only does this generate the most phenotypically accurate non-mammalian models for immediate investigation of disease biology and potential therapeutics, but the knowledge may be used in future studies to help inform the best strategy for model development. Key features of zebrafish and worm models are summarised in [Table 1.2](#).

TABLE 1.2: *C.elegans* and zebrafish as models of human neurodegenerative disease

Species	Group	Genetic homology	Nervous system	Primary advantages	Primary limitations
<i>C.elegans</i>	Invertebrate	approx 38% homology (Shaye and Greenwald, 2011), 65% human disease associated genes present (Sonhammer and Durbin, 1997)	Simple - 302 neurons, Lacks myelin (Bargmann, 1998)	Transparency allows ease of visualisation of simple nervous system. High throughput studies possible	Evolutionary distance from humans. Some pathways not conserved, eg inflammatory system.
<i>D.rerio</i>	Vertebrate	Over 70% homology, 80% human disease causing genes present (Howe et al., 2013)	Complex, segmented brain, Similar cells, structure and neurotransmitters as humans (Panula et al., 2010)	Closer genetically to humans than <i>C.elegans</i> with similar advantages.	Gene duplication during evolution can complicate model development (Lieschke and Currie, 2007). Non-mammalian.

It is not only the emergence of new model species that offers the opportunity to develop novel disease models, but also the continued discovery of novel ALS-linked gene mutations. Currently, mutations in known ALS-linked genes account for only 60% of FALS and 10% of SALS cases ([Robberecht and Philips, 2013](#)). Each new ALS-linked gene identified brings into focus potential pathogenic pathways and allows the generation of novel animal models to examine those pathways.

Exome capture and next generation sequencing technologies have greatly accelerated gene discovery in ALS. This is demonstrated by the recent identification of disease-linked mutations in the Valosin containing protein gene (*VCP*) in an ALS family ([Johnson et al., 2010](#)), and mutations in the cyclin F gene (*CCNF*) in ALS and FTD patients (manuscript submitted). The proteins encoded by these genes (*VCP* and cyclin F), both play a role in maintaining protein homeostasis and are the focus of this project.

VCP mutations are primarily associated with Inclusion Body Myopathy associated with Pagets disease of bone and frontotemporal dementia (IBMPFD), a multisystem degenerative disorder involving muscle, brain and bone tissue ([Ju and Weihl, 2010](#)). To date, 19 IBMPFD linked mutations and four ALS-linked mutations have been identified in *VCP* ([Johnson et al., 2010](#)) (Table 1.3).

TABLE 1.3: Mutations in *VCP* identified in ALS and IBMPFD patients

ALS-associated mutations	IBMPFD-associated mutations
R191Q	I27V
R159G	R93C
S592N	R95G/C
R155H	P137L
	R155C/P/L/S
	G157R
	R159C/H
	R191Q
	L198N
	A232E
	T262A
	N387H
	A439S
	D592N

Recently, in a large Australian family with ALS and FTD, our laboratory identified a mutation in *CCNF* that segregated with disease in the family. A worldwide collaborative effort has subsequently identified additional ALS and FTD-linked *CCNF* mutations in familial and sporadic patients, and rare single nucleotide polymorphisms (SNPs) in patients as well as control populations (Table 1.4).

TABLE 1.4: *CCNF* mutations identified in ALS/FTD patients and control populations

FALS-associated mutations	FTD/SALS-associated mutations	SNPs found in patients and controls
K97R	S3G	H69Y
S195R	T181I	A74T
S509P	T543I	G161R
S621G	E624K	V318G
I772T	R392T	R406Q
		R574Q
		F604I
		Q669STOP
		T698M
		V714M

Both VCP and cyclin F are integral components of one of the two major protein degradation pathways, the ubiquitin-proteasome system (UPS). The UPS is a selective system whereby specific proteins are tagged for degradation through the addition of ubiquitin molecules. Cyclin F is part of the E3 ubiquitin-protein ligase complex, which catalyses this ubiquitination. UPS chaperone proteins, one of which is VCP, recognise and bind to the ubiquitin molecules, then transfer the complex to the proteasome for degradation (Figure 1.1) (Nandi et al., 2006).

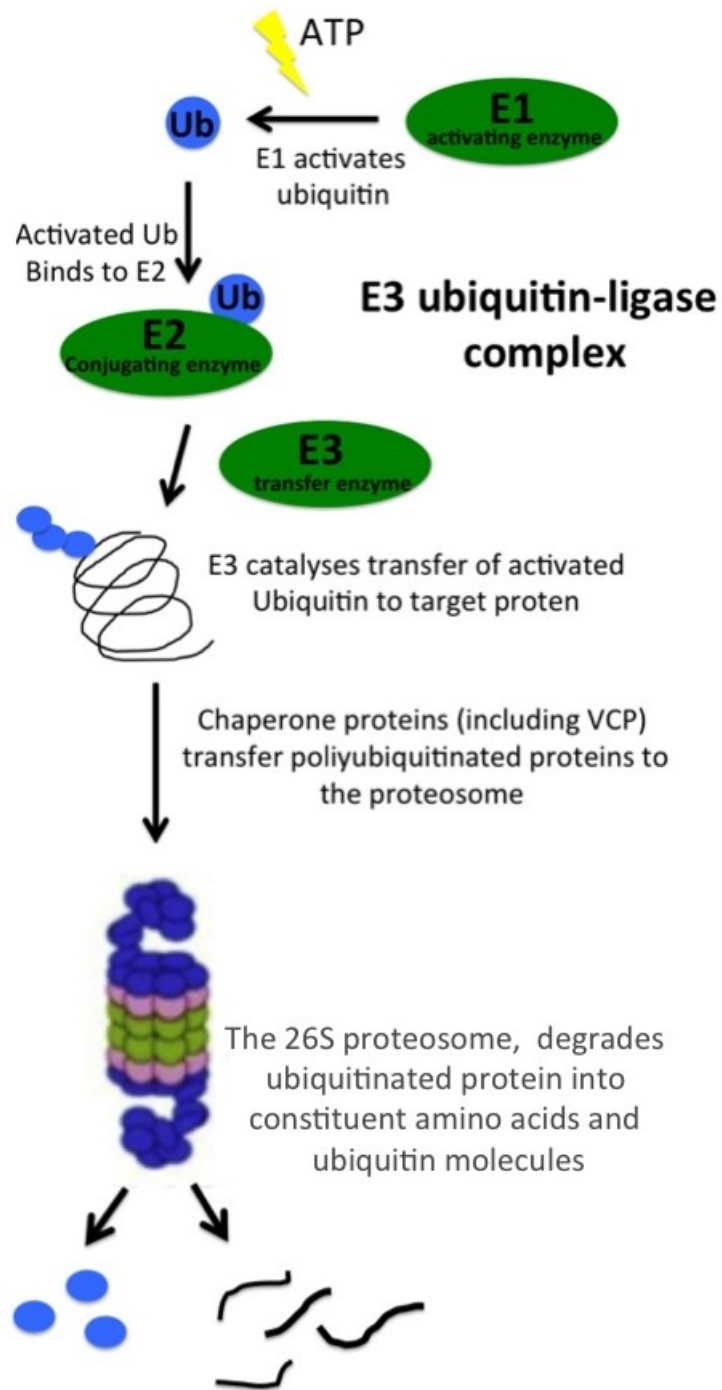


FIGURE 1.1: Schematic of the ubiquitin proteasome system (UPS) (Compiled from information presented in [Nandi et al. \(2006\)](#)). This figure illustrates the role of *CCNF* and *VCP* within the proteasome-mediated protein degradation pathway. *CCNF* is a component of the E3 ubiquitin ligase complex, responsible for catalyzing the transfer of ubiquitin to the target protein. *VCP* functions later in the UPS pathway, acting as a chaperone to transfer ubiquitinated proteins to the proteasome.

There is substantial evidence that failure of the UPS, and therefore a failure of protein homeostasis, has a significant role in ALS pathogenesis. Firstly, one of the pathological hallmarks of the disease is the cytoplasmic aggregation of ubiquitinated proteins ([Robberecht and Philips, 2013](#); [Bendotti et al., 2012](#)), implicating a failure of protein clearance by the UPS. Secondly, studies of a transgenic *SOD1* mouse model have demonstrated that the mutant SOD1 protein both escapes degradation by the UPS, and inhibits its activity, as indicated by reduced proteasome activity within the spinal cord ([Kabashi et al., 2004](#); [Cheroni et al., 2009](#)). Finally, a number of rare ALS-linked mutations have recently been identified in genes directly associated with the UPS, including *UBQLN2* ([Deng et al., 2011](#)), *SQSTM1* ([Fecto et al., 2011](#)), *VCP* ([Johnson et al., 2010](#)) and now *CCNF*.

At this stage, ALS-linked gene mutations known to affect protein homeostasis have not been used to generate animal models. However, two mouse models have been generated based on IBMPFD-associated *VCP* mutations (R155H and A232E) which demonstrate ALS-like pathology within their spinal cords. This pathology includes motor neuron degeneration with aggregation of TDP-43 positive ubiquitinated proteins ([Badadani et al., 2010](#); [Custer et al., 2010](#)). While these models do recapitulate some key pathological features of ALS, they do not develop the progressive, fatal ALS-like disease, and motor neuron degeneration is limited to the ventral horn of the spinal cord. Furthermore, the models also develop pathology consistent with IBMPFD that is not seen in ALS patients, such as degeneration of bony tissue.

This project aimed to address the current lack of ALS models based on gene mutations with a role in protein homeostasis and to investigate approaches to develop superior animal models to those currently available. Development of these models was based upon two hypotheses. First, that overexpression of an ALS-linked mutation in *CCNF* will produce a motor neuron disease phenotype in *C.elegans* and zebrafish, and second, that different transgenic techniques will generate models with distinct phenotypes.

The primary aim of the project therefore was to develop multiple novel animal models of ALS in two species, based on mutations in *CCNF*. Multiple species were selected for the project with the goal of maximising their potential downstream applications in biomolecular studies and high throughput preclinical trials. The second project aim, of developing superior models of ALS, was addressed through the use of different

transgenic strategies. Comparison of the resulting phenotypes from each strategy will provide knowledge that may be used to inform the future design of both non-mammalian and mammalian disease models. The development of animal models that better reflect the pathology seen patients will lead to more reliable insights into disease biology and provide a more accurate indication of the efficacy of potential therapeutics.

2

Methods

2.1 *VCP* gene mutation analysis

At the request of collaborators, patient DNA was screened for the presence of mutations within *VCP* as part of this project. The techniques used for mutation analysis of *VCP* include the polymerase chain reaction (PCR, Section 2.1.1), gel electrophoresis (Section 2.1.2), Sanger sequencing and chromatogram analysis (Section 2.1.3).

2.1.1 PCR

The 17 coding exons of *VCP* and 50 base pairs (bp) of adjacent flanking intronic sequences were amplified by PCR. PCR primers had been designed using ExonPrimer software (<http://ihg.gsf.de/ihg/ExonPrimer>) prior to the commencement of this project (Table 2.1). If the intronic region was small, two exons were amplified in a single PCR. Using a control DNA sample, PCR with each primer set was initially optimised with MyTaq DNA polymerase (Bioline) and Mastercycler pro (Eppendorf, USA) thermocycler conditions as shown in Table 2.2. An eight-temperature gradient was used to determine optimum annealing temperature (T_A) for each PCR reaction

(Table 2.3).

TABLE 2.1: PCR primers for amplification of *VCP* coding exons.

Primer	Sequence
VCP_Ex1_F	CTTGCCACCGCTCGTAG
VCP_Ex1_R	CTTTCCTGGTCTCCACCTCTC
VCP_Ex2-3_F	AAGTATGAGTTTTAGAGACTGGCG
VCP_Ex2-3_R	CTGTAATGCAGGCTATCTCTGG
VCP_Ex4_F	TTTGGACACCCAGTGCTTG
VCP_Ex4_R	AAGATGTTCCAAGGTTTATTCCC
VCP_Ex5_F	TGATGAGTTCTCACTTTGTCTTG
VCP_Ex5_R	GACAGTTACCACATGATGCCAC
VCP_Ex6_F	TGGAATGATTTAGAGAAACTCAGC
VCP_Ex6_R	GGACAGGATTAGACATTGGCAC
VCP_Ex7_F	AGCGCTAGTCAAGCCATTTTAG
VCP_Ex7_R	CCAGCTCATAAGCCCAGTTC
VCP_Ex8-9_F	ACCTGTCTCTGGGCCAAAC
VCP_Ex8-9_R	TGAAGGGCTTCAAGAGGATTAG
VCP_Ex10_F	TCACCCTAGGCCTGTCTCTTAC
VCP_Ex10_R	AGTTCCCAGCAACTGCCTAGAG
VCP_Ex11-12_F	TTGTCTCTGAGCCTCCTGC
VCP_Ex11-12_R	TGACACCCTGAGATCACCC
VCP_Ex13_F	TGGAGGGGATGCTTCTG
VCP_Ex13_R	AACAGCCTCTATTCCTTGCC
VCP_Ex14_F	CCACCACGTTTGCCTAGAG
VCP_Ex14_R	CTAAAGAGCACTCCGTACCAGC
VCP_Ex15_F	CCCAAAGATCTGCGTATCTCG
VCP_Ex15_R	ACTCCAGGGCATGGTGG
VCP_Ex16-17_F	TAAACTGCAGTAATGGGAGGC
VCP_Ex16-17_R	CCCCAGGGAACAAGGTC

TABLE 2.2: PCR conditions for amplification of *VCP*-coding exons.

Reagent	Volume (μ l)	Temperature	Time	Cycles
MyTaq DNA polymerase	5	95°C	10 min	1 ×
10mM F primer	0.4	94°C	15 sec	40 ×
10mM R primer	0.4	50-70°C	30 sec	40 ×
20ng control DNA	1	72°C	30 sec	40 ×
dH ₂ O	3.2	72°C	7 min	1 ×
10 μ l				

TABLE 2.3: Annealing temperature gradient for optimisation of *VCP* PCR conditions

Sample	Temperature
1	53.4°C
2	55.7°C
3	58.3°C
4	61.0°C
5	63.7°C
6	66.1°C
7	68.0°C
8	69.4°C

If the exon PCR failed to optimise with the conditions in Table 2.2, a second optimisation PCR (Table 2.4) was performed with the addition of 10 × PCR Enhancer (Life Technologies) and a refined eight-temperature annealing gradient (Table 2.5).

TABLE 2.4: PCR conditions for amplification of *VCP*-coding exons that failed to optimise under standard conditions.

Reagent	Volume (μ l)	Temperature	Time	Cycles
MyTaq DNA polymerase	5	95°C	10 min	1 ×
10mM F primer	0.4	94°C	15 sec	40 ×
10mM R primer	0.4	51-57 / 60-66°C	30 sec	40 ×
20ng control DNA	1	72°C	30 sec	40 ×
10x PCR enhancer	1	72°C	7 min	1 ×
dH ₂ O	2.2			
10 μ l				

TABLE 2.5: Narrowed annealing temperature gradients used to optimise exons 1 and 15

Temperature		
Column	Exon 1	Exon 15
1	51.2°C	53.4°C
2	52.7°C	55.7°C
3	54.4°C	58.3°C
4	56.1°C	61.0°C
5	57.8°C	63.7°C
6	59.4°C	66.1°C
7	60.7°C	68.0°C
8	61.6°C	69.4°C

Once optimal conditions were established (described in Results, 3.1), all *VCP* coding exons were amplified using 20 μ l PCR reactions for the patient DNA sample, a control DNA and a negative control (Tables 2.6 and 2.7). Two microlitres of each PCR product was visualised as described in Section 2.1.2.

TABLE 2.6: PCR reactions for exons 2–14 and 16–17

Reagent	Patient	Control	Blank
MyTaq DNA polymerase	10	10	10
10mM F primer	0.8	0.8	0.8
10mM R primer	0.8	0.8	0.8
20ng patient DNA	1	-	-
20ng control DNA	-	1	-
dH ₂ O	7.4	7.4	8.4
	20 μ l	20 μ l	20 μ l

TABLE 2.7: PCR reactions for exons 1 and 15

Reagent	Patient	Control	Blank
MyTaq DNA polymerase	10	10	10
10mM F primer	0.8	0.8	0.8
10mM R primer	0.8	0.8	0.8
10x PCR enhancer	2	2	2
20ng patient DNA	1	-	-
20ng control DNA	-	1	-
dH ₂ O	7.4	7.4	8.4
	20 μ l	20 μ l	20 μ l

2.1.2 Imaging of PCR products

Electrophoresis was used to separate PCR products on 0.75% – 1.5% w/v agarose gels in 1x TBE (90mM tris base, 90mM boric acid and 3mM Na₄EDTA). To allow visualisation of the bands under blue light, 1 \times Sybr Safe (Invitrogen) was added to the agarose gel. PCR products were electrophoresed on the agarose gels at 100V for 40 minutes unless otherwise specified. The relevant DNA ladders Hyperladder II (Bioline), 100bp plus (Bioline) or Hyperladder 1kb (Bioline) were used to determine the size of the PCR product.

Agarose gels were visualised and images captured on a Gel Doc EZ System (BioRad).

2.1.3 DNA sequencing and analysis

The remaining volume of PCR product (18 μ l) was sent to Macrogen (Korea) for purification and Sanger sequencing using a ABI3730XL sequencer and BigDye terminator sequencing (Life Technologies).

Every sequencing result was analysed using Sequencher v4.8 software (GeneCodes Corporation, USA) to trim the sequence of low quality bases and compare the sequenced product to a reference sequence.

2.2 Developing expression constructs for *in vivo* ALS models

2.2.1 Overview

C.elegans (nematode worm) constructs

Two sets of constructs were generated for expression in *C.elegans* using the Punc-25 vector. One set of constructs was designed to overexpress human *CCNF* (h*CCNF*) and the second set to overexpress h*CCNF* fused to a N-terminal mCherry fluorophore. Both sets were composed of a single wild-type h*CCNF* construct and 21 mutant constructs, one for each of the variants shown in Table 1.4, giving a total of 44 Punc-25 constructs for expression in *C.elegans*.

D.rerio (zebrafish) constructs

Four sets of constructs were developed for expression in zebrafish. Each set consisted of either wildtype h*CCNF*, the zebrafish orthologue (z*CCNF*), mutant p.S621G h*CCNF* or, the orthologous zebrafish mutation, p.S623G z*CCNF*.

Cloning techniques

Restriction enzyme cloning techniques were used to generate the Punc-25 constructs and the preliminary zebrafish constructs. Two different restriction sites were used to ensure the PCR product ligated into the vector in the correct orientation. The att site-specific Tol2 Gateway system (MultiSite Gateway Technology, Invitrogen) (Kwan et al., 2007) was used, and will be continue to be used to generate the final constructs for expression in zebrafish. The methods used are described in Sections 2.2.2 to 2.2.17 and the principles of the Tol2 cloning system are shown in Figure 2.1.

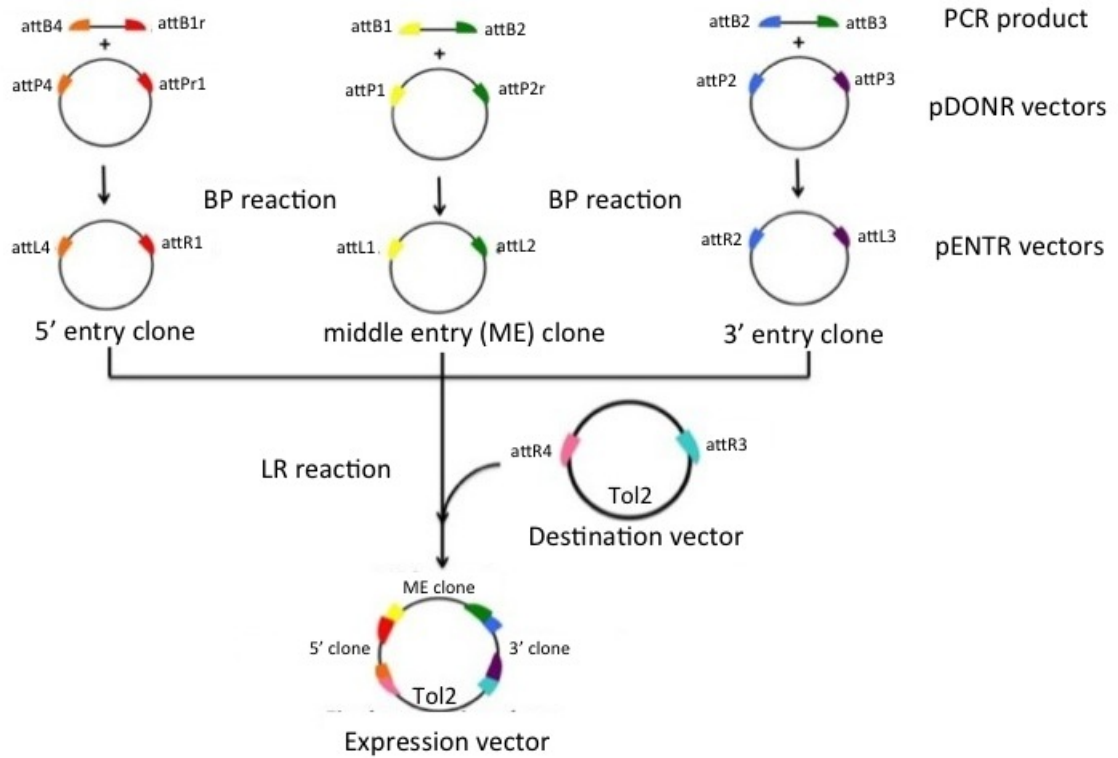


FIGURE 2.1: Principles of the Tol2 cloning system. Recombination reactions ligate complementary attB and attP sites present on a PCR product and a pDONR vector (BP reaction). This reaction yields entry clones that carry attL and attR sites. The LR reaction recombines the complementary attL and attR sites on the entry clones and a pDEST destination vector to generate the final expression clone (Kwan et al., 2007).

2.2.2 Alignment of zebrafish and human *CCNF* cDNA orthologues

The human and zebrafish orthologues of *CCNF* cDNA (NM_001761.2 and NM_207048.1) were compared by aligning the cDNA sequences using Clustal Omega 2.0 (<http://www.ebi.ac.uk/Tools/msa/clustalo/>). This enabled the identification of the specific nucleotide in the zebrafish sequence that needed to undergo site-directed mutagenesis (Section 2.2.9) to generate the equivalent mutation to the p.S621G mutation in the human *CCNF* cDNA sequence.

2.2.3 Designing primers

All primers used in this project were synthesised by Sigma-Aldrich Pty Ltd.

Site-directed mutagenesis primers

Site-directed mutagenesis primers enable the alteration of a single nucleotide in a PCR product by substituting the required nucleotide in the primer sequence. Primers for the Q5 site-directed mutagenesis PCR were designed using the New England Biolabs (NEB) online design software (www.NEBaseChanger.neb.com). The sequences for these primers and optimal annealing temperatures for each are shown in Table 2.8.

TABLE 2.8: Primers designed to generate each of the *CCNF* mutant constructs through Q5 site-directed mutagenesis

Primer	Sequence	T _A
NEBQ5_H69Y_F	GGTGGACAAC T ACGCCAGTGT	67°C
NEBQ5_H69Y_R	AGGTCCTTCAGCTGGGAG	
NEBQ5_K97R_F	GCTGCTGAAA G GGGGAATTTTC	58°C
NEBQ5_K97R_R	CCTTTCAAAGAGCTTCAG	
NEBQ5_G161R_F	GTCGGTGAGCA A AGCTGCTG	66°C
NEBQ5_G161R_R	CACGGAGGGCGGATGAAG	
NEBQ5_S195R_F	GAGTGCTGAG G CTGTTTCGAGG	67°C
NEBQ5_S195R_R	TGCCCCAAGCAGTGCAATATG	
NEBQ5_S509P_F	CAGGCAAGTC C CTCTGACCGC	67°C
NEBQ5_S509P_R	TAGTCCTTGGGGGCGTCA	
NEBQ5_R574Q_F	AAACGGAAGCA A GGAGAACAGCCTCC	70°C
NEBQ5_R574Q_R	GGTTCTCCGCCCGAGGG	
NEBQ5_S621G_F	CGACCAGGAG G GTGAGGGCGA	69°C
NEBQ5_S621G_R	CCTTCATAGCCAGAGCAGCAG	
NEBQ5_E624K_F	GAGTGAGGGCA A GAAGGAGGG	65°C
NEBQ5_E624K_R	TCCTGGTCGCCTTCATAG	
NEBQ5_T698M_F	AAGGACGTCA T GACCTCAGGGTACTCC	72°C
NEBQ5_T698M_R	CCCTGGCTCCCGGCTGGT	
NEBQ5_I772T_F	AACCTATGCAC A CACAGTGAG	60°C
NEBQ5_I772T_R	TATCCGCTTCACCTGTTG	
NEBQ5_F604I_F	GCTGGGCAGCA T CCTCGACTG	70°C
NEBQ5_F604I_R	AGCGTCTCCTCCTGGCTG	
NEBQ5_S3G_F	ATCCATGGGG G GCGGCGGCGT	72°C
NEBQ5_S3G_R	CTCTTGTCGTCATCGTCTTTGTAGTCCTTGACAGC	
NEBQ5_R392T_F	GACCTGGTGAG A ATGATGGGC	59°C
NEBQ5_R392T_R	CTCGTACTTGTAAGTGTTG	
NEBQ5_R406Q_F	GGGAAGATTCA A GTCCCCACTG	64°C
NEBQ5_R406Q_R	TTCCAAGGCGGAGACGAT	
NEBQ5_Q669stop_F	CCAGGACCCA T AGGCACTGGC	68°C
NEBQ5_Q669stop_R	GGTCCCTTGTCCTCTGGAC	
NEBQ5_A74T_F	CAGTGTGTGG A CATGTGCCAGC	68°C
NEBQ5_A74T_R	GCGTGGTTGTCCACCAGG	
NEBQ5_V318G_F	GACTGGCTGG G GGAAGTTGCC	67°C
NEBQ5_V318G_R	GATCAGAATGTACCTCATTGTGTCATTG	
NEBQ5_T327K_F	AAGGACTTCA A AAGCCTGTGC	64°C
NEBQ5_T327K_R	CATGGTGGCAACTTCCAC	
NEBQ5_V714M_F	CACAAGCTCC A TGGACGGTGG	68°C
NEBQ5_V714M_R	GGACTTGCGGTGCTGACG	
NEBQ5_T181I_F	CTGCAGAGGA T TCACAAAGCATC	64°C
NEBQ5_T181I_R	CTGGCACTCTGCCCTGAG	
NEBQ5_T543I_F	TTAGGAGTGAT A CAAGACAGCCC	65°C
NEBQ5_T543I_R	TGCAGCACACAACCTGGCT	
NEBQ5_ΔCCNF_S623G_F	AGACCGTGAG G GCGAGGGAGA	68°C
NEBQ5_ΔCCNF_S623G_R	CCCTCGTATCCAGAACAGGAA	

Blue indicates the nucleotide substitution in each primer set which generates the desired point mutation.

Restriction enzyme-site cloning primers

The primers used in restriction enzyme site cloning (Sections 2.2.10 and 2.2.11) were designed to contain the required restriction enzyme sequence and approximately 20 base pairs (bp) complementary to the template DNA as determined by NCBI primer blast tool (<http://www.ncbi.nlm.nih.gov/tools/primer-blast/>). Restriction enzyme site sequences were sourced from the NEB website (<http://www.neb.com/tools-and-resources/selection>). Primer sequences are shown in Table 2.9.

TABLE 2.9: Primers used to amplify *CCNF* with the addition of restriction enzyme sites

Primer	Sequence
NheI_mCherry_F	cagtGCTAGCgaatggtgagcaagggcgaggag
NheI_CCNF_cDNA_F	cagtGCTAGCgaatggggagcggcgcggtggt
EcoRI_CCNF_cDNA_R	cagtCTTAAGga ttacagcctcacaaggccca
XhoI_zCCNF_cDNA_F	cagtCTCGAGct atgaaagcgggcgcgctcca
EcoRI_zCCNF_cDNA_R	cagtGAATTCgatcagaagctcagaaagg

Restriction enzyme sites are shown in red, *CCNF*-complementary sequence in blue and filler sequences in black.

att-site cloning primers

The primers used in att-site cloning (Section 2.2.12 and 2.2.13) were designed to contain the required att sequence (~25bp) and 20bp complementary to the template DNA as determined by NCBI primer blast tool (<http://www.ncbi.nlm.nih.gov/tools/primer-blast/>). The att-site sequences were obtained from the MultiSite Gateway Three-Fragment Vector Construction Kit manual (Life technologies). Primer sequences are shown in Table 2.10).

TABLE 2.10: Primers used to generate PCR products for BP reactions

Primer	Sequence
mCherry_CCNF_cDNA_attB1_F	ggggACAAGTTTGTACAAAAAGCAGGCTGTatggtgagcaagggcgaggagga
mCherry_CCNF_cDNA_attB2_F	ggggACAGCTTTCTTGTACAAAGTGGGTatggtgagcaagggcgaggagga
hCCNF_cDNA_attB2_R	ggggACCACTTTGTACAAGAAAGCTGGGTAttacagcctcacaaggccag
hCCNF_cDNA_attB3_R	ggggACAACCTTTGTATAATAAAGTTGAattacagcctcacaaggccag
zCCNF_cDNA_attB2_R	ggggACCACTTTGTACAAGAAAGCTGGGTAttcagaagctcagaaaggct
zCCNF_cDNA_attB3_R	ggggACAACCTTTGTATAATAAAGTTGAAttcagaagctcagaaaggct

att site sequences are shown in red, *CCNF*-complementary sequence in blue and filler sequences in black.

2.2.4 RNA extraction from zebrafish

RNA extraction from 3-day post fertilisation (dpf) zebrafish embryos (n=50) was performed using a RNeasy Mini Kit (Qiagen). The embryos were euthanased, then submerged in RNAlater RNA Stabilization Reagent (Qiagen). The embryos were homogenised in Buffer RLT with a Dounce tissue grinder (Sigma Aldrich) and a 20 gauge needle and syringe. Extraction from this homogenised sample was performed as per manufacturers instructions. The RNA product was eluted into 30 μ l RNase-free water and immediately frozen at -30°C.

The concentration of all RNA and DNA solutions in this project was determined using 2 μ l of RNA or DNA on a NanoDrop ND-1000 spectrophotometer (Thermo Scientific).

2.2.5 Generation of a zebrafish cDNA library

A zebrafish cDNA library was generated from the extracted zebrafish mRNA using a Tetro cDNA Synthesis Kit (Bioline) according to manufacturer instructions (Table 2.11).

TABLE 2.11: Conditions for the generation of a cDNA library

Reagent	Volume (μ l)		
mRNA (up to 5 μ g)	10		
random hexamer primer	1	Temperature	Time
10mM dNTP mix	1	25°C	10 min
5 \times RT buffer	4	45°C	30 min
RNAse inhibitor	1	85°C	5 min
Tetro reverse transcriptase	1	Chill on ice	
dH ₂ O	2		
	20 μ l		

To determine the integrity of the cDNA library, RT-PCR was used with amplify the ubiquitously expressed β -actin with the primers shown in Table 2.12.

TABLE 2.12: β -actin primer sequences used to confirm the integrity of the zebrafish cDNA library

Primer	Sequence
β -actin_F	AGAGGGGAAATCGTGCGTGAC
β -actin_R	CAATAGTGATGACCTGGCCGT

2.2.6 *CCNF* PCR for subcloning

Three DNA polymerases, Accuzyme (Bioline), MyFi (Bioline) and Phusion High fidelity DNA polymerase (NEB), were used throughout the project for PCR amplification of *CCNF*. The primers used in these reactions are shown in Section 2.2.3. The PCR conditions used for each DNA polymerase are shown in Tables 2.13 to 2.15.

TABLE 2.13: PCR conditions with Accuzyme DNA polymerase

Reagent	Volume (μ l)	Temperature	Time	Cycles
Accuzyme mix	12.5	9°C	10 min	1 ×
20mM F primer	0.5	98°C	3 min	1 ×
20mM R primer	0.5	95°C	15 sec	30 ×
10ng plasmid template	1	55°C	15 se	30 ×
dH ₂ O	10.5	72°C	5 min	30 ×
	25 μ l			

TABLE 2.14: PCR conditions with MyFi DNA polymerase

Reagent	Volume (μ l)	Temperature	Time	Cycles
MyFi mix	25			
20mM F primer	1	95°C	1 min	1 ×
20mM R primer	1	95°C	15 sec	30 ×
200ng plasmid template	1	55 °C	15 sec	30 ×
dH ₂ O	22	72°C	1 min 40 sec	30 ×
	50 μ l			

TABLE 2.15: PCR conditions with Phusion DNA polymerase

Reagent	Volume (μ l)	Temperature	Time	Cycles
GC buffer	10			
10mM dNTPs	1			
20mM F primer	2.5	98°C	30 sec	1 ×
20mM R primer	2.5	98°C	10 sec	30 ×
10ng plasmid template	1	71°C	20 sec	30 ×
DMSO	1.5	72°C	90 sec	30 ×
Phusion polymerase	0.5	72°C	10 min	1 ×
dH ₂ O	31			
	50 μ l			

2.2.7 Generating an adenine overhang on a PCR product for TA cloning

TA cloning is the ligation of a PCR product flanked by adenine overhangs with a linear vector that carries thymine overhangs. The basic entry vector pGEM-T (Promega), was used for TA cloning in this project(Figure 2.2).

The *zCCNF* PCR product was amplified from a pCMV_SPORT6.1 vector (Millenium Science) with Phusion DNA polymerase (Section 2.2.3 and 2.2.6). Phusion DNA polymerase is a high fidelity, proof reading polymerase, and therefore generates a blunt ended PCR product, and the addition of the adenine overhang was required. This was achieved in by a 10 μ l reaction consisting of 1 unit Thermopol Taq polymerase (NEB), 1 × buffer (NEB), 0.2mM dATP nucleotide (NEB) and the *zCCNF* PCR product. The reaction was incubated at 72°C for 25 minutes.

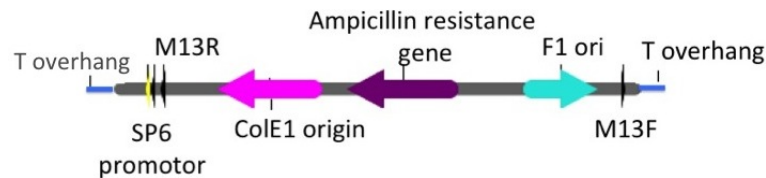


FIGURE 2.2: pGEM-T vector map. Schematic of the linear pGEM-T plamid (3kb) showing the T overhangs used for T-A ligation

2.2.8 Purification of PCR products

Gel purification

When gel purification of PCR products was required, electrophoresis was performed on a 0.75% w/v agarose gel with $1\times$ Sybrsafe (Invitrogen) at 100V for 1 hour. PCR products were visualised using a Safe Imager 2.0 Blue Light Transilluminator (Life Technologies), and the correct sized PCR bands were excised from the agarose gel using a scalpel blade. The extracted gel was weighed, and purified with an ISOLATE II PCR and Gel Kit (Bioline) according to manufacturer instructions. The purified PCR product was eluted in $25\mu\text{l}$ of sterile, deionized water.

2.2.9 Q5 site-directed mutagenesis

The Q5 site-directed mutagenesis kit (NEB) was used according to manufacturers instructions to introduce each of the 21 single nucleotide mutations into h*CCNF* in a pmCherry-C1 vector (Addgene) and to introduce the p.S623G mutation (c.207A>G) into z*CCNF* in the pGEM-T vector (Promega). The PCR reaction and thermocycler conditions used for these reactions are shown in Table 2.16.

TABLE 2.16: Q5 site-directed mutagenesis PCR conditions

Reagent		Volume (μl)
Q5 Hot-start high-fidelity $2\times$ mastermix		12.5
10mM F primer		1.25
10mM R primer		1.25
10ng plasmid template		1
dH ₂ O		9
		$25\mu\text{l}$
Temperature	Time	Cycles
98°C	30 sec	3 $1\times$
98°C	10 sec	25 \times
50-72°C *	30 sec	25 \times
72°C	90 sec	30 \times
72 °C	2 min	1 \times

*Annealing temperatures for each primer is shown in Table 2.8.

Kinase-Ligase-DpnI (KLD) reactions were performed on one microlitre of the PCR

product. The kinase enzyme phosphorylates the PCR product for subsequent ligation, and DpnI is a restriction enzyme that cleaves the methylated template DNA. One microlitre 10× KLD enzyme mix (supplied in kit) and 5μl of 2× KLD reaction buffer (supplied in kit) were added to 1μl of PCR reaction made up to a final volume of 10μl. The KLD/PCR product reaction was incubated at room temperature for 5 minutes prior to transformation (Section 2.2.14).

2.2.10 Restriction enzyme digestion

Vector restriction enzyme digestion

Vectors were digested in 50μl reactions consisting of 5μg of vector, 10× Cutsmart buffer (NEB) and 0.5μl of each restriction enzyme. Reactions were incubated at 37°C for a minimum 3 hours, maximum 16 hours, then heat-inactivated by a 15-minute incubation at 80°C.

One microlitre of Thermosensitive Alkaline Phosphatase (TSAP) was added per 1μg of digested vector to catalyze the removal of the 5' phosphate groups, thus preventing recircularisation of the digested vector. The TSAP reaction was incubated at 37°C for 15 minutes, then heat-inactivated by incubation at 80°C for 15 minutes. The digested product was gel purified as described in Section 2.2.8.

PCR product restriction enzyme digestion

CCNF PCR products generated from the primer sets in Section 2.2.3 were gel purified (Section 2.2.8), and eluted into 25μl. The restriction enzyme digestion reaction consisted of 25μl purified PCR product, 0.5μl of each required restriction enzyme, 3μl of 10× Cutsmart buffer (NEB) to a final volume of 30μl. This reaction was incubated at 37°C for a minimum of 1 hour, maximum of 16 hours.

2.2.11 Ligation

Ligation reactions were required to insert either the digested PCR product into the digested vector (Section 2.2.10), or the A-overhang *zCCNF* PCR product into the pGEM-T vector (Section 2.2.7). The ligation reactions (Table 2.17) were incubated at room temperature for 5 hours.

TABLE 2.17: Ligation reaction composition

Reagent	Quantity
T4 DNA ligase	1 μ l
Digested vector	50ng
Digested PCR product	150ng
1 μ l 2 \times Rapid Ligation Buffer (Promega)	2 μ l
	10 μ l

2.2.12 BP recombination

The BP reaction generates Tol2 entry clones by recombining attP sites present in a pDONR vector and attB sites present in a PCR product. This reaction yields clones that carry attL and attR sites for subsequent LR reactions to generate the final Tol2 constructs (2.1). In this project, middle entry clones (pENTR:221) and 3' entry clones (pENTR:P2R-P3) carrying mCherry-*CCNF* were required (Table 3.6). The pDONR vectors to generate these entry clones (Figure 2.3) were included as part of the Multisite Gateway cloning kit (Invitrogen).

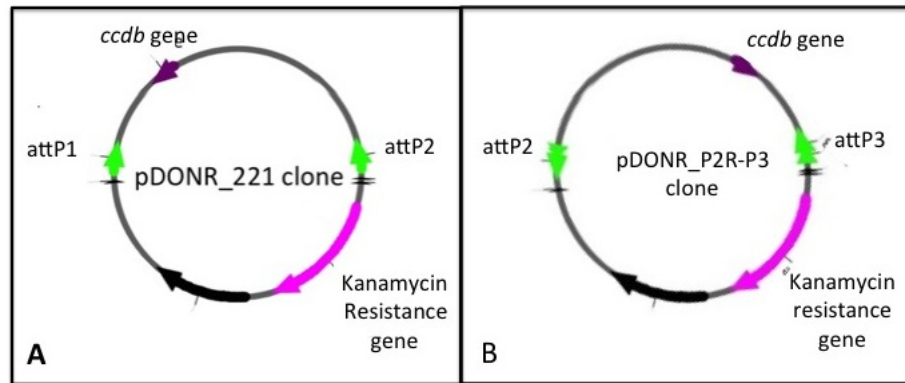


FIGURE 2.3: Vector maps of pDONR:221 (A) and pDONR:P2R-P3 (B) demonstrating the respective attP sites present

The amplicons containing h/z *CCNF* cDNA (wildtype and p.S621G/p.S623G mutant) fused to N-terminal mCherry sequence was generated through PCR as previously described (Section 2.2.6) using the appropriate att primers shown in Table 2.10.

The BP reaction was assembled as shown in Table 2.18. This reaction was assembled at room temperature, then incubated at 25°C for a minimum of one hour. One

microlitre of Proteinase K was added to the reaction to inactivate any nucleases present and this was incubated at 37°C for 10 minutes.

TABLE 2.18: Composition of the BP reaction

Reagent	Quantity
mCherry_ <i>CCNF</i> PCR product	50fmoles
pDONR vector	150ng
BP clonase enzyme mix	2 μ l
TE buffer pH8	$x\mu$ l
	10 μ l

2.2.13 LR recombination

The destination vectors pDEST:Tol2_pA2 and pDEST:Tol2_CG2 for use in the LR reaction (Table 2.19) were included as part of the Multisite Gateway cloning kit (Invitrogen). Eight LR recombination reactions were assembled on ice as shown in Table 2.19 using the entry clones shown in Table 2.20. Reactions were incubated at 25°C for 24 hours. Following incubation, one microlitre Proteinase K was added to the reaction, and incubated at 37°C for 10 minutes.

TABLE 2.19: Composition of the LR reaction

Reagent	Quantity
5' entry clone	10fmoles
Middle entry clone	10fmoles
3' entry clone	10fmoles
pDEST vector	20fmoles
LR clonase II enzyme mix	2 μ l
TE buffer pH8	$x\mu$ l
	10 μ l

TABLE 2.20: Entry clones used in LR recombination reactions

5' clone	Middle entry clone	3' clone	Tol2 backbone vector
CMV-SP6	mCherry_hCCNF_wt	poly A	pDEST:Tol2CG2
CMV-SP6	mCherry_hCCNF_S621G	poly A	pDEST:Tol2CG2
CMV-SP6	mCherry_zCCNF_wt	poly A	pDEST:Tol2CG2
CMV-SP6	mCherry_zCCNF_S623G	poly A	pDEST:Tol2CG2
β -actin	mCherry_hCCNF_wt	poly A	pDEST:Tol2pA2
β -actin	mCherry_hCCNF_S621G	poly A	pDEST:Tol2pA2
β -actin	mCherry_hCCNF_wt	poly A	pDEST:Tol2pA2
β -actin	mCherry_hCCNF_S623G	poly A	pDEST:Tol2pA2

2.2.14 Transformation of constructs into *E.coli*

Constructs generated from ligation reactions (Section 2.2.11) or att-recombination reactions (Sections 2.2.12 and 2.2.13) were transformed into Alpha-Select Gold efficiency competent cells (Bioline) using a heat-shock method. Two microlitres of ligation or recombination reactions was gently mixed with 25 μ l of competent cells, then cooled on ice for 30 minutes. Cells were heat shocked at 42°C for 30 seconds and immediately returned to ice. SOC medium (Life technologies) was added to the heat-shocked cells, (125 μ l), and the mixture incubated at 37°C with shaking at 200rpm for 1 hour.

For low efficiency transformations (LR reaction, Section 2.2.13), 2 μ l of the reaction was added to 50 μ l of competent cells and the incubation time with shaking was extended from 1 hour to 1.5 hours.

For propagation of constructs that carry a *ccbd* lethal gene (Tol2 pDONR and pDEST vectors), transformation into OneShot *ccdb* survival cells (Life Technologies) was performed, following the same heat-shock protocol.

The transformed competent cells were plated onto LB-agar plates containing the appropriate antibiotic for selection of the plasmid-carrying colonies (Table 2.21). The plates were inverted and incubated at 37°C overnight.

TABLE 2.21: Antibiotic resistance of each vector

Kanamycin resistance	Ampicillin resistance
pmCherry	Punc-25
pmCherry-C1	pGEM-T
pDONR:221 / pENTRY:221	pDEST:CG2
pDONR:P2R-P3 / pENTRY:P2R-P3	pDEST:pA2

2.2.15 PCR validation of constructs prior to sequencing

For each transformation reaction, multiple bacterial colonies were checked for the presence of the *CCNF* / *zCCNF* insert using PCR (Table 2.22). One vector specific and one insert specific primer was used in *hCCNF* PCR reactions (Table 2.23) to generate a PCR product ~ 200 bp in length. Two internal *CCNF* primers were used in the *zCCNF* PCR reactions (Table 2.23).

TABLE 2.22: PCR conditions for validation of constructs

Reagent	Volume (μ l)	Temperature	Time	Cycles
MyTaq mix	5			
20mM F primer	0.4	95°C	3 min	1 \times
20mM R primer	0.4	95°C	15 sec	30 \times
dH ₂ O	4.2	55°C	15 sec	30 \times
colony	+	72°C	1 min	30 \times
10 μ l				

TABLE 2.23: Internal *CCNF* primers for validation of colonies

Primer	Sequence
I772T_T698_A	CTATGAAGGCGACCAGGAGAG
T698_B	CCCTGAGGTCATGACGTCCTTC
<i>zCCNF</i> _cDNA_XhoI_F	CAGATCTCGAGCTATGAAAGCGGGCGCGCTCCA
NEBQ5_ <i>zCCNF</i> _S623G_R	CCCTCGTATCCAGAACAGGAA

2.2.16 Purification of plasmids

Following validation (Section 2.2.15), bacterial colonies confirmed as containing the desired construct were added to 5ml LB supplemented with 2.5 μ l kanamycin (100mg/ml) or 5 μ l ampicillin (100mg/ml) depending on their specific antibiotic resistance (Table 2.21), and incubated overnight at 37°C with shaking at 200rpm.

Glycerol stocks of each bacterial culture were prepared by adding 250 μ l of 100% glycerol (Sigma-Aldrich) to 750 μ l of culture and stored at –80°C.

Plasmids were purified from *E.coli* using either the ISOLATE II Plasmid Mini Kit (Bioline) or the Spin Miniprep Kit (Quiagen) as per manufactures instructions. Purified plasmid was eluted into 50 μ l of elution buffer provided with the kit.

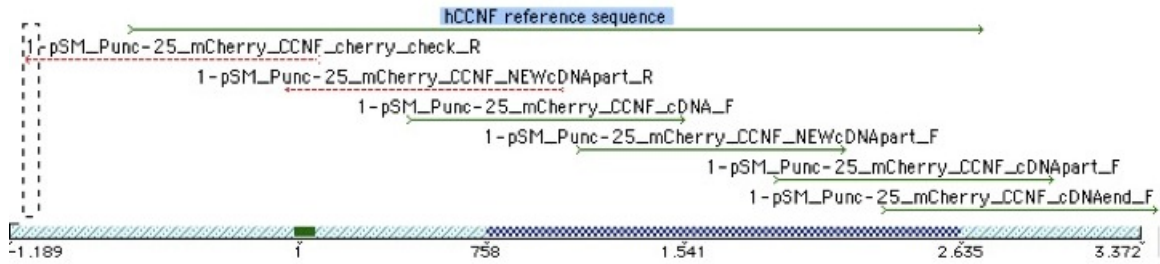
2.2.17 Validation of final constructs

Validation of mCherry-*CCNF* sequences

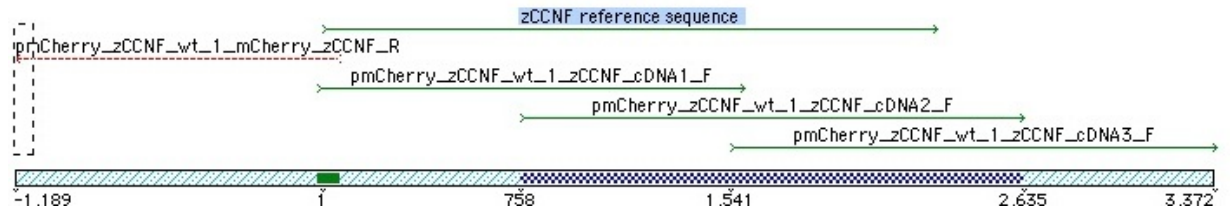
All constructs generated in this study were validated by Sanger sequencing (Macrogen). To confirm the nucleotide sequence of the h*CCNF* and the mCherry-h*CCNF* transgenes, primers shown in Table 2.24 were used to generate six overlapping sequence products (Figure 2.4), which were analysed using Sequencher. The primers used to confirm the nucleotide sequence of the z*CCNF* and mCherry-z*CCNF* transgenes were designed to generate products with less overlap, hence only four sequencing primers were required (Table 2.25, Figure 2.5).

TABLE 2.24: Primers used to sequence h*CCNF* constructs

Primer	Sequence
Cherry_check_R	CGCTCCCCATGGATCTCTTG
<i>CCNF</i> _NEWcDNApart_R	TGCACGGAGAAGACTTGTTG
<i>CCNF</i> _cDNA_F	CAACCACGCCAGTGTGT
<i>CCNF</i> _NEWcDNApart_F	GGAGGTGAGAGCTTCCAGTG
<i>CCNF</i> _cDNApart_F	AGGACAAGCGCTATGGAGAA
<i>CCNF</i> _cDNAend_F	CCTGAACCCAGAACAGCATT

FIGURE 2.4: Overlapping sequencing primers used to calidate h*CCNF* constructs.TABLE 2.25: Primers used to sequence z*CCNF* constructs

Primer	Sequence
z <i>CCNF</i> _cDNA1_F	CGGCGGCATGGACGAGCTGT
z <i>CCNF</i> _cDNA2_F	CACACTCAGGGACTACGCTG
z <i>CCNF</i> _cDNA3_F	ACACGTGTCATTAAGTGGAG
mCherry_z <i>CCNF</i> _R	GACGGCAGATGCTCGCTTTC

FIGURE 2.5: Overlapping sequencing primers used to calidate z*CCNF* constructs.

Validation of pmCherry-C1 constructs

Following sequencing, the ability of the four pmCherry-C1 constructs to express mCherry (and therefore *CCNF*) *in vivo* was validated prior to their use in the Tol2 expression vectors by microinjection of these constructs into zebrafish embryos at the single cell stage of development (Section 2.3).

Validation of Tol2 expression vectors

Prior to sequencing of the Tol2 clones generated in the LR reaction, restriction enzyme digests were performed to confirm the presence of the expected entry clones. One

restriction site found only within the Tol2 backbone vector and one restriction site found only in the middle entry or 3' entry clone were selected (Table 2.26) and the restriction reactions (Table 2.27) performed. These reactions were incubated at 37°C for a minimum of 20 minutes, and the digested vector was gel electrophoresed and imaged.

TABLE 2.26: Restriction enzymes used in digestion reactions for preliminary validation of correct insert in Tol2 expression clones

Tol2 Construct	Restriction enzymes	Expected fragment size
CMV-SP6	BamHI and AngI	1371 bp and 4284 bp
β -actin 2	BamHI and AngI	1371 bp and 8422 bp
HB9	BamHI and ClaI	943bp

TABLE 2.27: Digestion reactions to validate LR reaction products

Reagent	Volume (μl)
LR reaction product	500ng
Restriction enzyme active in 5' clone	0.5
Restriction enzyme active in 3' clone	0.5
10 x Cutsmart buffer	1
dH ₂ O	x
	10 μ l

2.3 Microinjection of pmCherry-C1_ *CCNF* constructs into zebrafish embryos

The four pmCherry-C1_ *CCNF* constructs were microinjected into the animal pole of single celled zebrafish embryos to generate transient expression models that demonstrate mosaic expression of the transgene. Completion of the Tol2 constructs for microinjection and model analysis is part of an ongoing project.

2.3.1 Zebrafish ethics

The housing, breeding and experimental protocols used in this project were approved by the Animal Ethics Committee, Macquarie University (NSW, Australia) and follow the guidelines as detailed in The Zebrafish Book ([Westerfield, 2000](#)).

2.3.2 Collection of embryos

Injections of the pmCherry-C1 constructs were performed into wild-type zebrafish. Injection of future Tol2 constructs will be into the a *HuC*-GFP line ([Park et al., 2000](#)), which demonstrates motor neuron expression of GFP.

To collect embryos for injections, one male and one female zebrafish were kept overnight in a false bottom, pair-mating tank separated by a plastic divider. Removal of the divider in the morning allowed the fish to come into contact, which initiated spawning. The eggs passed through the false bottom of the tank and were collected by straining the tank water through a plastic tea strainer. The eggs were rinsed with system water and transferred to a Petri dish containing E3 embryo medium with 0.5% methylene blue (Sigma-Aldrich).

The eggs were examined under a microscope to confirm fertilisation prior to injection.

2.3.3 Microinjection

Eggs collected from each breeding pair were divided into two groups: one to be injected with the mCherry-C1 vector (*hCCNF*_wt, *hCCNF*_S621G, *zCCNF*_wt and *zCCNF*_S623G) and one control to remain uninjected.

The pmCherry_C1_ *CCNF* constructs were microinjected into the animal pole of the single stage zebrafish embryos at a concentration of 25ng/ μ l. One microlitre of phenol red was added to 3 μ l of the diluted plasmid to allow visualisation of the injected product (Figure 2.6).

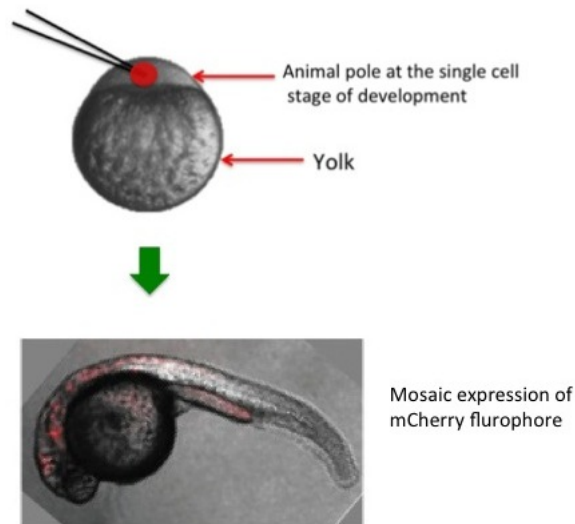


FIGURE 2.6: Microinjection into zebrafish embryos. Illustration of microinjection of a plasmid into the animal pole of zebrafish embryo at the single cell stage of development and subsequent mosaic expression of the mCherry fluorephore

Standard protocol was followed for the injections ([Westerfield, 2000](#)), using a Nikon SMZ745 stereomicroscope, and a PicospritzerTM II Microinjection Dispense System (General ValveTM corporation). Pipettes were pulled with a micropipette puller (Model 700 D, David Kopf Instruments Tujunga, CA) and the tips broken by gentle contact with forceps under the stereomicroscope.

Following injection, embryos were incubated at 28°C for 24 hours in a petri dish containing E3 embryo medium (5mM NaCl, 0.17mMKCl, 10mM HEPES, 0.33mM MgSO₄, 0.33mM CaCl₂ to pH 7.8). Each embryo was then screened for expression of the mCherry fluorephore using Leica M165FC stereo dissection microscope (Leica).

2.3.4 Imaging of embryos

Prior to imaging, embryos were manually dechorionated using Dumont #5 watchmaker forceps (World Instruments).

Embryos were euthanased at 30 hours post fertilisation (hpf) in Tricaine methanesulfonate anaesthetic solution of pH 7.0 (mixed from 400 mg tricaine powder, 97.9 ml deionised water 2.1 ml 1 M Tris (pH 9) (**Westerfield, 2000**)).

Expression of the mCherry tagged transgene was confirmed through florescence microscopy, performed on a Leica M165FC stereo dissection microscope (Leica) using a ProRes CJ cool camera (Jenoptic). UV illumination was provided by an external light source for fluorescence excitation (EL6000, Leica) using an mCherry filter cube (Leica) (594nm).

3

Results

3.1 *VCP* mutation analysis

Individuals with mutations in *VCP* coding exons frequently present with a specific neuronal pathology characterised by VCP- and ubiquitin-positive cytoplasmic and nuclear aggregates (Watts et al., 2004; Schroder et al., 2005). Our collaborators identified an Australian patient with this distinctive pathology in post-mortem tissue. To determine whether the patient had a *VCP* mutation, DNA extracted from brain tissue was screened for *VCP* mutations as part of this project.

Optimal PCR conditions for 15 of the 17 *VCP* exons were established using a MyTaq DNA polymerase protocol (Figure 3.1). The remaining two exons were successfully optimised using a modified PCR protocol (outlined in Table 2.4, Section 2.1.1) Figure 3.2.

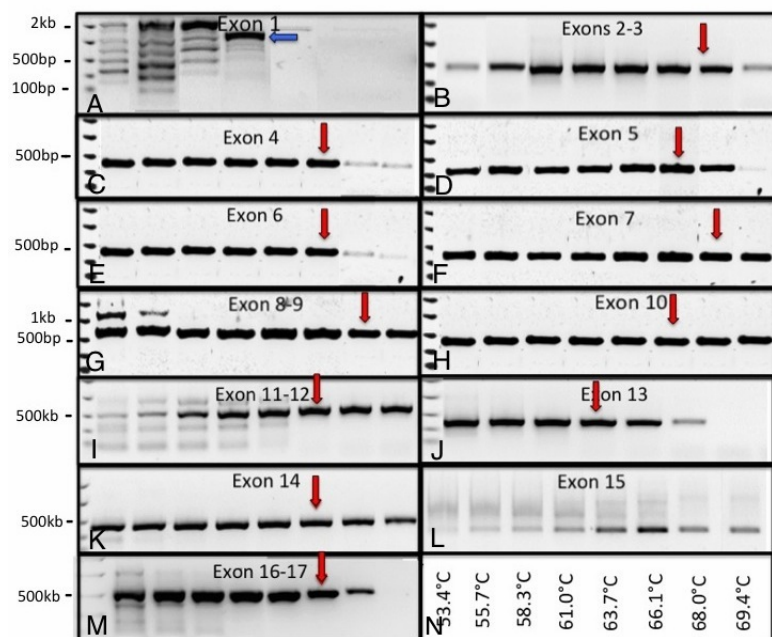


FIGURE 3.1: PCR optimisation for *VCP* exon amplification. Agarose gels of *VCP* PCR products demonstrating optimal annealing temperatures for each exon (red arrows) with the exception of Exon 1 (A) and Exon 15 (L). The blue arrow in A indicates the amplification of a non specific product in Exon 1. Annealing temperatures indicated in (N) apply to all reactions.

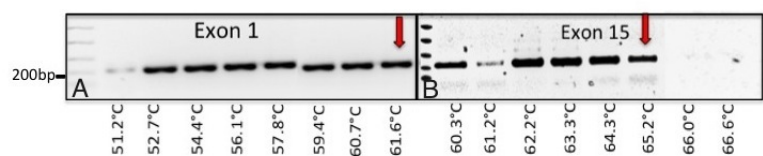


FIGURE 3.2: PCR optimisation for amplification of *VCP* exons 1 and 15. Agarose gels indicating sucessful optimisation of Exon 1 (A) and Exon 15 (B) with the addition of PCR enhancer and a refined temperature range as indicated. Red arrows indicate the selected annealing temperature for subsequent PCR reactions.

The selected PCR conditions for each exon (Table 3.1), were used to sucessfully amplify all *VCP* exons from the ALS patient DNA sample and from a control DNA sample. A negative control was also included in each exon PCR (Figure 3.3). The resultant PCR products were outsourced to Macrogen (Korea) for purification and Sanger sequencing. The outcome of mutation analysis of each exon is summarised in Table 3.2.

TABLE 3.1: Optimised PCR conditions for each *VCP* exon using MyTaq DNA polymerase

Exon	[T _A]	Conditions
1	61°C	MyTaq + PCR enhancer
2–3	68°C	MyTaq
4	66°C	MyTaq
5	66°C	MyTaq
6	66°C	MyTaq
7	69°C	MyTaq
8–9	68°C	MyTaq
10	66°C	MyTaq
11–12	66°C	MyTaq
13	64°C	MyTaq
14	66°C	MyTaq
15	64°C	MyTaq + PCR enhancer
16–17	66°C	MyTaq

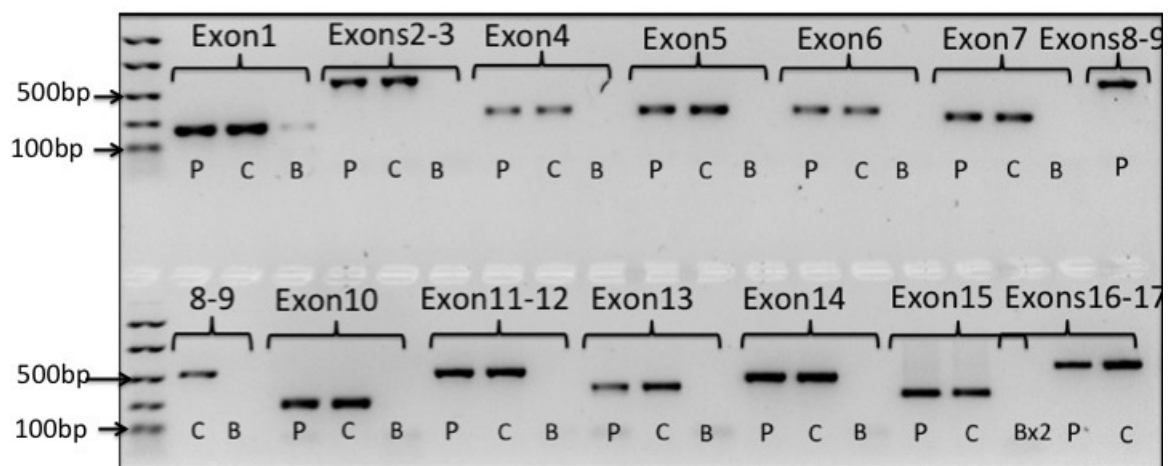
FIGURE 3.3: Amplification of *VCP* exons. Gel electrophoresed samples of PCR products for each of the 17 exons of *VCP*. P = patient sample DNA, C = control DNA and B = blank sample. Note the blank samples for exons 15 and 16–17 are in the same well: Bx2.

TABLE 3.2: Analysis results of *VCP* gene screening

Exon	Sequencing result
Exon 1	no polymorphisms
Exons 2–3	no polymorphisms
Exon 4	no polymorphisms
Exon 5	c.475C>T
Exon 6	no polymorphisms
Exon 7	no polymorphisms
Exons 8–9	no polymorphisms
Exon 10	no polymorphisms
Exons 11–12	no polymorphisms
Exon 13	no polymorphisms
Exon 14	c.1839-1847 delA
Exon 15	no polymorphisms
Exons 16–17	no polymorphisms

Across all 17 exons, two variants were identified. The first variant was identified in exon 5 (Figure 3.4) and substitutes a C to T at nucleotide position 475 (c.475C>T), resulting in an amino acid change of arginine to cysteine at position 159 (p.R159C).

The second variant is a deletion of an adenosine nucleotide within a polyA region of Exon 14 (Figure 3.5).

Both mutations were validated by repeating the PCR and sequencing in both forward and reverse orientation.

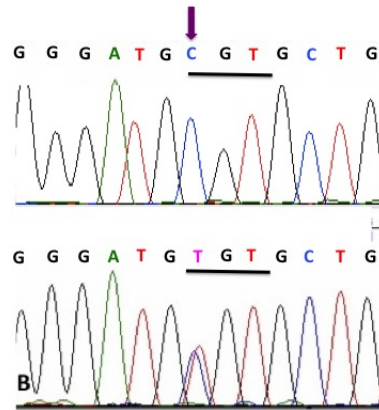


FIGURE 3.4: *VCP* missense mutation in exon 5. Sequence traces from an unaffected control (A) and the patient (B). The arrowhead indicates the base position at which *VCP* is mutated (c.475C>T)

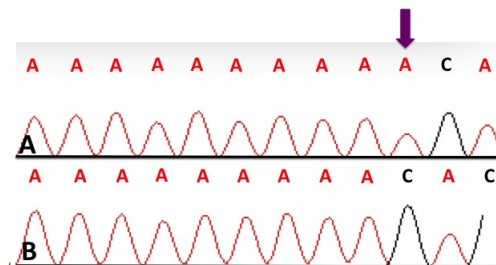


FIGURE 3.5: *VCP* deletion mutation in ooly A region of exon 14. Sequence traces from an unaffected control (A) and the patient (B).

3.2 Developing expression constructs for *in vivo* ALS models

3.2.1 Overview

To date, no *in vivo* models have been developed to specifically examine the effect of ALS-linked mutations in protein degradation pathway genes. The constructs that this project aimed to generate (summarised in Table 3.3) are based on *CCNF* variants previously identified in FALS, SALS and FTD patients (unpublished data, Table 1.4) and were designed to be expressed in either *C.elegans* or zebrafish.

TABLE 3.3: *CCNF* constructs to generate novel animal models of ALS

Construct	Species	Model	Species of origin for <i>CCNF</i> sequence	Expression	Fluorescent tag
Punc-25	<i>C.elegans</i>	Stable	Human	Neuronal	Nil
Punc-25-mCherry	<i>C.elegans</i>	Stable	Human	Neuronal	mCherry
CMV-SP6	Zebrafish	Transient / stable	Human / zebrafish	Ubiquitous	mCherry
β -actin2	Zebrafish	Stable	Human / zebrafish	Ubiquitous	mCherry
HB9-4x	Zebrafish	Stable	Human / zebrafish	Motor neuron	mCherry
HB9-12x	Zebrafish	Stable	Human / zebrafish	Motor neuron	mCherry

3.2.2 Site-directed mutagenesis

For the downstream *in vivo* analysis of mutant *CCNF*, site directed mutagenesis was used to introduce the known sequence variants into *CCNF* cDNA. Q5 mutagenesis (Section 2.2.9) was used to successfully introduce each of the variants from Table 1.4 separately into the h*CCNF* cDNA in the pmCherry-C1.h*CCNF* vector, and to introduce the p.S623G mutation into z*CCNF* cDNA in the pGEM-T_z*CCNF* vector. In total, 22 mutant pmCherry_*CCNF* constructs were created.

Each mutant construct was transformed, propagated and purified (Methods sections 2.2.14 and 2.2.16).

Sequencing of a 1000bp fragment overlapping the target site was used to confirm the presence of the variant in each construct (Figures 3.6 to 3.8). Additional sequencing across the entire *CCNF* cDNA and mCherry sequence ensured that mutagenesis had not introduced any additional nucleotide changes into these fusion constructs.

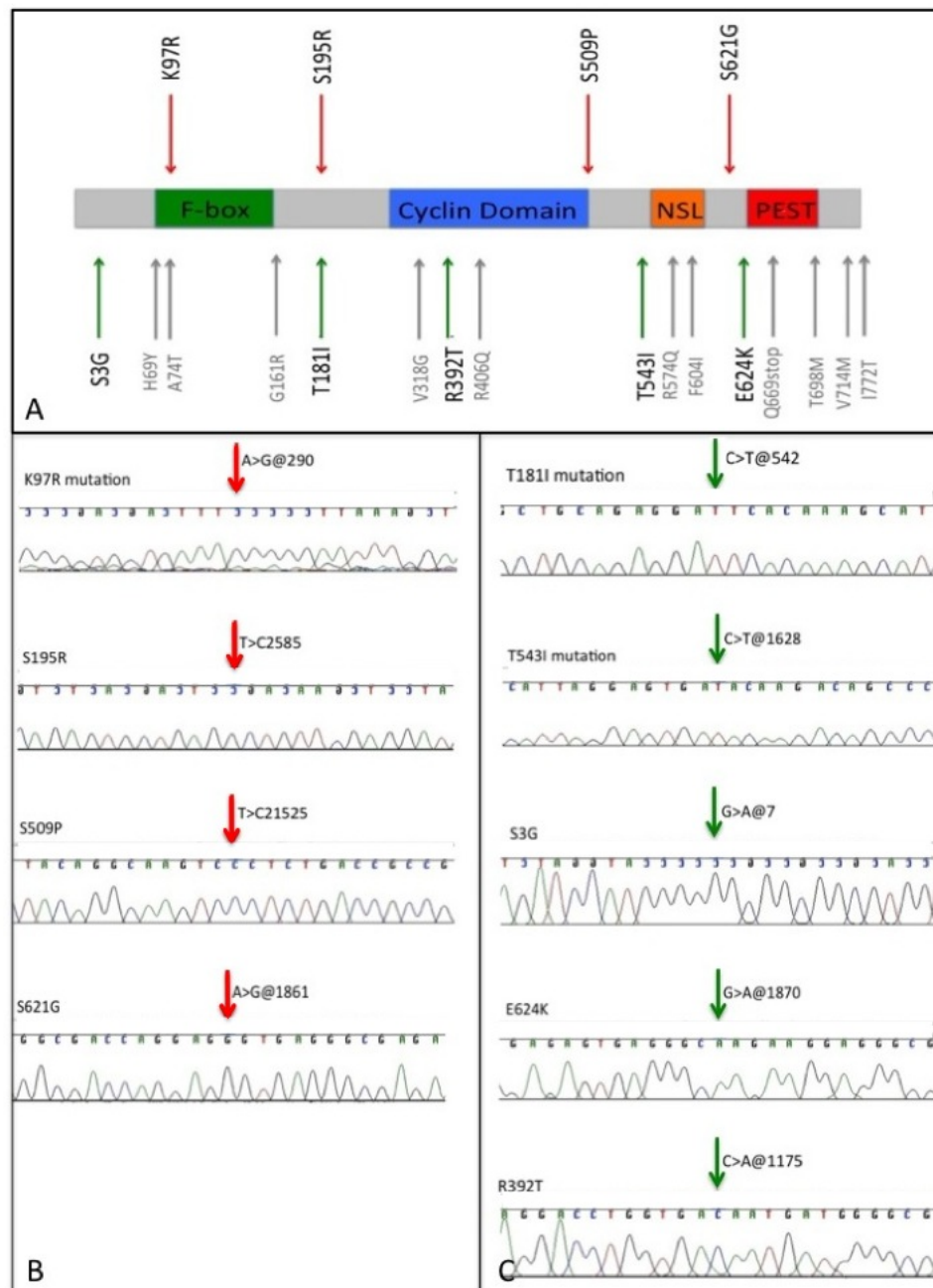


FIGURE 3.6: Generation of mutant h*CCNF* constructs 1. **A**. Schematic of the location of known mutations/SNPs within *CCNF*. Red arrows indicate mutations found in FALS patients, green arrows indicate mutations found in SALS patients, grey arrows indicate SNPs found in patients and controls. **B**. Chromatograms generated from sequencing of h*CCNF* constructs based on FALS-associated mutations. **C**. Chromatograms generated from sequencing of h*CCNF* constructs based on SALS-associated mutations. Arrows indicate the location of each point mutation.

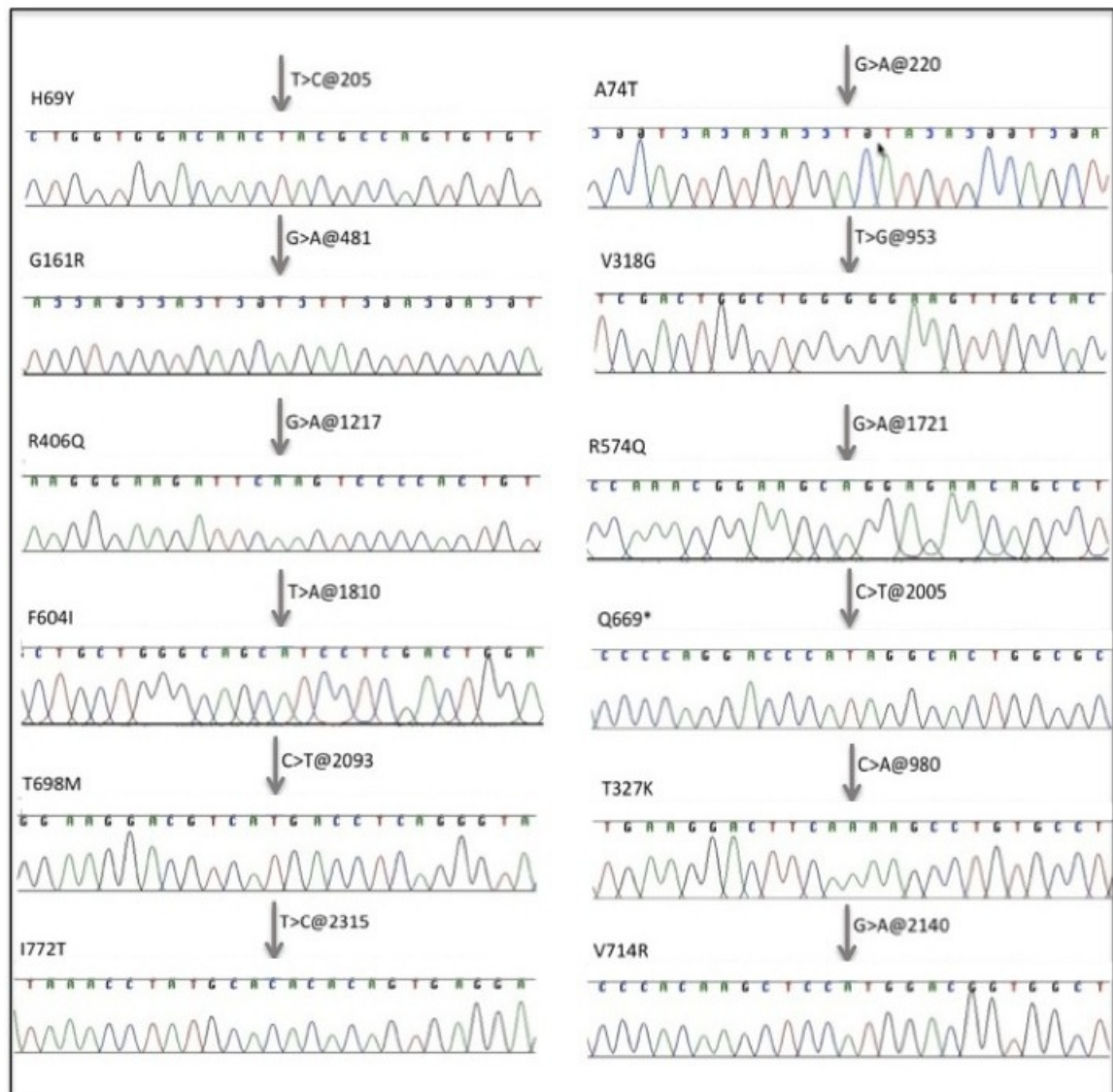


FIGURE 3.7: Generation of mutant *hCCNF* constructs 2. Chromatograms generated from sequencing of *hCCNF* constructs based on SNPs identified in public databases and present in ALS and/or FTD patients and controls. Arrows indicate the location of each point mutation.

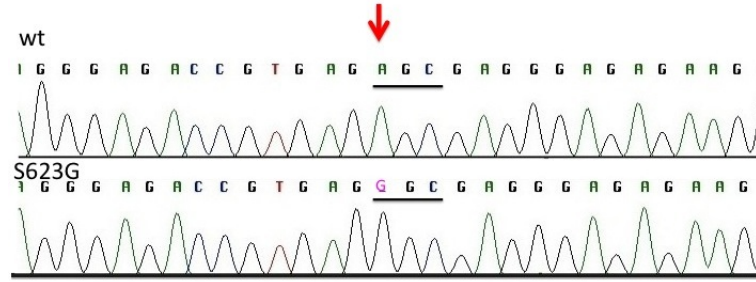


FIGURE 3.8: Generation of mutant *zCCNF* constructs. Chromatograms generated from sequencing of wild-type *zCCNF* (top) and mutant *zCCNF* (bottom) based on the p.S623G mutation (equivalent to human p.S621G mutation). Arrow indicates the location of the point mutation c.1867A>G.

3.2.3 Generation of Punc-25 expression constructs

The Punc-25 expression constructs were designed to contain either the *hCCNF* cDNA (2,361bp) or the *hCCNF* cDNA fused with an N-terminal mCherry (3,099bp) within the multiple cloning site of the Punc-25 vector. The *NheI* and *EcoRI* restriction sites present in the multiple cloning site were used to generate these constructs (Figure 3.9).

Wild type and mutant *hCCNF* cDNA and wild type and mutant fusion mCherry-*hCCNF* cDNA was PCR amplified from the pmCherry-C1 constructs (Section 2.2.6). Forward primers used in the PCR carried a *NheI* restriction site at the 5' end, and reverse primers carried a *EcoRI* site at the 3' end (Table 2.9, Section 2.2.3). The 42 mutant and two wildtype PCR products generated are shown in Table 3.4.

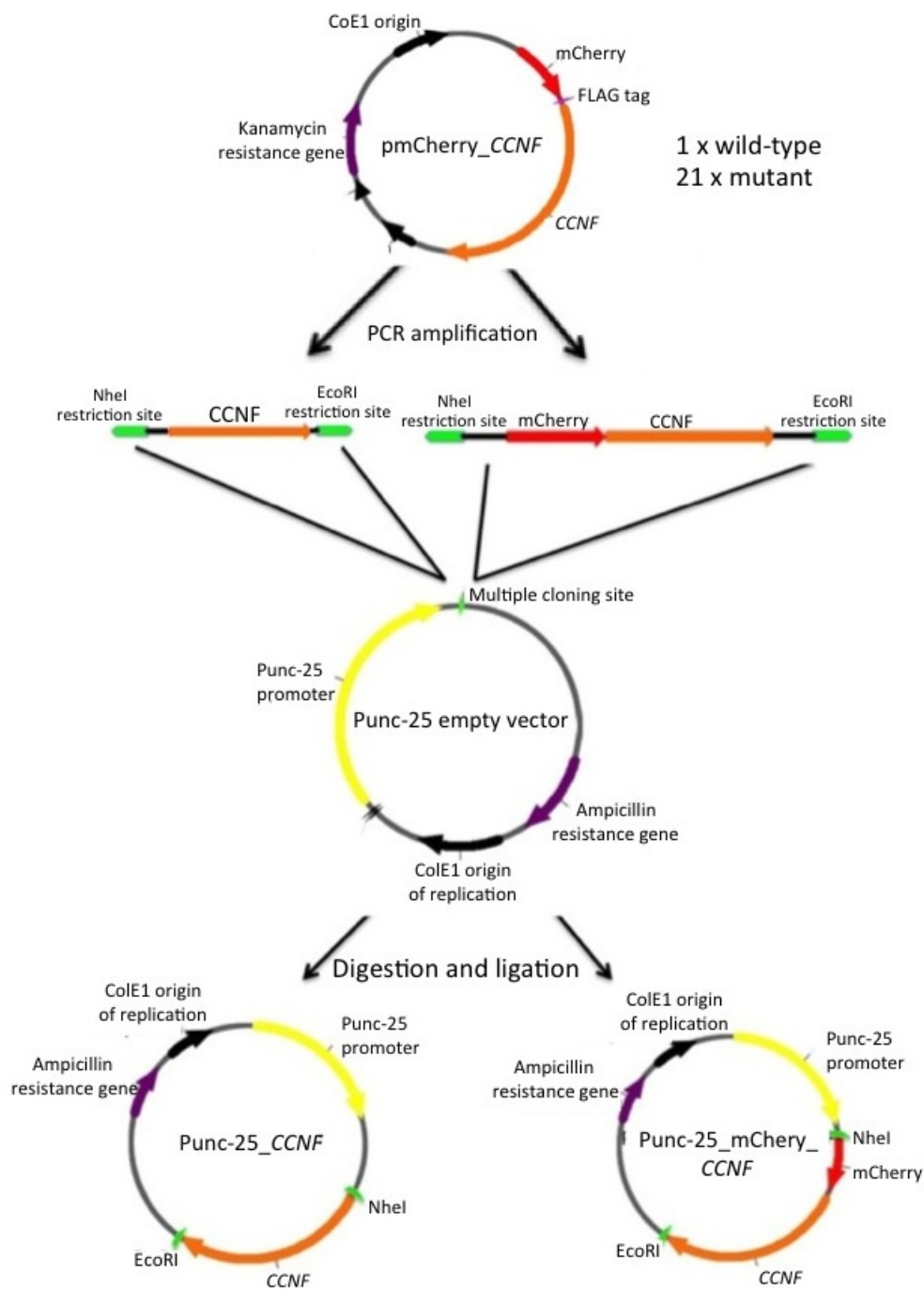


FIGURE 3.9: Generation of Punc-25 expression constructs. Schematic summarising the successful generation of the Punc-25_*CCNF* and Punc-25_mCherry_*CCNF* constructs for expression in *C.elegans* through PCR amplification of *CCNF* (Section 2.2.6), digestion of the amplicon and the Punc-25 vector (Section 2.2.10), gel purification (Section 2.2.8), ligation (Section 2.2.11), transformation and purification of the resulting plasmids (Sections 2.2.14 and 2.2.16)

TABLE 3.4: hCCNF cDNA PCR products.

hCCNF amplicon	Expression construct generated from the amplicon
hCCNF_wt	Punc-25_hCCNF_wt
mCherry_hCCNF_wt	Punc-25_mCherry_hCCNF_wt
hCCNF_S3G	Punc-25_hCCNF_S3G
mCherry_hCCNF_S3G	Punc-25_mCherry_hCCNF_S3G
hCCNF_H69Y	Punc-25_hCCNF_H69Y
mCherry_hCCNF_H69Y	Punc-25_mCherry_hCCNF_H69Y
hCCNF_A74T	Punc-25_hCCNF_A74T
mCherry_hCCNF_A74T	Punc-25_mCherry_hCCNF_A74T
hCCNF_K97R	Punc-25_hCCNF_K97R
mCherry_hCCNF_K97R	Punc-25_mCherry_hCCNF_K97R
hCCNF_G161R	Punc-25_hCCNF_G161R
mCherry_hCCNF_G161R	Punc-25_mCherry_hCCNF_G161R
hCCNF_T181I	Punc-25_hCCNF_T181I
mCherry_hCCNF_T181I	Punc-25_mCherry_hCCNF_T181I
hCCNF_S195R	Punc-25_hCCNF_S195R
mCherry_hCCNF_S195R	Punc-25_mCherry_hCCNF_S195R
hCCNF_V318G	Punc-25_hCCNF_V318G
mCherry_hCCNF_V318G	Punc-25_mCherry_hCCNF_V318G
hCCNF_R392T	Punc-25_hCCNF_R392T
mCherry_hCCNF_R392T	Punc-25_mCherry_hCCNF_R392T
hCCNF_R406Q	Punc-25_hCCNF_R406Q
mCherry_hCCNF_R406Q	Punc-25_mCherry_hCCNF_R406Q
hCCNF_S509P	Punc-25_hCCNF_S509P
mCherry_hCCNF_S509P	Punc-25_mCherry_hCCNF_S509P
hCCNF_T543I	Punc-25_hCCNF_T543I
mCherry_hCCNF_T543I	Punc-25_mCherry_hCCNF_T543I
hCCNF_R574Q	Punc-25_hCCNF_R574Q
mCherry_hCCNF_R574Q	Punc-25_mCherry_hCCNF_R574Q
hCCNF_F604I	Punc-25_hCCNF_F604I
mCherry_hCCNF_F604I	Punc-25_mCherry_hCCNF_F604I
hCCNF_S632G	Punc-25_hCCNF_S632G
mCherry_hCCNF_S632G	Punc-25_mCherry_hCCNF_S632G
hCCNF_E624K	Punc-25_hCCNF_E624K
mCherry_hCCNF_E624K	Punc-25_mCherry_hCCNF_E624K
hCCNF_Q669STOP	Punc-25_hCCNF_Q669STOP
mCherry_hCCNF_Q669STOP	Punc-25_mCherry_hCCNF_Q669STOP
hCCNF_T698M	Punc-25_hCCNF_T698M
mCherry_hCCNF_T698M	Punc-25_mCherry_hCCNF_T698M
hCCNF_V714M	Punc-25_hCCNF_V714M
mCherry_hCCNF_V714M	Punc-25_mCherry_hCCNF_V714M
hCCNF_I772T	Punc-25_hCCNF_I772T
mCherry_hCCNF_I772T	Punc-25_mCherry_hCCNF_I772T

The PCRs successfully amplified the required hCCNF sequence or the mCherry_hCCNF fusion sequence, however, a non-specific product of approximately 400bp was also amplified (Figure 3.10). The correct PCR product was gel purified (Section 2.2.8), and then digested with NheI and EcoR1 restriction enzymes (Section 2.2.10).

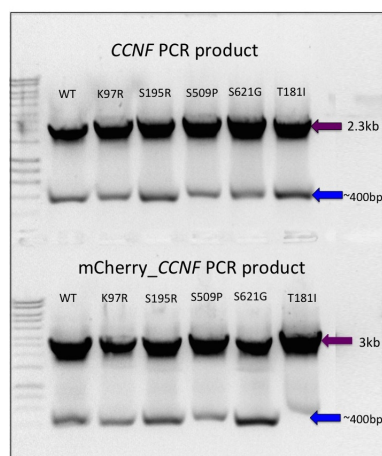


FIGURE 3.10: PCR amplification of *hCCNF* from pmCherry-C1 vector. Representative agarose gel of electrophoresed PCR products *hCCNF* and mCherry-*hCCNF* with size marker Hyperladder 1 (Bioline). Purple arrows indicate products of expected size, blue arrows indicate the presence of a non-specific product.

The Punc-25 vector was prepared by also digesting with *NheI* and *EcoRI* restriction enzymes (to generate sticky ends complementary to those of the PCR products), treated with TSAP, gel purified and ligated with the *CCNF* PCR products (Sections 2.2.10, 2.2.16 and 2.2.11).

Ligation reactions were transformed (Section 2.2.14) and recombinant clones identified by colony PCR validation (Section 2.2.15) using internal *CCNF* primers described in Table 2.23. A representative gel of electrophoresed products amplified by colony PCR validation is shown in Figure 3.11.

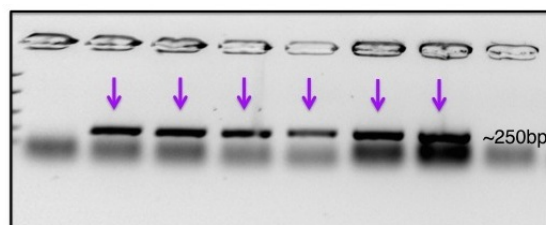


FIGURE 3.11: Validation of recombinant clones. Representative agarose gel of electrophoresed PCR products generated to validate recombinant clones carrying the *CCNF* transgene (purple arrows). Note the two negative colonies at either end of the gel.

Validated colonies were propagated and the plasmid DNA was successfully purified (Section 2.2.16). DNA concentration and 260/280 ratios of each of the 44 constructs were determined using nanodrop (Table 3.5).

TABLE 3.5: PCR products and Punc-25 constructs generated

Construct	Concentration (ng/ μ l)	260/280
pSM Punc-25_CCNF_wt	747.3	1.89
pSM Punc-25_mCherry_CCNF_wt	690.9	1.87
pSM Punc-25_mCherry_CCNF_S3G	496.0	1.86
pSM Punc-25_CCNF_S3G	478.6	1.87
pSM Punc-25_CCNF_H69Y	613.3	1.87
pSM Punc-25_mCherry_CCNF_H69Y	650.4	1.89
pSM Punc-25_CCNF_A74T	451.9	1.8
pSM Punc-25_mCherry_CCNF_A74T	498.8	1.86
pSM Punc-25_CCNF_K97R	482.7	1.87
pSM Punc-25_mCherry_CCNF_K97R	639	1.87
pSM Punc-25_CCNF_G161R	734.9	1.86
pSM Punc-25_mCherry_CCNF_G161R	657.0	1.88
pSM Punc-25_CCNF_T181I	630.1	1.86
pSM Punc-25_mCherry_CCNF_T118I	530.7	1.87
pSM Punc-25_CCNF_S195R	846.6	1.86
pSM Punc-25_mCherry_CCNF_S195R	684.8	1.86
pSM Punc-25_CCNF_V318G	894.5	1.87
pSM Punc-25_mCherry_CCNF_V318G	436.5	1.89
pSM Punc-25_CCNF_T327K	545.	1.87
pSM Punc-25_mCherry_CCNF_T327K	550.6	1.87
pSM Punc-25_CCNF_R372T	829	1.88
pSM Punc-25_mCherry_CCNF_R372T	563.7	1.86
pSM Punc-25_CCNF_R406Q	586.6	1.86
pSM Punc-25_mCherry_CCNF_R406Q	536.2	1.87
pSM Punc-25_CCNF_S509P	622.5	1.89
pSM Punc-25_mCherry_CCNF_S509R	655.5	1.87
pSM Punc-25_CCNF_T543I	557.8	1.89
pSM Punc-25_CCNF_mCherry_T543I	418	1.86
pSM Punc-25_CCNF_R574	830.9	1.87
pSM Punc-25_mCherry_CCNF_R574Q	663.9	1.86
pSM Punc-25_CCNF_F604T	720.0	1.84
pSM Punc-25_mCherry_CCNF_F604I	542.6	1.86
pSM Punc-25_CCNF_S621G	874.8	1.86
pSM Punc-25_mCherry_CCNF_S621G	690.8	1.87
pSM Punc-25_CCNF_E624K	722.4	1.87
pSM Punc-25_mCherry_CCNF_E624K	682.8	1.87
pSM Punc-25_CCNF_Q669*	623	1.86
pSM Punc-25_mCherry_CCNF_Q669*	583.3	1.86
pSM Punc-25_CCNF_T698M	881.5	1.89
pSM Punc-25_mCherry_CCNF_T698M	483.7	1.87
pSM Punc-25_CCNF_V714M	308.3	1.88
pSM Punc-25_mCherry_CCNF_V714M	597.6	1.86
pSM Punc-25_CCNF_I772T	821.8	1.86
pSM Punc-25_mCherry_CCNF_I772T	542.1	1.89

All constructs were diluted to 100ng/ μ l for sequencing. Analysis of sequence data confirmed the correct *CCNF* or mCherry-*CCNF* fusion sequence within the Punc-25 vector. If errors were present in the plasmid sequence, additional PCR validated colonies were propagated, purified and sequenced to identify a valid Punc-25-*CCNF* construct or Punc-25-mCherry-*CCNF* fusion construct. All validated constructs were sent to Dr Massimo Hilliard's laboratory at the Queensland Brain Institute for expression and ongoing studies in *C.elegans*. A representative image of the *C.elegans* model generated from expression of the Punc-25-*CCNF*-wt construct in the *juIs76_vdIs4* strain is shown in Figure 3.12.



FIGURE 3.12: Expression of Punc-25-*CCNF*-wt in *C.elegans*. Representative image of the *C.elegans* *CCNF* model using **A.** A GFP filter cube (395nm) to image the GABAergic neurons through the *juIs76* ((Punc-25-GFP) transgene present in the transgenic line utilised and **B.** A mCherry filter cube (594nm) to image the pre-synaptic sites through the *vdIs4* (Punc-25-mCherry-RAB3) transgene, also present in the transgenic line.

3.2.4 Alignment of zebrafish and human *CCNF* orthologues

Alignment of the human and zebrafish *CCNF* cDNA sequences (NM.001761 and NM.207048) demonstrated a 61.2% sequence homology between the two species. The p.S621G mutation in the human gene is orthologous to p.S623G in z*CCNF* (Figure 3.13). The nucleotide substitution required in the zebrafish *CCNF* is c.1867A>G.

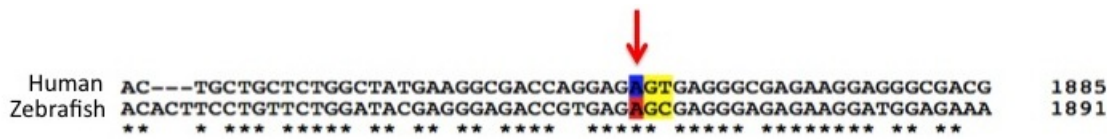


FIGURE 3.13: Clustal Omega alignment of zebrafish and human *CCNF* orthologues. Representative sample of the Clustal Omega analysis of h*CCNF* and z*CCNF*. The red arrow indicates the location of the S621G mutation, which occurs at nucleotide position c.1861 in h*CCNF*. The equivalent z*CCNF* mutation occurs at nucleotide position c.1867 (p.S623G.)

3.2.5 RNA extraction from zebrafish embryos

Zebrafish RNA was successfully extracted from embryos (Section 2.2.4), as demonstrated by the presence of strong bands representative of the two dominant RNA species (18S and 28S) in an electrophoresed sample (Figure 3.14). The concentration of this RNA was determined to be 200ng/ μ l (eluted in 30 μ l).

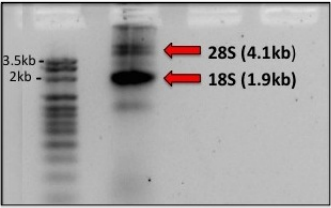


FIGURE 3.14: RNA extracted from zebrafish embryos. Agarose gel of electrophoresed RNA extracted from zebrafish embryos demonstrating the presence of the two dominant rRNA species 18S and 28S. This confirms the integrity of the extracted RNA.

The RNA was used for reverse transcription cDNA synthesis, generating a cDNA library with a concentration of 400ng/ μ l (Section 2.2.5). To determine the integrity of the cDNA library, the ubiquitously expressed β -actin cDNA was successfully amplified using the RT-PCR reaction in Table 2.15, Section 2.2.6 and primers in Table 2.12, (Figure 3.15).

However, there was repeated failure to RT-PCR amplify full-length *zCCNF* from this cDNA library. Upon careful inspection of the designed *zCCNF* primers, an error was identified in the design of the reverse primer (corrected primer sequence is shown in Table 2.9). Due to time constraints in this project, a vector containing full-length *zCCNF* cDNA (pCMV_SPORT6.1*zCCNF* vector) was obtained from a zebrafish construct repository and used for the remainder of this project.

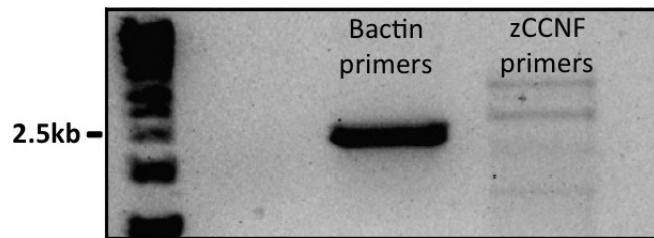


FIGURE 3.15: RT-PCR amplification of β -actin from zebrafish cDNA library. Agarose gel of electrophoresed samples of β -actin and *zCCNF* RT-PCR amplified from the zebrafish cDNA library, demonstrating successful amplification of the β -actin product, and failure of amplification of *zCCNF*. This failure was found to be due to an error in primer design.

3.2.6 Subcloning into pmCherry-C1 vector

The pmCherry-C1 vector used for subcloning of *hCCNF* and the fused mCherry-*hCCNF* sequence into the *C.elegans* vector was obtained through Addgene, a repository for constructs generated by other research laboratories. The Addgene vector (Figure 3.16) carries a FLAG tag (24bp) between the N-terminal mCherry sequence and *CCNF*, in lieu of the multiple cloning site. As such, *zCCNF* could not be subcloned into this vector. Instead, to maintain standardised constructs, both *hCCNF* (wild type and p.S621G mutant) and *zCCNF* (wild type and p.S623G mutant) were subcloned into the multiple cloning site of fresh pmCherry-C1 vector (Clontech).

Subcloning of h*CCNF*

h*CCNF* (wildtype and p.S621G mutant) was directly subcloned into the Clontech pmCherry-C1 vector using PCR amplification to introduce EcoRI and XhoI restriction sites, (Table 2.9, Section 2.2.6) followed by digestion and ligation reactions (Sections 2.2.10 and 2.2.11). Sequencing of the new fusion constructs (pmCherry-C1_*CCNF*_wt and pmCherry-C1_*CCNF*_S621G, (Figure 3.16), confirmed the insert was present in the correct orientation with no undesired spontaneous mutations.

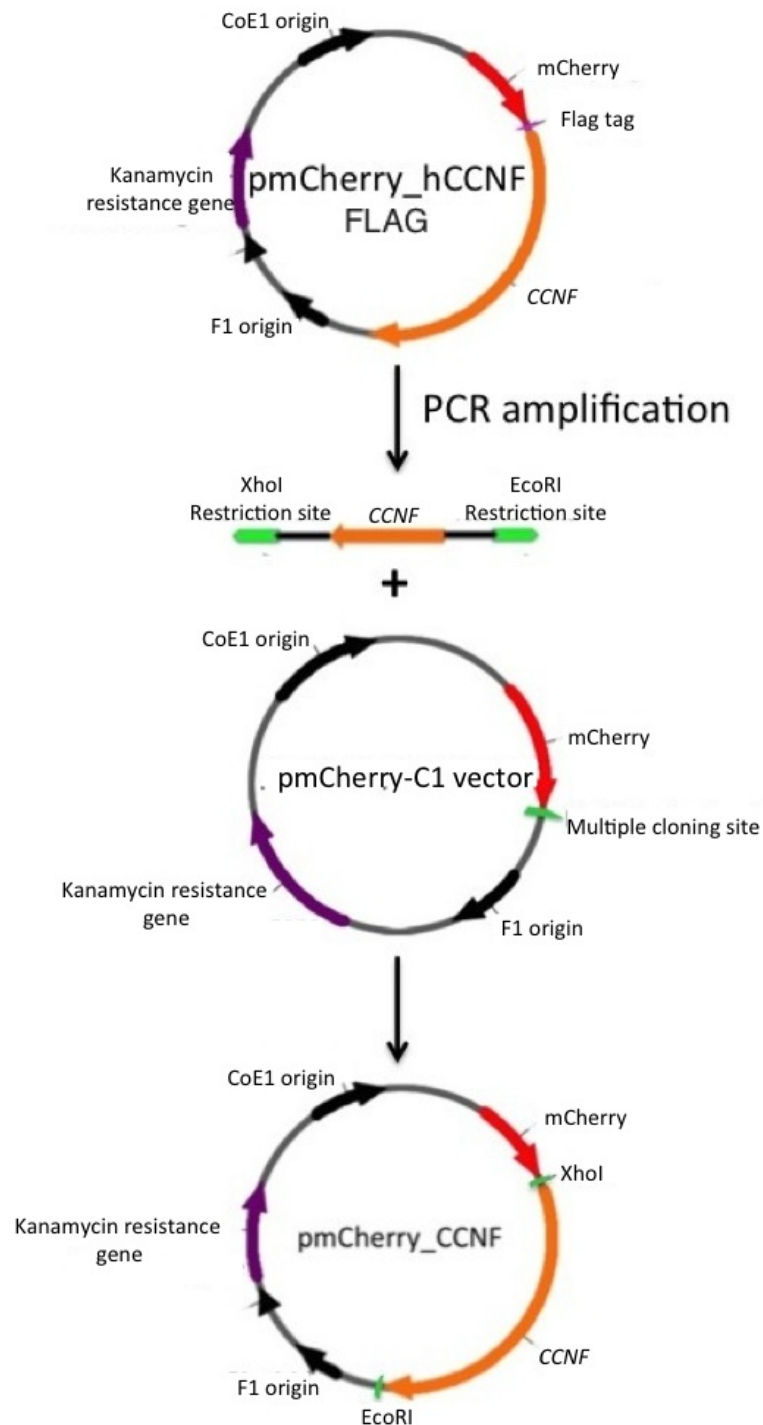


FIGURE 3.16: Subcloning of *hCCNF* into pmCherry-C1 vector. Schematic summarising the successful generation of the pmCherry-C1_*hCCNF* vectors through PCR amplification of *hCCNF* from the pmCherry-FLAG vector (Section 2.2.6), digestion of the amplicon and the pmCherry-C1 vector (Section 2.2.10), gel purification (Section 2.2.8), ligation of digested products (Section 2.2.11), transformation and purification of the resulting plasmids (Sections 2.2.14 and 2.2.16).

Subcloning of *zCCNF*

Primers containing XhoI and EcoRI restriction sites were used to PCR amplify a *zCCNF* amplicon from the pCMV_SPORT6.1_*zCCNF* vector (Section 2.2.3 and 2.2.6), with the aim of subcloning the amplicon directly into pmCherry-C1. However, attempts to ligate the XhoI and EcoRI digested PCR product into a similarly digested pmCherry-C1 repeatedly failed despite extensive troubleshooting.

To overcome this, the *zCCNF* cDNA flanked by EcoRI and XhoI restriction sites was PCR amplified from the pmCherry-FLAG tag vector and ligated into pGEM-T (Promega) through TA cloning (Section 2.2.7). This construct was subsequently transformed, propagated and purified. Sanger sequencing verified the correct *zCCNF* cDNA sequence in the pGEM-T vector (Sections 2.2.14, 2.2.16 and 2.1.3).

Q5 site-directed mutagenesis was used to introduce the p.S623G mutation into the pGEM-T_*zCCNF* vector (Section 2.2.9). The resulting pGEM-T_*zCCNF*_S623G construct was verified by Sanger sequencing.

Wild-type and mutant p.S623G *zCCNF* were digested out of the pGEM-T clones using the introduced XhoI and EcoRI restriction sites (Section 2.2.10) and gel purified (Section 2.2.8).



FIGURE 3.17: Digested pGEM-T_*zCCNF* clones. Image of gel electrophoresed sample of digested pGEM-T_*zCCNF* wild type and p.S623G mutant clones. Purple boxes indicate section of gel removed for purification of *zCCNF* product.

The pmCherry-C1 vector was digested with XhoI and EcoRI restriction enzymes, gel purified, and ligated with the digested *zCCNF* products (wildtype and p.S623G). Troubleshooting established that a modified transformation procedure designed for ligation reactions with a low efficiency (Section 2.2.14) was required for successful colony growth to occur. Following PCR validation (Section 2.2.15), the pmCherry-C1_*zCCNF*_wt and the pmCherry-C1_*zCCNF*_S623G fusion constructs were purified and sequenced. Figure 3.18 illustrates the steps taken to subclone *zCCNF* into the pmCherry_C1 vector.

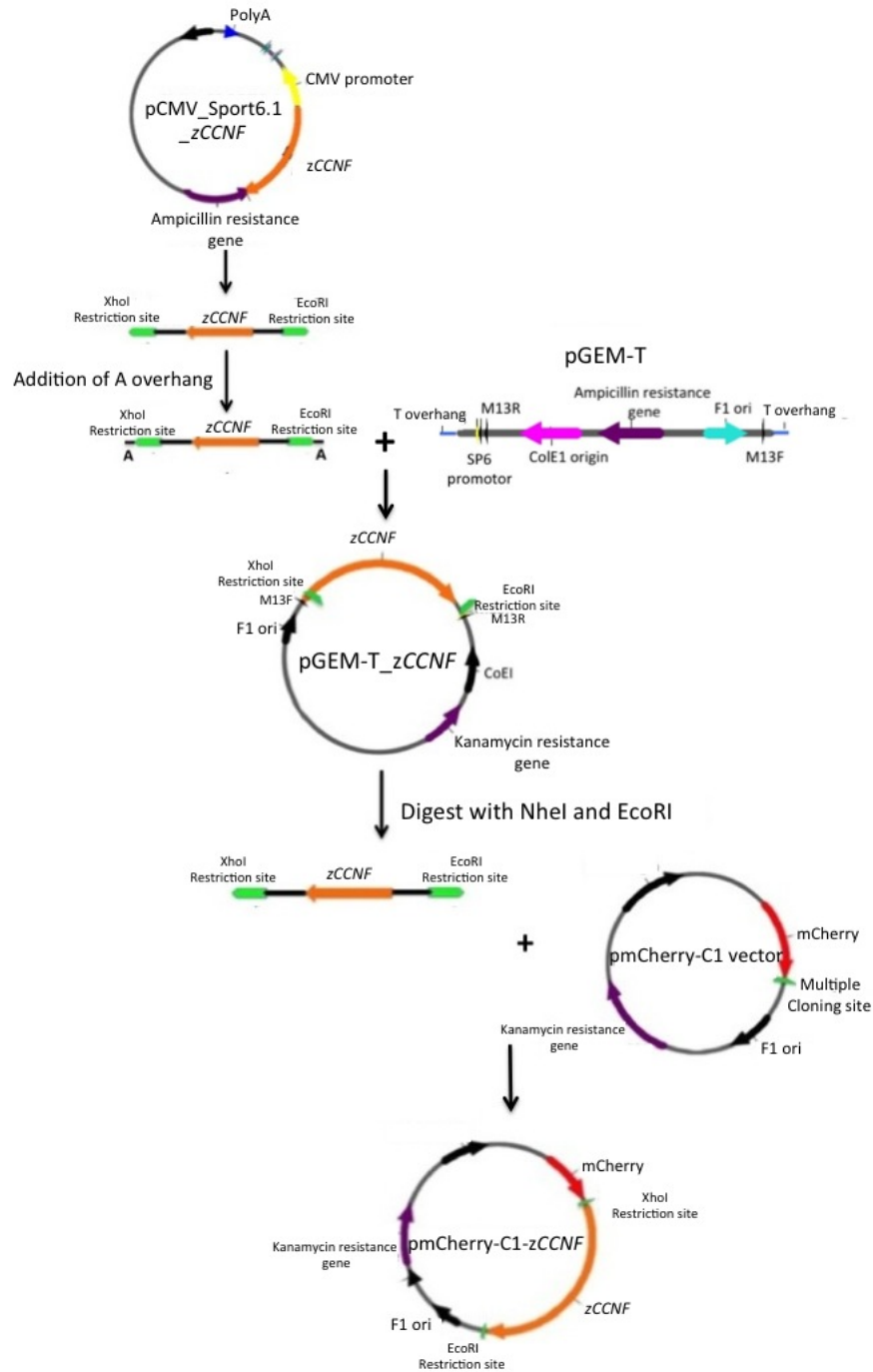


FIGURE 3.18: Subcloning of *zCCNF* into pmCherry-C1 vector. Schematic summarising the successful generation of the pmCherry-C1-*zCCNF* vectors through PCR amplification of *zCCNF*_{wt} (Section 2.2.6), addition of an adenine overhang and subsequent TA cloning into the pGEM-T vector (Section 2.2.7), digestion of the amplicon from the pGEM-T vector (Section 2.2.10), gel purification (Section 2.2.8), ligation with similarly digested pmCherry-C1 vector (Section 2.2.11), transformation and purification of the resulting plasmids (Sections 2.2.14 and 2.2.16).

3.2.7 Expression of pmCherry-C1 constructs

To confirm that mCherry-*CCNF* amplicons were in the correct frame and would allow for protein expression *in vivo*, the pmCherry-C1-*CCNF* constructs (pmCherry-C1_h*CCNF*_wt, pmCherry-C1_h*CCNF*_S621G, pmCherry-C1_z*CCNF*_wt and pmCherry-C1_z*CCNF*_S623G) were transiently expressed in zebrafish embryos. The pmCherry-C1 vector carries a CMV promoter, that drives expression of the mCherry-*CCNF* fusion sequences *in vivo*.

Zebrafish embryos were microinjected with the constructs and screened for mCherry expression at 30 hpf. Approximately 30% of injected embryos demonstrated transient and mosaic expression of the mCherry-*CCNF* transgene, as illustrated in Figure 3.19.

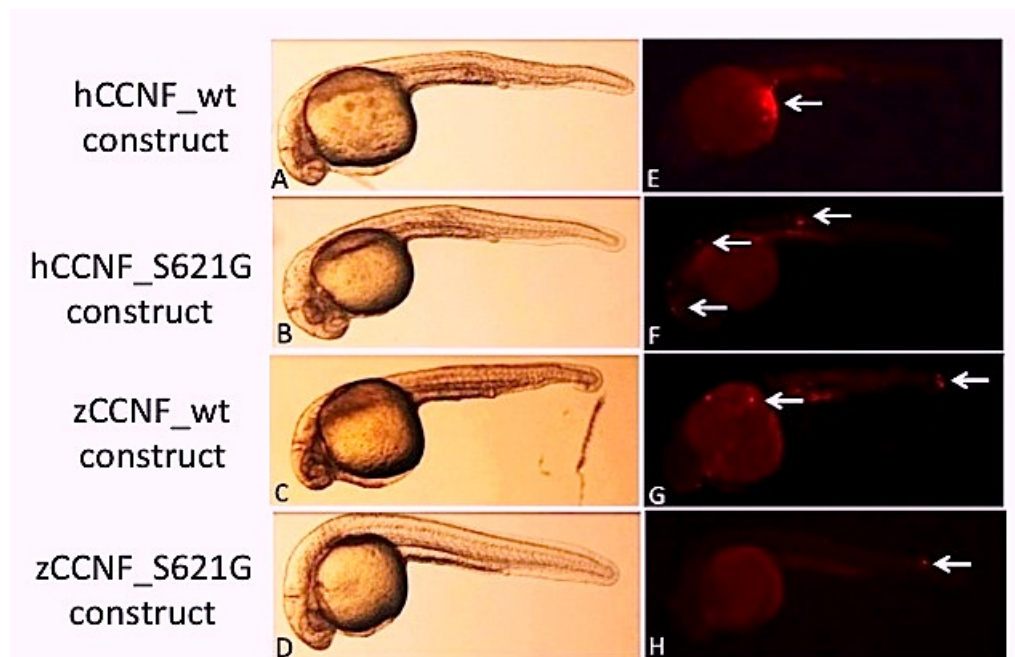


FIGURE 3.19: Expression of pmCherry-*CCNF* constructs in zebrafish embryos. Representative images of 30hpf zebrafish embryos microinjected with each of the four pmCherry-*CCNF* constructs. **A-D**: white light images of the zebrafish embryos. **E-H**: Images of the same embryos under mCherry filter cube (594nm), demonstrating mosaic expression of the mCherry fluorephore as highlighted by the white arrows.

3.2.8 Generation of *CCNF* Tol2 constructs

The long-term project aims to generate expression constructs for each of the four pmCherry-C1-*CCNF* constructs using a three-fragment vector Tol2 kit (Kwan et al., 2007). This kit allows for the order- and orientation-specific recombination of a 5' entry clone (p5E), a middle entry clone (pME), and a 3' entry clone (p3E) with a Tol2 backbone vector in a single reaction to generate a Tol2 expression clone Figure 2.1.

The clones designed for this project will generate models that demonstrate ubiquitous expression (driven by the CMV and β -actin promoters) and motor neuron expression (driven by the HB9 promoter). HB9 is a weak promoter, therefore the GAL4-UAS / KalTax systems were selected to amplify expression levels. The degree of amplification required to generate suitable expression levels cannot be predicted, therefore two clones were selected: one to amplify expression four-fold and one to amplify expression 12-fold. The entry clones used are summarised in Table 3.6.

TABLE 3.6: Tol2 clones used to generate zebrafish constructs

Construct	5' Clone	ME clone	3' clone	Destination vector
CMV-SP6.h/z <i>CCNF</i>	p5E:CMV - ubiquitous promoter. Allows generation of <i>CCNF</i> mRNA	pENTR:221_mcherry- <i>CCNF</i>	PolyA	pDest:Tol2CG2 (Tol2 vector carrying a cardiac GFP reporter)
Bactin2.h/z <i>CCNF</i>	P5E:Bactin2 - ubiquitous promoter	pENTR:221_mcherry- <i>CCNF</i>	PolyA	PDest:Tol2pA2 - no fluorescent reporter
HB9.h/z <i>CCNF</i>	p5E:HB9 - motor neuron promoter	pME:kalTax4 amplifies expression of MN promoter x4	pENTR:P2R-P3_mCherry- <i>CCNF</i>	PDest:Tol2pA2
HB9.h/z <i>CCNF</i>	p5E:HB9 - motor neuron promoter	pME:GAL4_UASx12 amplifies expression of MN promoter x12	pENTR:P2R-P3_mCherry- <i>CCNF</i>	PDest:Tol2pA2

The entry clone containing the CMV promoter, the β actin2 promoter and the PolyA tail, in addition to the pDest:Tol2pA2 and pDest:Tol2CG2 destination vectors were sourced from the Chien laboratory (<http://chien.neuro.utah.edu/Tol2kitwiki>), while the p5E:HB9, pME:KalTax4 and the pME:GAL4-UAS x12 entry clones were a kind gift from the Cole laboratory (Macquarie University). Each vector was amplified by transformation, propagation and purification (Sections 2.14, 2.17), then validated by Sanger sequencing using M13_F (GTTTTCCCAGTCACGAC) and M13_R (CAGGAAACAGCTATGAC) primers, available as universal sequencing primers at Macrogen (Korea).

Validation of gifted Tol2 entry clones

The Tol2 Entry clones HB9, KalTax4 and the GAL4-UASx12 obtained as gifts from the Cole laboratory were validated prior to performing BP and LR reactions. The KalTax4 clone was gifted as a GAL4-UASx4 clone, however the sequenced vector failed to align with the reference sequence and upon analysis it was determined that no UAS site was present.

The NCBI BLAST software (<http://www.ebi.ac.uk/Tools/sss/ncbiblast/vectors.html>) was used to confirm the gifted vector carried a KalTax4 sequence. This sequence has the same function as the GAL4-UAS clone and consequently, was used as an alternative in the project.

BP reactions to generate Tol2 entry clones

The four mCherry-*CCNF* fusion sequences (human and zebrafish wildtype and mutant) were PCR amplified from the pmCherry-C1 constructs with Phusion DNA polymerase and att B site primers (Sections 2.2.3 and 2.2.6).

Gel electrophoresis of the PCR products demonstrated the amplification of non-specific sequences (Figure 3.20). This necessitated gel purification (Section 2.9) of the 3.1kb mCherry-*CCNF* product. The purified PCR products were used in a BP reaction (Section 2.12) as illustrated in Figure 3.21.

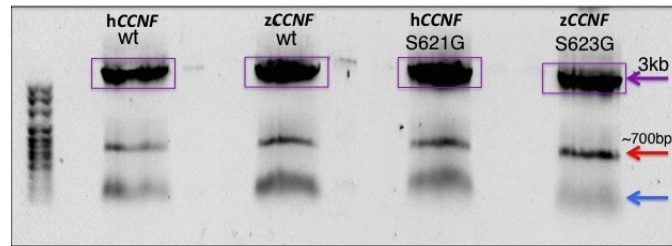


FIGURE 3.20: PCR amplification of *hCCNF* and *zCCNF* fusion sequences. Image of gel electrophoresed PCR products generated from the amplification of *hCCNF* and *zCCNF* from the pmCherry-C1 vectors. Purple arrow indicates product of expected size which was subsequently gel purified, red arrow indicates the non-specific product amplified and blue arrow indicates primer dimer formation.

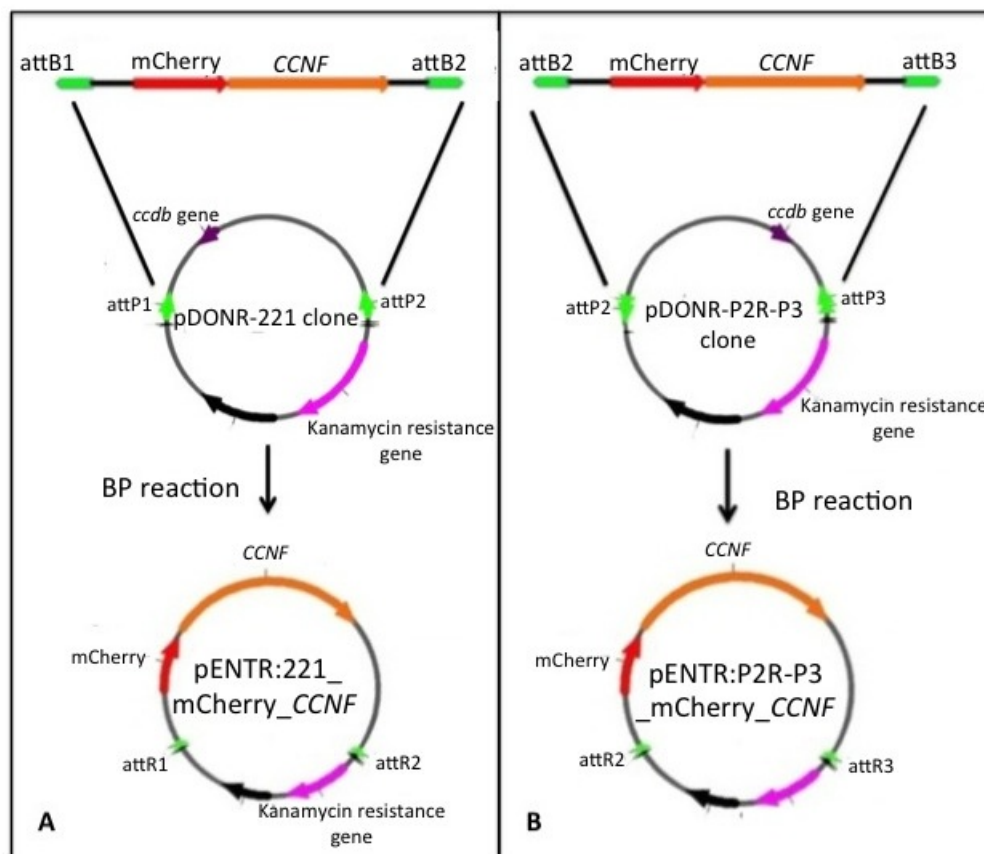


FIGURE 3.21: BP recombination reaction. Schematic illustrating the strategy used for the generation of mCherry-*CCNF* entry clones in a BP reaction. **A.** Generation of middle entry pENTR:221_mcherry-*CCNF* clones through PCR amplification of mCherry-*CCNF* with attB1 forward primer and attB2 reverse primers. **B.** Generation of a 3' pENTR:P2R-P3_mCherry-*CCNF* entry clone through PCR amplification with attB2 forward primer and attB3 reverse primer.

These reactions generated the entry clones shown in Table 3.7.

TABLE 3.7: Tol2 entry clones generated through BP reactions

Middle Entry clones	3' Entry clones
pENTR:221_h <i>CCNF</i> _wt	pENTR:P2R-P3_h <i>CCNF</i> _wt
pENTR:221_h <i>CCNF</i> _S621G	pENTR:P2R-P3_h <i>CCNF</i> _S621G
pENTR:221_z <i>CCNF</i> _wt	pENTR:P2R-P3_z <i>CCNF</i> _wt
pENTRY:221_z <i>CCNF</i> _S622G	pENTR:P2R-P3_z <i>CCNF</i> _S622G

All constructs were sequenced to confirm the presence of the correct mCherry-*CCNF* insert within each entry clone.

LR reactions to generate Tol2 expression vectors

The 5'-, middle- and 3'- entry vectors that were either purchased, gifted or generated by BP reactions in Section 2.2.12 were recombined in LR reactions with one of two Tol2 destination vectors - pDEST:Tol2-PA2 or pDEST:Tol2-CG2 (Section 2.2.13). Due to time constraints, only 8 of the 16 planned LR reactions were performed, as described in Section 2.2.13.

Due to low recombination efficiencies, the incubation time for the LR reaction was extended from the recommended 16 hours at 25°C to 24 hours at 25°C. Despite this, the reaction still had a very low efficiency, so a modified transformation protocol with an extended recovery time was used (Section 2.2.14).

The constructs were propagated and purified (Section 2.2.16), then examined by restriction enzyme digestion (2.2.17) and gel electrophoresis (Section 2.1.2). Products of the expected size failed to be digested from these constructs, despite repetition of the reaction (Figure 3.22). Sequencing of the clones confirmed the presence of the expected entry clones, however the clones were present in the incorrect locations and orientation.

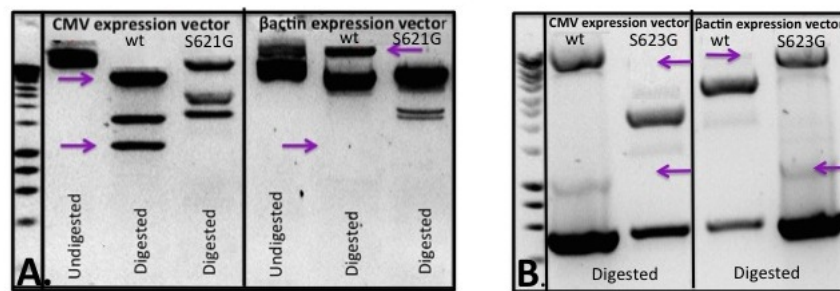


FIGURE 3.22: Restriction enzyme digests of Tol2 expression clones. Representative image of gel electrophoresed products generated by digestion of **A.** Tol2 h*CCNF* expression vectors and **B.** z*CCNF* expression vectors, with size marker Hyperladder 1kb plus. Arrows indicate expected size of the products of digestion. The presence of additional products of digestion and an absence of expected products indicates a failure of the LR reaction.

Time constraints of this project precluded repetition of the BP and LR reactions for these constructs. An ongoing project will generate these constructs and establish the sixteen stable lines of zebrafish expressing *CCNF* for further analysis.

4

Discussion

4.1 ALS gene discovery

Gene mutations are the only known cause of ALS and gene discoveries have provided insight to possible functional pathways responsible for this devastating disease. However, the pathological mechanisms underlying ALS remain poorly understood and currently only 60% of familial cases, and 10% of sporadic cases have an identified causal gene mutation (**Robberecht and Philips, 2013**). The ongoing identification of ALS-linked genes and gene mutations is essential to further our understanding of the molecular mechanisms of the disease and facilitate development of disease models, which in turn will aid the design and testing of targeted therapeutics.

The identification of novel ALS genes or novel mutations in known ALS genes can also be of benefit to patients as it presents the opportunity to identify the specific disease mutation in an individual or within a family. The confirmation of a gene mutation in a patient does not currently affect treatment decisions, however it does provide an opportunity to prevent that mutation from being inherited by subsequent generations through the use of genetic testing of embryos and *in vitro* fertilisation (IVF). Furthermore, identification of a mutation within a patient provides a definitive

diagnosis of ALS and in some cases, allows a more informed prognosis to be given, as different mutations within the same gene can be associated with different age of onset and rapidity of progression (Chen et al., 2013). Without ALS-linked gene identification, diagnosis is reliant on observing disease progression and can take up to 12 months.

There is great promise that ALS gene discovery will affect treatment decisions in the near future with the rapid development of gene therapy techniques. For example, a study using an antisense morpholino to reduce expression levels of mutant SOD1 in patients has now entered a Phase 1 clinical trial. While results regarding efficacy of the therapy are not yet available, the potential treatment was well tolerated by patients, providing hope for the therapeutic approach (Miller et al., 2013).

Exome sequencing analysis performed in our laboratory recently identified ALS-linked mutations in *CCNF* in a large Australian ALS family and worldwide collaborative gene screening efforts subsequently identified *CCNF* mutations in familial and sporadic ALS and FTD patients with a global frequency of 0.6 to 3.3%. This project aimed to generate non-mammalian animal models based on mutations within this gene. In the future, these *CCNF* models will be used for *in vivo* studies to investigate disease pathology, and for preliminary testing of potential therapeutics. In addition to generating animal models, this project performed mutation screening of *VCP*, a known ALS- and IMBPFD-associated gene in a pathologically implicated patient.

4.1.1 Mutation screening of *VCP*

The patient involved in this study was referred to the Macquarie Motor Neuron Disease Research Centre genetics laboratory for mutation screening of the *VCP* gene (encoding valosin-containing protein) due to the presence of pathological features consistent with *VCP* mutations. These pathological features typically consist of *VCP*- and TDP-43-positive ubiquitinated protein aggregates in muscles and neurons (Watts et al., 2004; Schroder et al., 2005). To date, four ALS-causative mutations (Koppers et al., 2012) and 19 IMBPFD-causative mutations (Kimonis et al., 2008; Ju and Weihl, 2010) have been identified in *VCP*, with the majority of mutations occurring within exon five.

The first *VCP* variant identified in this project (c.475C>T, p.R159C) is absent from the public variant database dbSNP release141 (<http://www.ncbi.nlm.nih.gov/SNP/>) and absent from 6500 exomes in the Exome Variant Server database (<http://www.evs.gs.washington.edu/EVS/>). The variant is located in exon 5 and has previously been reported in an IBMPFD patient in America (Spina et al., 2013). Furthermore, alternate mutations in the same codon (p.R159G and p.R159H) have been identified in two patients in an Italian ALS-FTD family (Johnson et al., 2010) and four members of an Austrian IMBPFD family (Haubenberger et al., 2005), which suggests a mutation hotspot in this region. The mutated arginine residue is highly conserved across species (Figure 4.1) which, in combination with the characteristic pathology displayed by the patient, is highly suggestive that the variant identified in this project is the pathological mutation in this patient.

<i>H.sapiens</i> (human)	GKRIHVLPIDDTVEGITGNLFEVYLKPYFLEAYRPIRKGDIFLVRGGMRAVEFKVVETDP	170
<i>P.troglodytes</i> (chimpanzee)	GKRIHVLPIDDTVEGITGNLFEVYLKPYFLEAYRPIRKGDIFLVRGGMRAVEFKVVETDP	170
<i>M.musculus</i> (mouse)	GKRIHVLPIDDTVEGITGNLFEVYLKPYFLEAYRPIRKGDIFLVRGGMRAVEFKVVETDP	170
<i>C.lupus</i> (dog)	GKRIHVLPIDDTVEGITGNLFEVYLKPYFLEAYRPIRKGDIFLVRGGMRAVEFKVVETDP	170
<i>S.cerevisiae</i> (yeast)	ATRISVLPIADTIEGITGNLFDVFLKPYFVEAYRPIRKGDHFFVVRGGMRAVEFKVVETDP	180
<i>D.rerio</i> (zebrafish)	GKRIHVLPIDDTVEGITGNLFEVYLKPYFLEAYRPIRKGDIFLVRGGMRAVEFKVVETDP	170
<i>G.gallus</i> (junglefowl)	GKRIHVLPIDDTVEGITGNLFEVYLKPYFLEAYRPIRKGDIFLVRGGMRAVEFKVVETDP	170
<i>R.norvegicus</i> (rat)	GKRIHVLPIDDTVEGITGNLFEVYLKPYFLEAYRPIRKGDIFLVRGGMRAVEFKVVETDP	170
<i>B.taurus</i> (cattle)	GKRIHVLPIDDTVEGITGNLFEVYLKPYFLEAYRPIRKGDIFLVRGGMRAVEFKVVETDP	170
<i>C.elegans</i> (worm)	GTRIVLPIDDTIEGLTGNLFDVFLKPYFLEAYRPLHKGDIPTVQAAMRTVEFKVVETDP	176
<i>D.melanogaster</i> (fly)	GKRVRLPIDESTEGVTGNLFEIYLKPYFLEAYRPIHMGDNFIVRAAMRTVEFKVVETDP	167
<i>X.tropicalis</i> (frog)	GKRIHVLPIDDTVEGITGNLFEVYLKPYFLEAYRPIRKGDIFLVRGGMRAVEFKVVETDP	170

FIGURE 4.1: Evolutionary conservation of amino acid 159 in *VCP* (highlighted in yellow). This amino acid is substituted from an arginine to cysteine (p.R159C) in the patient sample screened in this project.

The second variant identified during mutation screening was a deletion of an adenine nucleotide in a polyA region of exon 14. Cloning of exon 14 from gDNA to allow sequencing of both alleles suggest that the polymorphism is heterozygous (i.e. 8 and 9 adenine nucleotides respectively). Further analysis is required to establish the standard size of this polyA region in a large population of ALS patients and controls. The deletion seen in this patient would produce a frameshift mutation, the significance of which is uncertain.

The location of the polyA region within exon 14 of *VCP* is unusual. Evolution has largely selected against the presence of long polyA sequences within protein coding regions as they increase the incidence of slippage of RNA polymerase during transcription, leading to errors in gene expression. Furthermore, slippage events during DNA replication are also hypothesised to occur with greater frequency in polyA regions, resulting in a greater incidence of mutational events in these areas ([Linton et al., 1997](#)). A number of diseases are known to be associated with differential polyA site transcription and alternate polyadenalation, for example Fragile X syndrome, the most common form of inherited intellectual disability ([Hollerer et al., 2014](#)). The deletion of an adenine nucleotide in *VCP* exon 14 of the patient screened in this project is potentially pathogenic, however its significance remains unclear. Studies using real time quantitative reverse transcriptase PCR (qRT-PCR) will be performed in an ongoing project to identify and validate isoforms that result from this variant, and to determine any effects of the polyA variant on *VCP* expression.

4.1.2 PCR optimisation for screening of *VCP*

Optimisation of the PCR conditions for the majority of the *VCP* exons in this project was relatively straightforward however, exons 1 and 15 proved more difficult. In the case of exon 1, this may have been a consequence of its relatively high CG content (59.2%) compared to the other *VCP* exons. CG-rich sequences can be significantly more challenging to amplify as a result of their strong secondary structure that interferes with efficient denaturing. In addition, primers designed to anneal to CG-rich targets have a tendency to form intermolecular secondary structures that compete for annealing position, and therefore limit amplification efficiency (Frey et al., 2008).

It is more difficult to explain why PCR enhancer was required to amplify exon 15. The CG content of this exon is not substantially higher than the other exons (51.6%), and the size of the amplicon is not excessively large (294bp). It was hypothesised that suboptimal primer design could be the reason for poor PCR efficiency. Complementary sequences between primers can result in primer dimer formation, while complementary sequences within a single primer can result in primer hairpinning. Additionally, complementary sequences in the template DNA at multiple sites can result in amplification of non-specific products. However, analysis with Primer-BLAST software (<http://www.ncbi.nlm.nih.gov/tools/primer-blast>) determined that the primers designed to amplify *VCP* exon 15 were specific to the target sequence. Suboptimal primer design therefore, is unlikely to be a contributor to the PCR inefficiency.

Through a process of elimination therefore, an inappropriate magnesium (Mg) concentration in the PCR reaction appears to be the most likely cause of the inefficiency of the reaction. Optimal Mg concentration in a PCR varies between reactions as template DNA concentration, deoxynucleotide triphosphate (dNTPs) concentration and the presence of any proteins or chelating agents all influence Mg requirement. Insufficient Mg inactivates DNA polymerase, while excessive Mg can reduce enzyme fidelity and increase non-specific amplification.

The contents of the PCR enhancer reagent from Invitrogen used in this study is proprietary, but they are typically composed of additives aimed at enhancing denaturing efficiency (such as betane, formamide and DMSO (Henke et al., 1997; Sarkar et al., 1990)), increasing DNA polymerase stability (BSA, gelatin and non-ionic detergents (Varadaraj and Skinner, 1994)), or increasing specificity of primer annealing by

reducing primer secondary structures (7-deaza-2-deoxyguanosine, ([Jung et al., 2002](#))). The addition of glycerol or ammonium chloride makes the PCR more tolerant of sub-optimal conditions through unknown mechanisms. The combination of these reagents in the PCR enhancer used in this project is unknown, therefore the specific chemical responsible for optimising the PCR for exons 1 and 15 cannot be determined.

4.2 Animal models of ALS

The major aim of this project was to generate multiple novel non-mammalian animal models of ALS, with the future intent of identifying which techniques produce a model that best reflects the disease phenotype. Not only will this allow the use of models with optimum design for immediate use in functional studies, but the knowledge may also be applied to the design of future animal models. Projects aimed at developing improved animal models are essential as no current model adequately reflects the pathological features of ALS. Additionally therapeutic trials in these models have demonstrated poor predictive ability of the efficacy of therapeutics in human patients.

Currently there is an over-reliance on the G93A *SOD1* transgenic mouse model, particularly for therapeutic testing. This model is recognised as the most phenotypically accurate nonprimate model of ALS as it reflects many of the pathological hallmarks of the disease, including progressive motor neuron degeneration, microglial activation and aggregates of ubiquitinated protein (Bruijn et al., 1997; Gurney et al., 1994; Wong et al., 1995). However, these models do not demonstrate physiologically accurate gene expression, as they carry 23 copies of the *SOD1* transgene. Furthermore, neither *SOD1* patients, nor *SOD1* models demonstrate TDP-43 positive protein aggregates, a pathological hallmark in approximately 90% of ALS patients (Neumann et al., 2006; Arai et al., 2006).

It is not only the mutation upon which animal models are based that needs to be assessed, but also the technical strategy used to generate them. Models based on mutations within *TARDBP* (TDP-43) are a good example. The caveat of the vast majority of these models is that they significantly over-express *TARDBP* under neural promoters (Vaccaro et al., 2012; Ash et al., 2010; Liachko et al., 2010; Hanson et al., 2010; Li et al., 2010). This is in contrast to the expression pattern of endogenous TDP-43, which is ubiquitous and moderate. While reflecting some of the aspects of ALS pathology, these models fail to demonstrate ubiquitinated TDP-43 positive aggregates (Swarup et al., 2011). Two *TARDBP* mouse models with more physiologically accurate gene expression have recently been developed, and both of these models demonstrate cytoplasmic ubiquitinated aggregates with TDP-43 pathology (Swarup et al., 2011; Arnold et al., 2013). This improved phenotypic accuracy provides a strong argument for continual re-assessment of available models and the techniques used to generate them.

It must be recognised however, that even if optimal techniques are identified, the perfect animal model of ALS may never be developed. One reason for this is that species differences can affect model phenotype, even within mammals. This fact is demonstrated by a study that generated *TARDBP* transgenic cynomolgus monkeys and rats using the same techniques. Both species developed upper and lower motor neuron degeneration and ubiquitinated TDP-43 positive neuronal aggregates. However, only the non-human primates demonstrated cytoplasmic TDP-43 mislocalisation and Bunina bodies (Uchida et al., 2012). The physiological reasons behind the different phenotypes remains unclear, however the study highlights the limitation of non-primate models to reflect all of the aspects of human disease. These species differences may in some part explain the failure thus far of therapeutic benefits to translate from animal models to human clinical trials (Schnabel, 2008).

In addition to the influence of species differences, models based on a single gene mutation, housed under standard laboratory conditions, cannot accurately mimic disease modifiers. Epigenetic factors are believed to contribute to the substantial phenotypic variability and irregular disease penetrance seen between carriers of the same ALS-linked gene mutation (Kearney, 2011). Furthermore, discordant disease phenotypes are seen within sets of identical twins (Xi et al., 2014), suggesting a significant role of environmental factors in disease development.

Despite the inability of any animal model of ALS to accurately reflect all of the pathological features of the disease, they currently remain the only means to study cellular disease biology *in vivo*. This reliance on imperfect models leads to a need for multiple models, each of which reflect different aspects of ALS pathology. This can be achieved by basing models on mutations within ALS-linked genes that function in different cellular pathways, or different locations within these pathways. The majority of models established thus far are based on mutations that primarily influence antioxidant activity (*SOD1*), and RNA processing (*TARDBP* and *FUS*). Still required are models based on mutations that influence other primary pathways, particularly protein homeostasis, and other cellular processes such as excitotoxicity, defective axonal transport and mitochondrial dysfunction.

4.3 *C.elegans* models generated in this project

4.3.1 Nematode strain

One of the major advantages of *C.elegans* as models of neurodegenerative disease is that they maintain transparency throughout life, allowing *in vivo* imaging and analysis of neurons as they develop and degenerate. To capitalise on this advantage the *juIs76_vdIs4* transgenic line of *C.elegans* has been used by collaborators at the Queensland Brain Institute for expression of the constructs generated in this project. The *juIs76* transgene (Punc-25_GFP) expresses GFP in the GABAergic nerves and the *vdIs4* (Punc-25_mCherry_RAB3) transgene expresses mCherry at the pre-synaptic sites of these neurons. The use of this transgenic line therefore allows visualisation of the GABAergic motor neurons and their synapses without the need for fixing and staining, which which permits sequential analysis to be performed throughout the worms lifetime.

4.3.2 Features of the *C.elegans* expression vectors

Punc-25 vector

The Punc-25 vector was used in this project at the request of collaborators. The *unc-25* gene promoter is expressed exclusively in GABAergic neurons, therefore the *CCNF* models based on the Punc-25 constructs will demonstrate stable, neuronal expression of the transgene. *Unc* promoters (-25 and -47) have previously been used to generate *C.elegans* models of ALS (Li et al., 2013; Vaccaro et al., 2012), and these models demonstrate an ALS-like phenotype that includes neuronal degeneration and cytoplasmic protein aggregates.

mCherry fluorephore

The two sets of Punc-25 constructs generated in this project are differentiated by the presence or absence of a mCherry fluorescent reporter at the N terminus of the *CCNF* sequence. Fluorescent reporters are currently the gold standard method for examining protein expression and cellular localisation, however their potential to affect model phenotype must be recognised. Two recent studies have highlighted this; both demonstrating altered behavior of a target protein as a consequence of a fluorescent

tag (Landgraf et al., 2012; Huang et al., 2014).

Landgraf et al. (2012) examined the effect of fluorescent tags on protein degradation and localisation within bacteria. They demonstrated that all tags tested, including the commonly used GFP, distorted proteolysis to some extent. Furthermore, some tags resulted in significant mislocalisation of the tagged protein and increased the tendency of the proteins to aggregate. The second study (Huang et al., 2014) examined the effect of a mCherry fluorophore on lysosome behavior in cell culture. They found that direct fusion of a mCherry tag to the protein of interest (TPP1) affected lysosomal targeting. Linker sequences between the tag and the protein were required to eliminate this effect.

Altered protein homeostasis, protein aggregation and protein mislocalisation are all pathological features of ALS, thus the findings of these studies are directly relevant to models of the condition. Multiple *C.elegans* and mouse models of ALS have been established that express a fluorescent reporter (Wang et al., 2009; Li et al., 2013; Zhang et al., 2011; Li et al., 2014; Ayers et al., 2014), and all demonstrate some of the pathological features of ALS. The two sets of *C.elegans* constructs generated in this project will allow a comparison of cyclin F behaviour in the presence and absence of a fluorescent tag.

Analysis of these models is currently in progress at the Queensland Brain Institute.

4.3.3 Transgenic techniques in *C.elegans*

Collaborators at the Queensland Brain Institute will co-inject the Punc-25-*CCNF* plasmids with a fluorescent marker into the gonad of an adult worm to generate the *C.elegans* models. The *CCNF* transgene will form extra-chromosomal concatamers within the gonads, which will be stably inherited with reasonable efficiency (Berkowitz et al., 2008).

There is a second technique to generate transgenic *C.elegans* lines, known as biolistic transformation (Isik and Berezikov, 2013; Hochbaum et al., 2010). This technique uses DNA-coated gold particles to introduce exogenous DNA into the germline. When exposed to calcium chloride, the gold particles form a complex with the endogenous

DNA, integrating the transgene. This approach requires significantly less operator skill than microinjection, however has a much lower efficiency, therefore a larger number of worms must be treated.

4.3.4 Caveats of the *C.elegans* models

The evolutionary distance between *C.elegans* and humans is the most significant caveat of the models. This distance is reflected by a lack of conservation of some genes, including *CCNF* (<http://www.asia.ensembl.org>), and some physiological systems, such as an adaptive inflammatory system. The role of the inflammatory system in ALS is unclear, but neural inflammation with microglial activation is a pathological characteristic of the disease (Turner et al., 2004). Therefore, the effect of an innate as opposed to an adaptive inflammatory system on model phenotype is potentially significant.

The second significant caveat of the *C.elegans* model is a consequence of the GABAergic neuron expression produced by the *unc-25* promoter. Endogenous cyclin F (encoded by *CCNF*) is a ubiquitously expressed protein (Bai et al., 1994), and it is unclear how this expression pattern will reflect the pathology seen in patients.

A further potential caveat of the *C.elegans* models is the use of a N-terminal mCherry fluorescent reporter. The position of a fluorescent reporter fused to a gene of interest has the potential to affect protein behaviour as shown by Stadler et al. (2013). This study compared the cellular localisation of over 500 human proteins in the presence of a N-terminal reporter and a C-terminal reporter (cyan fluorescent protein, CFP or yellow fluorescent protein, YFP). 26% of proteins examined demonstrated dissimilar localisation patterns. Therefore, to minimise the possibility of localisation artifacts, this study ideally would have generated additional constructs expressing a C-terminal mCherry reporter.

Prior to the commencement of this project, attempts were made to generate C-terminal mCherry-*CCNF* constructs for expression in cell culture. Generation and sequencing of the constructs was challenging and transfected fibroblasts failed to demonstrate any mCherry expression. The N-terminal mCherry tag was successfully trialled as an alternative and consequently used for all future work.

4.3.5 Characterisation of the *C.elegans* models

Preliminary analysis of the *C.elegans* models is underway at the Queensland Brain Institute. These models will be examined over the coming months, to quantify spontaneous motility, characterise any paralysis that may develop with respect to time of onset and severity, analyse neuronal degeneration through measurement of motor neuron length and aberrant branching, examine the GABAergic neuronal synapses for indications of early degeneration, determine *CCNF* protein localisation and the presence or absence of protein aggregates within the neurons of the models.

The first hypothesis for this study is that comparison of these criteria will establish a difference in phenotype between the *CCNF* variants that correlates with the patient groups in which the variants have been found. The mutations considered high priority, as they are found in FALS and SALS cases, are theorised to result in a more severe, earlier onset motor neuron phenotype than the low priority SNPs found in patients and controls (Table 1.4, Introduction).

The second hypothesis is that comparison of the mCherry-*CCNF* transgenic worms and the *CCNF* transgenic worms will demonstrate differences in protein localisation and/or protein aggregation as a consequence of the fluorescent tag. This will be the first *in vivo* study to directly compare tagged and untagged models of neurodegenerative disease.

4.4 Zebrafish models generated in this project

4.4.1 Zebrafish strains

Like *C.elegans*, embryonic zebrafish are transparent, but pigment is deposited through the larval stage, leading to a loss of transparency by adulthood. There is a transgenic line of zebrafish that maintains its transparency throughout life that was considered for use in this project (Casper line)(White et al., 2008). However, the lack of pigment in the adult fish relies on mutations in two genes, *Nacre* and *Roy*, both of which must be present in the homozygous state. Establishing the *CCNF* models with stable

expression will require out-crossing of two generations, so maintaining a homozygous *Nacre* and *Roy* state would be experimentally challenging, costly and time-consuming. Additionally, *Roy* is still an uncharacterised zebrafish gene (<http://www.zfin.org>), therefore any effect of the mutation within the Casper line, other than a loss of pigment, remains unknown. The *HuC*-GFP line of zebrafish was instead selected for this project. This is a well-characterised line developed to express GFP in the motor neurons. This expression will allow sequential analysis of motor neuron development and structure *in vivo* throughout the embryonic stage of development.

4.4.2 Zebrafish models

mCherry-C1 Zebrafish models

The pmCherry-C1 zebrafish models demonstrating transient and mosaic mCherry-*CCNF* expression were developed with the aim of validating the constructs prior to progressing to Tol2 cloning. The highly variable mosaic expression that results from injection of plasmid DNA means no definitive conclusions can be drawn from analysis of these models. The models that will be generated from the Tol2 constructs in an ongoing project will demonstrate either transient or stable ubiquitous expression of the transgene and will undergo thorough analysis as discussed below.

Tol2 zebrafish models

Expression of the Tol2 constructs shown in Table 4.1 will allow a detailed analysis of the phenotype that results from overexpression of human, compared to zebrafish *CCNF*. As shown in this project, zebrafish and human *CCNF* share only 61.4% homology. It is therefore reasonable to hypothesise that overexpression of z*CCNF* will produce a different phenotype than overexpression of h*CCNF*. Differences in species physiology, and the different temperatures at which the respective proteins naturally function (28°C vs 37°C), further strengthen this hypothesis.

TABLE 4.1: Tol2 expression constructs

Constructs for ubiquitous expression	Constructs for motor neuron expression
CMV-SP6_h <i>CCNF</i> _wt	HB9_KalTax4_h <i>CCNF</i> _wt
CMV-SP6_h <i>CCNF</i> _S621G	HB9_KalTax4_h <i>CCNF</i> _S621G
CMV-SP6_z <i>CCNF</i> _wt	HB9_KalTax4_z <i>CCNF</i> _wt
CMV-SP6_z <i>CCNF</i> _S623G	HB9_KalTax4_z <i>CCNF</i> _S623G
β -actin_h <i>CCNF</i> _wt	HB9_Gal4-UAS_h <i>CCNF</i> _wt
β -actin_h <i>CCNF</i> _S621G	HB9_Gal4-UAS_h <i>CCNF</i> _S621G
β -actin_z <i>CCNF</i> _wt	HB9_Gal4-UAS_z <i>CCNF</i> _wt
β -actin_z <i>CCNF</i> _S623G	HB9_Gal4-UAS_z <i>CCNF</i> _S621G

To date, there is only one published study describing an ALS zebrafish model that overexpresses a zebrafish transgene (*SOD1*) and six zebrafish models that overexpress a human transgene (*SOD1*, *TARDBP*, *FUS*, *C9orf72* and *VAPB*) (Table 4.2). The model based on the zebrafish *SOD1* transgene (z*SOD1*) cannot be directly compared to the models based on the human *SOD1* orthologue, as the z*SOD1* construct also carried an 11.7 kb region upstream and a 4.5 kb sequence downstream from the *SOD1* gene, the effects of which cannot be quantified. Studies using the Tol2 constructs in Table 4.1 therefore will be the first to examine whether models based on a mutation within the human gene, or models based on a mutation within the zebrafish gene demonstrate a similar phenotype.

TABLE 4.2: Established zebrafish models of ALS.

Transgene	Species	Expression	Promoter	Reference
<i>TARDBP</i>	Human	Transient	pCS2+	Kabashi et al. (2010)
<i>SOD1</i>	Zebrafish	Stable	Endogenous	Ramesh et al. (2010)
<i>TARDBP</i> & <i>FUS</i>	Human	Transient	pCS2+	Kabashi et al. (2011a)
<i>SOD1</i>	Human	Transient and stable	pCS2+ and CMV	Sakowski et al. (2012)
<i>C9orf72</i>	repeat sequence	Transient	pCS2+	Lee et al. (2013)
<i>VABP</i>	Human	Transient	PCS2+	Kabashi et al. (2013)
<i>SOD1</i>	Mutation introduced into endogenous gene with ENU*	Stable	endogenous	Da Costa et al. (2014)

*ENU = N-ethyl-N-nitrosourea, chemical mutagen.

Additionally, the Tol2 models will be the first to allow a direct comparison of the effect of different expression patterns on model phenotype. All established zebrafish models have been generated either through injection of mRNA (transient, mosaic expression), or with promoters that drive stable ubiquitous expression (Table 4.2). The Tol2 constructs will generate models with ubiquitous and motor neuron expression of

the *CCNF* transgene at two different levels of overexpression.

4.4.3 Features of the Tol2 constructs

Ubiquitous Promoters Two ubiquitous promoters will be used in the Tol2 constructs, CMV-SP6 and β -actin. The CMV-SP6 promoter has the advantage of allowing *in vitro* generation of mRNA to develop transient models for immediate analysis, in addition to driving ubiquitous transgene expression in stable lines. Significant variation in activity levels has been demonstrated between different promoters (Papadakis et al., 2004), and no study has yet determined the optimal ubiquitous promoter for generating phenotypically accurate zebrafish models of ALS. The Tol2 constructs generated through this project will be the first to allow a direct comparison of the phenotype produced by different ubiquitous promoters in a zebrafish model.

HB9 motor neuron-specific promoter The two sets of HB9 constructs will allow a direct comparison of the phenotype generated by different expression levels of the h*CCNF* and z*CCNF* transgenes in motor neurons. The KalTaX4 system amplifies the expression of the weak HB9 promoter 4-fold, while the GAL4-UAS system will amplify this expression 12-fold. The optimal expression level of a transgene is unknown. Sufficient levels are required to produce a phenotype, however excessive expression levels are not physiologically relevant. Generating two models at different ends of the spectrum remains the only method available to determine optimum expression levels.

Tol2 backbone vectors The final component of the Tol2 constructs is the Tol2 backbone vector. Two different vectors will be used, pDEST:Tol2-CG2 and pDEST:Tol2-PA2, both of which carry a multisite Gateway cloning cassette (att sites), a polyA signal and flanking Tol2 ends (Figure 4.6). The pDEST:TOL2-CG2 vector has an additional cmlc2:EGFP-pA cassette that drives GFP expression in the developing zebrafish heart. The GFP cardiac reporter is a brighter fluorophore than mCherry, and therefore will aid early screening of the founder fish which will demonstrate mosaic transgenic expression.

The limitation of the GFP cardiac reporter is that there is potential for the regulatory

sequences of the fluorescent marker to drive expression of the *CCNF* transgene, and vice versa (Mosimann et al., 2011). This could result in cardiac expression of *CCNF* in the motor neuron lines, or GFP expression in organs other than the heart, potentially interfering with analysis of protein expression. The GFP reporter therefore, was restricted to use with the CMV constructs as these are expected to demonstrate the weakest expression of all the promoters, minimising the risk of cross-talk, and aiding what would otherwise be difficult embryo selection, based on weak, mosaic mCherry expression.

4.4.4 Troubleshooting

A number of issues arose during the generation of the zebrafish constructs which required extensive troubleshooting. Problems encountered included errors in primer design, plasmid contamination, inappropriate DNA polymerase for specific purposes and multiple problems ligating, propagating and therefore subcloning. The primary issues are discussed below.

Failure to generate z*CCNF* cDNA

The integrity of the zebrafish cDNA library generated through reverse transcription of fresh RNA was demonstrated by the amplification of β -actin cDNA using pre-designed and validated primers (Table 2.12) as shown in Figure 3.14. Upon review of the z*CCNF* primers originally designed for this project, it was discovered that the sense target sequence was used to design the reverse primer rather than the antisense sequence. Therefore the primer set was unable to amplify the z*CCNF* cDNA product. A primer with the correct sequence was designed and used to successfully amplify z*CCNF* in subsequent reactions.

Subcloning z*CCNF* into pmCherry-C1

Direct subcloning of z*CCNF* from the pCMV_SPORT-6.1 vector into the pmCherry-C1 vector using EcoRI and XhoI restriction sites repeatedly failed despite troubleshooting. It was discovered that the use of an intermediate vector, pGEM-T, was required. Further, an extended recovery time during transformations was required for successful growth of colonies carrying the pmCherry-C1.z*CCNF* construct. The troubleshooting

process described in detail below suggests that there were multiple issues interfering with subcloning of the *zCCNF* amplicon. The presence of an unmapped restriction site(s) in the pCMV_SPORT6.1_*zCCNF* vector was hypothesised to be one of these issues, and the second was a poor efficiency of transformation. This inefficiency may have been due to contamination of the pmCherry-C1 vector, or the result of an unexplained incompatibility between *zCCNF* and the competent cells used for transformation.

The *zCCNF* cDNA sequence in the pCMV-SPORT-6.1_*zCCNF* vector was validated through sequencing, however the complete vector sequence was not validated in this way due to unnecessary costs. The vector may carry an unmapped restriction site(s) since it was obtained from a repository, rather than a company, which could have interfered with direct subcloning of *zCCNF*. This hypothesis was reached through a process of elimination of other factors. Successful PCR amplification of *zCCNF* flanked by *EcoI* and *XhoI* restriction sites from the pCMV-SPORT6.1 vector was confirmed by Sanger sequencing. Validation of successful digestion of the pmCherry-C1 vector was confirmed by gel electrophoresis and imaging (Figure 4.2). To determine if the failure of subcloning was due to poor ligation efficiency, a number of changes to the protocol were tested. First, all reagents used in the ligation reaction were replaced with fresh aliquots, second, the vector:insert ratio was varied from 1:5 to 5:1, and finally, the incubation time of the ligation reaction was extended to 16 hours. However, transformation of these ligated products repeatedly failed to produce any colonies.

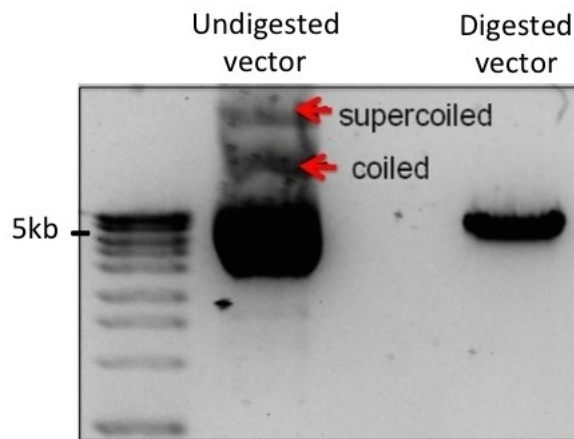


FIGURE 4.2: Digestion of pmCherry-C1. Gel electrophoresis of pmCherry-C1 vector pre- and post-digestion with EcoRI and XhoI restriction enzymes. The absence of coiled and supercoiled products in the digested vector indicate successful linearisation of the plasmid.

To validate the XhoI and EcoRI restriction sites flanking *zCCNF*, the PCR product was subcloned into the pGEM-T vector through TA cloning and subsequently digested from this vector with XhoI and EcoRI digestion enzymes. The pGEM-T vector was chosen as an intermediate vector as it does not contain either of these restriction sites, therefore, successful digestion of pGEM-T *zCCNF* with EcoRI and XhoI (Figure 4.3) confirmed the presence and functionality of the EcoRI and XhoI sites.

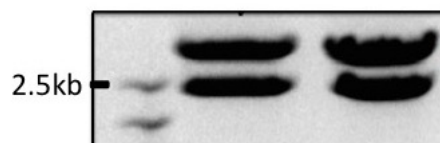


FIGURE 4.3: Digestion of pGEM-T *zCCNF* vector. Gel electrophoresis image of digested pGEM-T *zCCNF* vector with Hyperladder 100bp plus, illustrating separation of the *zCCNF* product (2.3kb) and the pGEM-T vector (3kb).

The digested *zCCNF* product was gel purified and ligated with the digested pmCherry-C1 vector. The efficiency of the ligation and transformation was very low and only two colonies were generated, both of which were propagated, purified and Sanger sequenced. Sequencing analysis confirmed the presence of the *zCCNF* amplicon within the pmCherry-C1 vector, however the original PCR reaction from pCMV-SPORT-6.1 *zCCNF*

had introduced multiple (non-synonymous) variants into the products. PCR of *zCCNF* from pCMV-SPORT6.1 was repeated, using a proof reading DNA polymerase and the process of subcloning into pGEM-T, and then digesting from the vector repeated.

To investigate the low efficiency of the ligation reaction between pmCherry-C1 and the *zCCNF* insert, the (undigested) vector was electrophoresed for an extended time to determine if any degradation or contamination had occurred. This demonstrated the presence of three non-specific products in the pmCherry-C1 vector (Figure 4.4), indicating that the aliquot used for these experiments was contaminated. Therefore a new pmCherry-C1 preparation was propagated and purified from a validated glycerol stock using fresh reagents following decontamination of benches and pipettes. However, gel electrophoresis of the newly prepared pmCherry-C1 demonstrated the presence of the same three bands and efficiency of the ligation reaction remained poor. This problem was circumvented by extending the incubation time during transformation. Whether this poor efficiency was due to contamination of the original pmCherry-C1 vector, or due to an incompatibility of *zCCNF* and the competent cells remains undetermined.

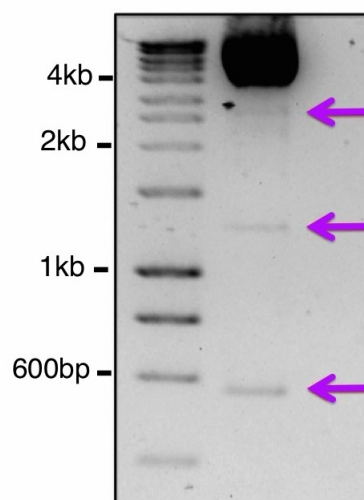


FIGURE 4.4: Contamination of pmCherry-C1 vector. Gel electrophoresis image of pmCherry-C1 vector with size marker Hyperladder 1kb Plus demonstrating the vector at the expected size (4.7kb) and three non specific products (red arrows), suggesting contamination of the vector.

Failure of LR reactions to generate correct Tol2 expression vectors

Tol2 att recombination reactions are site-specific, which should prevent incorrect positioning of entry clones within the final expression vector. However, sequencing of the constructs generated by LR reactions in this project demonstrated incorrect orientation and incorrect placement of the entry clones within the destination vector.

Retrospective analysis of the sequencing results of the preceding BP reactions yielded an explanation. The sequencing results were initially analysed to confirm no errors had been introduced to the mCherry-*CCNF* sequences within the entry clone, however the att-site sequences were not validated. Careful sequence examination revealed that the incorrect att site (att3 instead of att1) was present at the 5' end of the mCherry-*CCNF* sequence, a consequence of the incorrect primer being used in the initial PCR amplification. Six of the amino acids present in the att1 and att3 sites are complementary (Figure 4.5), which appears to be sufficient to allow the BP recombination to occur, although at a low efficiency. The lack of an att1 site and the presence of two att3 sites in the LR reaction resulted in the incorrect orientation and placement of the entry clones within the expression vector.

att1	----TTTGTACAAAAAAG	14
att3	CAACTTTATTATACA---	15

FIGURE 4.5: att site sequences. Complementary nucleotides between att1 and att3 recombination sites highlighted in yellow.

Time constraints prevented repeat PCR of pmCherry-*CCNF* from the pmCherry-C1 vectors and subsequent BP and LR reactions, however this will be performed as part on an ongoing project.

4.4.5 Future completion of the Tol2 constructs

Due to time constraints in this project, future work will be required to complete the Tol2 constructs (Figure 4.6) as described in the Methods section.

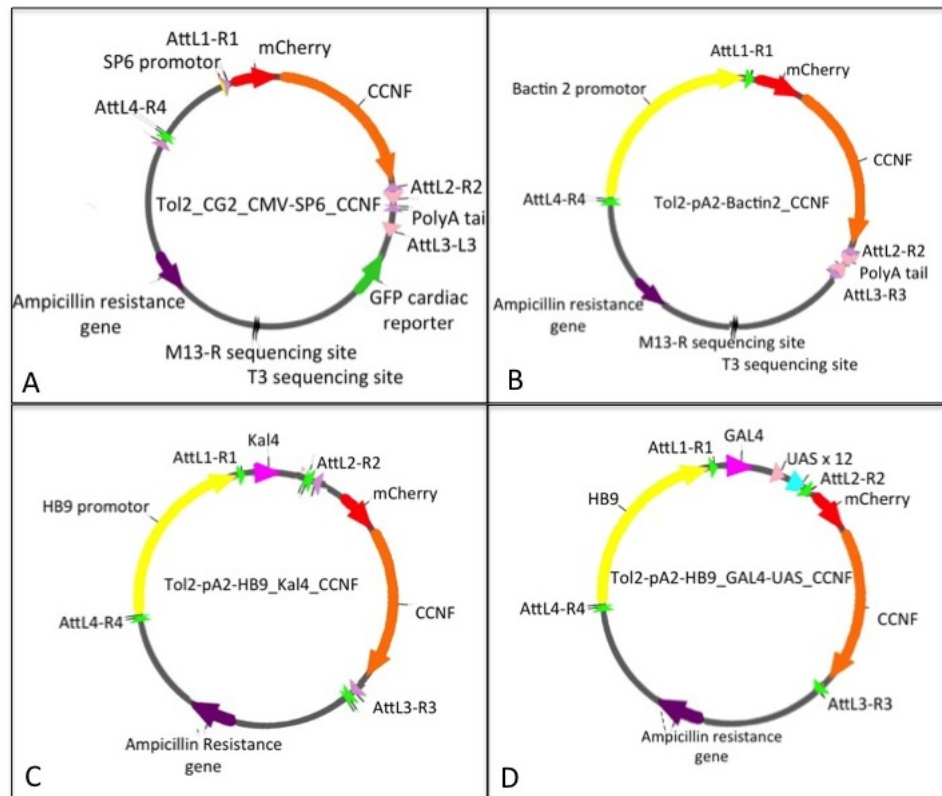


FIGURE 4.6: Construct maps of the final Tol2 expression vectors that will be developed from the pmCherry-C1 constructs. (A.) CMV-SP6 construct from which mRNA will be generated to develop transient models for immediate analysis and from which stable lines demonstrating ubiquitous expression will be generated. (B.) β -actin construct from which stable lines demonstrating ubiquitous expression will be generated. (C.) HB9-KalTax4 construct from which stable lines expressing *CCNF* in motor neurons at 4x amplification will be generated. (D.) HB9-Gal4-UAS construct from which stable lines expressing *CCNF* in motor neurons at 12 x amplification will be generated.

4.4.6 Transgenic techniques in the zebrafish

Traditional techniques

The majority of zebrafish models that demonstrate stable expression of a transgene have been generated using the techniques utilised in this project. The microinjection of plasmid DNA (eg. the pmCherry-C1 constructs) results in relatively slow integration into the host genome, and therefore, high levels of mosaicism and low germline transmission rates (Stuart et al., 1988). The use of vectors, such as Tol2, results in earlier integration of the transgene and consequently higher germline transmission rates. The Tol2 transposon system is one of the most commonly used vectors, along with retroviral

vectors and vectors that carry meganuclease restriction sites (Table 4.3).

8

TABLE 4.3: Comparison of transgenic techniques in the Zebrafish.

Technique	1st zebrafish study	Germline transmission rates	Primary limitation
Plasmid DNA	Stuart et al. (1988)	approx 5%	High levels of mosaicism limit analysis of F0 generation, random integration
Retroviral vectors	Lin et al. (1994)	70–100%	Challenging to manipulate, stringent safety requirements and random integration.
Meganucleases	Thermes et al. (2002)	20–30%	Random integration, unknown how efficiency is increased.
Transposon vectors	Kawakami et al. (2000)	30–50%	Random integration

The Tol2 transposon system used in this project is the most popular of these techniques. Transposon constructs demonstrate germline transmission rates up to 50% (Suster et al., 2009) with low concatemeric formation and early integration into the host genome, reducing mosaicism (Kwan et al., 2007). Like all of the traditional transgenic techniques however, Tol2 randomly integrates the transgene into the host genome, which can result in significant positional effects and consequently, variable gene expression.

One zebrafish study has overcome this limitation by co-injecting the Tol2 construct with a site-specific integrase enzyme (PhiC31) (Mosimann et al., 2013) . This technique is the transgenic method of choice in *Drosophila*, in which a large number of PhiC31 integrase recombination sites have been inserted into the genome and their position mapped (Groth et al., 2004; Bischof et al., 2007). However, this is not yet the case with zebrafish. The recent study had to first establish a transgenic line of zebrafish that carry a PhiC31 site at the desired genomic location before microinjection of the Tol2 construct. This approach was beyond the scope of the current project.

Genome editing techniques

The rapidly emerging genome editing techniques look set to supersede traditional transgenic techniques, including Tol2, in the near future. This new approach makes use of sequence-specific DNA binding domains in the form of zinc finger nucleases (ZFNs), transcription activator-like effector nucleases (TALENs) or clustered regularly

interspaced short palindromic repeats (CRISPRs). The site-specific binding domain is fused to a non-specific nuclease, which generates a double strand break in the host genome at the target site, allowing for the removal of a target gene, or the insertion of a co-injected transgene. This results in site-specific gene knock out, or gene insertion, eliminating positional effects and multi-site transgenic integration. Theoretically, this should produce models with more physiologically accurate gene expression ([Gaj et al., 2014](#)). Further, the technique confers the ability to alter multiple genes simultaneously ([Wang et al., 2013](#)), rather than having to first establish, then interbreed two stable lines. This will enable the development of more complex, potentially more accurate models of multifactorial diseases in the future.

While these techniques have enormous potential to produce improved animal models of disease, they are still in the early stages of development, which is why they were not considered for this project. A number of zebrafish knock-out models targeting a range of genes (unrelated to ALS) have been established using ZFNs, TALENs and CRISPRs ([Meng et al., 2008](#); [Huang et al., 2011](#); [Foley et al., 2009](#); [Doyon et al., 2008](#); [Dahlem et al., 2012](#)), however, to date only relatively short transgenes have been successfully integrated into the zebrafish genome. This limited size restricts the capacity for fusion of a fluorescent tag or regulatory sequences to the transgene.

A recent study demonstrated the first insertion of a GFP-tagged transgene into the zebrafish genome using TALENS ([Zu et al., 2013](#)). However, the efficiency of germline transmission was extremely low (1.5%) and the GFP tag either failed to express, or was expressed in non-targeted tissue. The ability to efficiently and reliably insert large DNA fragments without random integration must be established before the technique can be widely adopted for gain-of-function models of disease. Currently, novel models generated through genome editing still require validation through established techniques, thus even if superseded in the future, the models generated in this study will still have value.

4.4.7 Establishing stable zebrafish transgenic lines

To establish the 16 stable zebrafish lines, approximately 300 embryos will be injected with each Tol2 construct. These embryos (F0 generation), will be screened for mCherry or GFP expression at 24hpf. Those F0 fish that incorporate the pmCherry-tagged

transgene into their genome with the lowest levels of mosaicism will be selected and raised to maturity (founder fish).

The founder fish will demonstrate mosaic expression of *CCNF*, and only approximately 30% will incorporate the transgene into their germline. To determine which individuals comprise that 30%, the founder fish will be out-crossed to wild-type *HuC*-GFP-line fish to establish the F1 generation. F1 fish that demonstrate mCherry_*CCNF* expression will do so ubiquitously/within the motor neurons. However, each fish will be distinct, differentiated by the number of transgenic insertions at a single location and the frequency of insertion throughout the genome.

To develop stable lines that produce offspring with predictable transgenic expression, a generation must be established that carries the transgene at a single location. This will be achieved by outcrossing the F1 generation to wild-type *HuC*-GFP fish. Transgenes are inherited in Mendelian fashion in the F2 generation, therefore, if 50% of the F2 embryos express mCherry_*CCNF*, it will be assumed the F1 parent carries the transgene at a single genomic location, and the stable line is established. Higher percentages of mCherry_*CCNF* positive offspring will suggest the presence of multiple insertions in the F1 generation and further outcrossing will be necessary (Figure 4.7).

Each stable line will demonstrate a distinct expression pattern due to positional effects and variations in the copy number of transgenes present at the insertion location. Therefore, once established, individual transgenic lines will be assessed to determine those which demonstrate the optimal expression pattern.

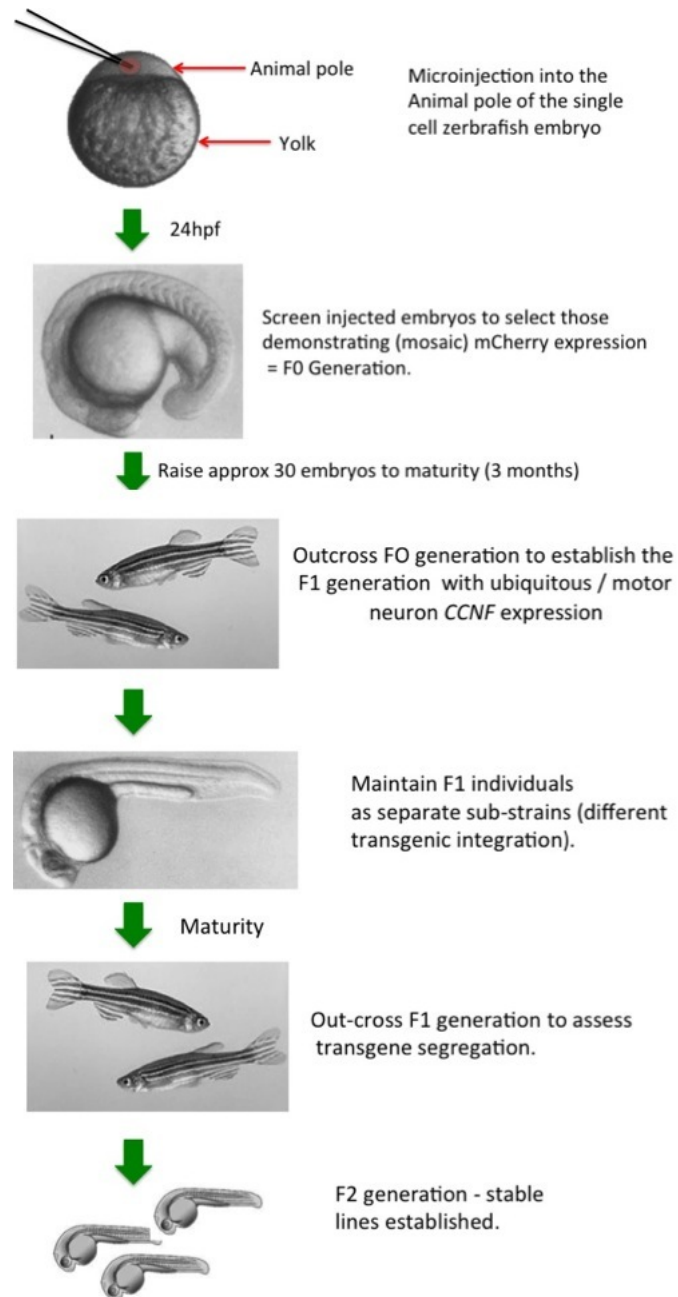


FIGURE 4.7: Establishing stable lines of zebrafish. Schematic demonstrating the multiple generations required to establish stable lines of zebrafish that carry the *CCNF* transgene at a single genomic location.

4.4.8 Caveats of the zebrafish models

Zebrafish are evolutionarily closer to humans than the invertebrate *C.elegans*. This is reflected in the high conservation of physiological systems and the main architecture, cell types, and neurotransmitters of the nervous system between the species. The physiological processes of zebrafish do however, function at a significantly lower temperature than humans, and the influence of this on pathological changes associated with ALS-linked mutations is undetermined.

A second caveat of the models is that like the *C.elegans* models, all constructs generated carry the mCherry fluorescent reporter at the N-terminal of the protein. Ideally a second set of constructs would be generated carrying a C-terminal reporter to ensure no localisation artefacts are produced.

The primary limitations of the zebrafish models however, are a consequence of the transgenic technique used. Traditional techniques, like Tol2, result in random transgenic integration at multiple locations in the host genome. These factors have significant potential to influence the phenotype of the resulting models. Furthermore, the zebrafish models are designed to overexpress *CCNF*, rather than express the transgene at physiologically accurate levels.

4.4.9 Characterisation of the zebrafish models

Analysis of the transient models generated by injection of mRNA (synthesised from the CMV-SP6 constructs) will include quantification of motor neuron axonal length, assessment of any aberrant axonal branching and examination of mobility through a touch evoked swimming response trial. Furthermore, the mCherry fluorescent tag will allow analysis of cyclin F localisation and aggregation in these models.

Once established, the stable transgenic lines will be characterised using the same criteria, however more in depth characterisation will also be possible with the longer time frame available. This will include immunofluorescence analysis to identify protein aggregates. These studies will aim to establish whether any protein aggregates that form are ubiquitinated, and whether they are positive for endogenous TDP-43. Mutations in other ALS-linked genes, including *VCP* and *UBQLN2*, both of which function in the UPS, have been shown to result in co-aggregation of the mutant protein with wild-type

TDP-43. Analysis of these models will determine whether mutant cyclin F acts in the same way.

Analysis of the neuromuscular junctions (NMJ) at various time-points in the zebrafish development may also be performed. NMJ defects are the earliest pathological changes seen in ALS patients and some current zebrafish models reflect this (Hartley et al., 2000; Ramesh et al., 2010). The integrity of the NMJ will be examined using the SV2 antibody as a marker for the pre-synaptic terminal and α -bungarotoxin as a marker of the post-synaptic terminal. Determining whether NMJ defects are seen pre-symptomatically in the transgenic lines will contribute to establishing the phenotypic accuracy of the models.

Furthermore, neural inflammation with microglial activation has been demonstrated in ALS patients. The ability of the zebrafish models to reflect this pathology may be examined through the use of immunohistochemistry (IHC) studies targeting inflammatory markers.

Finally, characterisation of each of the transgenic lines will include a determination of the transgene copy number present through quantitative PCR (qPCR), and assessment of cyclin F expression levels through western blotting. This analysis will allow a determination of which transgenic line demonstrates the most physiologically accurate gene expression.

This in-depth characterisation will determine the optimum transgenic lines for use in functional studies and establish which technique(s) used to generate the stable lines produces a phenotype that best reflects that seen in ALS patients. This knowledge may be used to inform the design of future zebrafish models of ALS based on other gene mutations. The knowledge may also be extended to ALS model development in other species for which it is too costly or time consuming to examine multiple strategies.

4.5 Future applications of the *CCNF* models

The models generated by this project will provide a novel opportunity to investigate the cellular consequences of ALS-linked mutations within a gene known to function in protein homeostasis. The models will be highly suited to primary studies investigating

the early changes that occur in the neuromuscular system and they will be ideal for functional studies into the pathophysiology of ALS, with the aim of identifying potential therapeutics and biomarkers as early indicators of disease. Furthermore, the advantages of the two model species used in this project make them ideal for therapeutic testing, both on a small scale with pharmaceuticals directed at a specific target, and on a large scale in high throughput chemical screens. The advantage of generating models based on the same mutation in two species is that comparison of the results of functional and therapeutic studies is possible, which will provide an indication of the consistency of the findings across species.

4.5.1 Determination of effect of mutant *CCNF* on protein behaviour

The models generated by this project will be the first animal models based on ALS-linked mutations within *CCNF*. Therefore, initial functional studies are likely to focus on characterising the mutant protein, specifically its cellular localisation and its effects on the UPS.

Mutant proteins encoded by some ALS-associated genes (TDP-43 and FUS) have been shown to mislocalise to the cytoplasm. This mislocalisation appears to lead directly to motor neuron degeneration, most likely through a loss of function mechanism ([Igaz et al., 2011](#); [Lanson et al., 2011](#); [Xia et al., 2012](#)). Cyclin F functions in the UPS, which degrades both cytoplasmic and nuclear proteins and consequently, wild-type cyclin F is found in both cellular compartments. If the mutant protein is found to localise solely to either the nucleus or the cytoplasm, this could result in a loss of function in one compartment and subsequent cell death.

Mislocalisation of a mutant protein is not however, essential for cell death to occur in ALS, as illustrated by models based on mutations within *UBQLN2*. Like *CCNF*, *UBQLN2* is an ALS-associated gene which functions within the UPS. The mutant protein, ubiquilin2, has not been shown to mislocalise in these models ([Deng et al., 2011](#)). Therefore, whether *CCNF* will induce cellular toxicity through mislocalisation is unclear. Both the *C.elegans* and the zebrafish models will be highly suited to establishing this.

In addition, these models will be used to establish the functional consequences of mutant cyclin F on UPS activity. The G93A *SOD1* mouse models has demonstrated reduced activity levels of the proteasome in muscle and spinal cord ([Kabashi et al., 2004](#); [Cheroni et al., 2009](#)), and ubiquitin-mediated proteasomal degradation has been showed to be impaired in a cellular model based on mutant *UBQLN2* ([Deng et al., 2011](#)). It is theorised that mutant *CCNF* will have a similar effect on UPS function. The activity levels of the proteasome in muscle and the spinal cord of models can be assayed with kits such as the Proteasome-Glo assay kit (Promega) which will be suited for use in the models generated by this study.

4.5.2 Functional studies in *C. elegans* models

In addition to these studies aimed at characterising the direct impact of mutant cyclin F, the *C.elegans* models will be highly suited to a range of further studies investigating the cellular processes involved in disease pathogenesis. For example, the transparency of the *C.elegans* models make them ideal for studies examining stress granule formation *in vivo* in real time. Stress granules are commonly found in ALS patient tissue and most of the components of these granules are conserved between species ([Therrien and Parker, 2014](#)). One *C.elegans* model has demonstrated their suitability for such studies using heat as a stressor to induce granule formation ([Sun et al., 2011](#)). To date however, only cell culture studies have examined the effect of other stressors, such as oxidative stress, on granule formation ([Vance et al., 2013](#)). Oxidative stress plays a significant role in aging and is also believed to be involved in ALS pathogenesis, therefore, such studies are definitely warranted.

The transparency of the *C.elegans* models also make them ideal for propagation studies, to examine any prion-like activity of the mutant cyclin F. Mutant SOD1 ([Munch et al., 2011](#)), TDP-34 ([Nonaka et al., 2013](#)) and FUS ([Robberecht and Philips, 2013](#)) have been shown to demonstrate prion-like activity, which is hypothesised to contribute to the pattern of progressive motor neuron death seen in ALS patients. The *C.elegans* models provide the first opportunity to determine whether mutant cyclin F demonstrates the same properties.

Furthermore, the simplicity of the *C.elegans* nervous system lends the models to the study of interactions between different cells of the nervous system. Recent evidence suggests that glial cells play a significant role in motor neuron degeneration ([Lasiene](#)

and Yamanaka, 2011). Examining how glial cells and motor neurons interact is challenging in higher order mammals, but can be relatively simple in *C.elegans*, given their nervous system is comprised of only have 302 neurons and 56 glial cells (Oikonomou and Shaham, 2011).

4.5.3 Functional studies in zebrafish models

The *C.elegans* and zebrafish models will be equally suited to many of the same functional studies, however, the zebrafish models are likely to better reflect some aspects of disease pathology. For example, they will be the superior model for functional studies into the role of the inflammatory system in disease pathogenesis. Unlike *C.elegans*, the zebrafish immune system is remarkably similar to the human system, demonstrating both innate and adaptive immunity. Consequently, zebrafish have been used as models to investigate the acute inflammatory response, the interaction of the inflammatory system with various pathogens and the inflammatory response to injury (for review, see Meeker and Trede (2008)). Therefore, the models generated through this study will be ideal to investigate the role of neural inflammation with microglial activation in ALS pathology.

Furthermore, given their larger size in comparison to the *C.elegans* models, and their greater similarities to humans physiologically, the transgenic zebrafish may be the preferred model for other functional studies. Such studies include investigations of the role of mitochondrial dysfunction, excitotoxicity, axonal transport and the endoplasmic reticulum unfolded protein response in disease pathogenesis (Turner et al., 2013; Ling et al., 2013).

Finally, the transgenic zebrafish lines carrying h*CCNF* will be suitable for direct comparison with established zebrafish lines in our laboratory (*TARDBP* and *FUS*), all of which are based on the human gene.

4.5.4 Therapeutic trials

The models generated through this project will be ideal for therapeutic testing both on a small and a large scale. Both models share the advantage of simplicity of drug delivery because therapeutics can be added to the liquid culture of *C.elegans*, or the

tank water of the zebrafish. Additionally, their high fertility and fecundity coupled with rapid development allows for statistically significant numbers to be included in therapeutic trials (Gosai et al., 2010; Lieschke and Currie, 2007). While both model species share these advantages, the zebrafish models may be superior to the *C.elegans* models due to the fact that like humans, they have a blood-brain barrier, which regulates access of therapeutic agents to the CNS (Jeong et al., 2008).

The advantages of the *C.elegans* and zebrafish models will be most evident in high throughput therapeutic screening of compound libraries. Such screening has become increasingly utilised over the past decade and has successfully identified a number of effective pharmaceuticals that are now FDA approved for a range of conditions (reviewed in Macarron et al. (2011)). A recent study used a TDP-43 *C.elegans* model of ALS to screen over 4000 FDA approved compounds. The study identified a number of pharmaceuticals that reduced TDP-43 toxicity in the models by altering the endoplasmic stress response (Therrien and Parker, 2014). Testing of these drugs is yet to progress to clinical trials, however, the study does highlight the promise of the high throughput approach in drug discovery. A significant advantage of screening drugs already FDA approved is the increased speed of progression through clinical trials and, if found to be beneficial, rapid availability to patients.

The ability of animal models to predict the therapeutic effect of drugs in ALS patients has been questioned due to repeated failures of translation. Only one drug that demonstrated positive results in animal model testing, riluzole, has shown any benefit in human patients and remains the only approved therapeutic for ALS. The benefit of the drug however is very modest - it has been found to extend the lifespan of sufferers by an average of only two months (Miller et al., 2003). All other drugs that have shown promise in animal models and progressed to clinical trials have failed to demonstrate even this minimal effect.

Animal models that fail to adequately reflect the disease phenotype may be partially responsible for this failure of translation, but poor study design has also been shown to be a major contributor. A review of animal therapeutic trials demonstrated numerous cases of inadequate sample size, failure of appropriate randomisation, selection of inappropriate criteria and inappropriate statistical analysis. The review retested several compounds that showed positive results in major animal studies using the G93A *SOD1* mouse (minocycline, creatine, celecoxib, sodium phenylbutyrate, ceftriaxone,

WHIP131, thalidomide, and riluzole). Repeating these studies using an optimal study design demonstrated no survival benefit for any of these compounds, including riluzole (Scott et al., 2008).

Therefore, it is not only improved animal models of ALS that are required, but improved studies with more robust design. The advantages of *C.elegans* and zebrafish as models allow high numbers of animals to be included in therapeutic trials. This lends greater statistical power to such studies, thereby enhancing study design and consequently producing more reliable results.

4.6 Summary

Mutation analysis in this project identified two variants in *VCP* coding exons in a patient with characteristic *VCP* pathology. Ongoing projects will clarify the role of the *VCP* variants in sporadic ALS.

This project developed 44 expression constructs based on mutations in *CCNF* for expression in *C.elegans*. In addition, four transgenic zebrafish models were generated to validate the mCherry-*CCNF* fusion construct and the process was commenced to generate 16 stable lines of zebrafish. Future work aims to complete the 16 transgenic zebrafish models (Table 4.1) and analyse the phenotype produced by over-expression of mutant *CCNF*. This analysis will indicate which of the numerous strategies used generates the most phenotypically accurate model of ALS, information that may be used to inform the design of future models in fish and other species.

While the models generated through this study may not reflect all of the pathological characteristics of ALS, they are novel models based on a mutation in a gene that affects one of the major pathogenic pathways implicated in ALS pathogenesis. As such they have great potential to increase our knowledge regarding ALS pathology through a variety of biomolecular studies. Such knowledge is crucial to identify accurate disease biomarkers and effective therapeutics for what currently remains an invariably fatal condition.

References

- Aoki, M., Kato, S., Nagai, M., and Itoyama, Y. (2005), Development of a rat model of amyotrophic lateral sclerosis expressing a human SOD1 transgene, *Neuropathology*, 25, 4, 365–370 [3](#)
- Arai, T., Hasegawa, M., Akiyama, H., Ikeda, K., Nonaka, T., Mori, H., et al. (2006), TDP-43 is a component of ubiquitin-positive tau-negative inclusions in frontotemporal lobar degeneration and amyotrophic lateral sclerosis, *Biochem. Biophys. Res. Commun.*, 351, 3, 602–611 [73](#)
- Arnold, E. S., Ling, S. C., Huelga, S. C., Lagier-Tourenne, C., Polymenidou, M., Ditsworth, D., et al. (2013), ALS-linked TDP-43 mutations produce aberrant RNA splicing and adult-onset motor neuron disease without aggregation or loss of nuclear TDP-43, *Proc. Natl. Acad. Sci. U.S.A.*, 110, 8, E736–745 [73](#)
- Ash, P. E., Zhang, Y. J., Roberts, C. M., Saldi, T., Hutter, H., Buratti, E., et al. (2010), Neurotoxic effects of TDP-43 overexpression in *C. elegans*, *Hum. Mol. Genet.*, 19, 16, 3206–3218 [3](#), [73](#)
- Ayers, J. I., Fromholt, S., Koch, M., DeBosier, A., McMahon, B., Xu, G., et al. (2014), Experimental transmissibility of mutant SOD1 motor neuron disease, *Acta Neuropathol.*, 128, 6, 791–803 [76](#)
- Badadani, M., Nalbandian, A., Watts, G. D., Vesa, J., Kitazawa, M., Su, H., et al. (2010), VCP associated inclusion body myopathy and paget disease of bone knock-in mouse model exhibits tissue pathology typical of human disease, *PLoS ONE*, 5, 10 [3](#), [11](#)
- Bai, C., Richman, R., and Elledge, S. J. (1994), Human cyclin F, *EMBO J.*, 13, 24, 6087–6098 [77](#)

- Bargmann, C. I. (1998), Neurobiology of the *Caenorhabditis elegans* genome, *Science*, 282, 5396, 2028–2033 [6](#)
- Barmada, S. J., Skibinski, G., Korb, E., Rao, E. J., Wu, J. Y., and Finkbeiner, S. (2010), Cytoplasmic mislocalization of TDP-43 is toxic to neurons and enhanced by a mutation associated with familial amyotrophic lateral sclerosis, *J. Neurosci.*, 30, 2, 639–649 [1](#)
- Benatar, M. (2007), Lost in translation: treatment trials in the SOD1 mouse and in human ALS, *Neurobiol. Dis.*, 26, 1, 1–13 [4](#)
- Bendotti, C., Marino, M., Cheroni, C., Fontana, E., Crippa, V., Poletti, A., et al. (2012), Dysfunction of constitutive and inducible ubiquitin-proteasome system in amyotrophic lateral sclerosis: implication for protein aggregation and immune response, *Prog. Neurobiol.*, 97, 2, 101–126 [11](#)
- Berkowitz, L. A., Knight, A. L., Caldwell, G. A., and Caldwell, K. A. (2008), Generation of stable transgenic *C. elegans* using microinjection, *J Vis Exp*, , 18 [76](#)
- Bischof, J., Maeda, R. K., Hediger, M., Karch, F., and Basler, K. (2007), An optimized transgenesis system for *Drosophila* using germ-line-specific phiC31 integrases, *Proc. Natl. Acad. Sci. U.S.A.*, 104, 9, 3312–3317 [88](#)
- Bruijn, L. I., Becher, M. W., Lee, M. K., Anderson, K. L., Jenkins, N. A., Copeland, N. G., et al. (1997), ALS-linked SOD1 mutant G85R mediates damage to astrocytes and promotes rapidly progressive disease with SOD1-containing inclusions, *Neuron*, 18, 2, 327–338 [73](#)
- Bruijn, L. I., Houseweart, M. K., Kato, S., Anderson, K. L., Anderson, S. D., Ohama, E., et al. (1998), Aggregation and motor neuron toxicity of an ALS-linked SOD1 mutant independent from wild-type SOD1, *Science*, 281, 5384, 1851–1854 [3](#)
- Cai, H., Lin, X., Xie, C., Laird, F. M., Lai, C., Wen, H., et al. (2005), Loss of ALS2 function is insufficient to trigger motor neuron degeneration in knock-out mice but predisposes neurons to oxidative stress, *J. Neurosci.*, 25, 33, 7567–7574 [3](#)
- Chen, S., Sayana, P., Zhang, X., and Le, W. (2013), Genetics of amyotrophic lateral sclerosis: an update, *Mol Neurodegener*, 8, 28 [68](#)

- Chen, Y., Yang, M., Deng, J., Chen, X., Ye, Y., Zhu, L., et al. (2011), Expression of human FUS protein in *Drosophila* leads to progressive neurodegeneration, *Protein Cell*, 2, 6, 477–486 [3](#)
- Cheroni, C., Marino, M., Tortarolo, M., Veglianesi, P., De Biasi, S., Fontana, E., et al. (2009), Functional alterations of the ubiquitin-proteasome system in motor neurons of a mouse model of familial amyotrophic lateral sclerosis, *Hum. Mol. Genet.*, 18, 1, 82–96 [11](#), [95](#)
- Ciura, S., Lattante, S., Le Ber, I., Latouche, M., Tostivint, H., Brice, A., et al. (2013), Loss of function of C9orf72 causes motor deficits in a zebrafish model of Amyotrophic Lateral Sclerosis, *Ann. Neurol.* [3](#)
- Custer, S. K., Neumann, M., Lu, H., Wright, A. C., and Taylor, J. P. (2010), Transgenic mice expressing mutant forms VCP/p97 recapitulate the full spectrum of IBMPFD including degeneration in muscle, brain and bone, *Hum. Mol. Genet.*, 19, 9, 1741–1755 [3](#), [11](#)
- Da Costa, M. M., Allen, C. E., Higginbottom, A., Ramesh, T., Shaw, P. J., and McDermott, C. J. (2014), A new zebrafish model produced by TILLING of SOD1-related amyotrophic lateral sclerosis replicates key features of the disease and represents a tool for in vivo therapeutic screening, *Dis Model Mech*, 7, 1, 73–81 [80](#)
- Dahlem, T. J., Hoshijima, K., Jurynek, M. J., Gunther, D., Starker, C. G., Locke, A. S., et al. (2012), Simple methods for generating and detecting locus-specific mutations induced with TALENs in the zebrafish genome, *PLoS Genet.*, 8, 8, e1002861 [89](#)
- Dal Canto, M. C. and Gurney, M. E. (1995), Neuropathological changes in two lines of mice carrying a transgene for mutant human Cu,Zn SOD, and in mice overexpressing wild type human SOD: a model of familial amyotrophic lateral sclerosis (FALS), *Brain Res.*, 676, 1, 25–40 [3](#)
- Dal Canto, M. C. and Gurney, M. E. (1997), A low expressor line of transgenic mice carrying a mutant human Cu,Zn superoxide dismutase (SOD1) gene develops pathological changes that most closely resemble those in human amyotrophic lateral sclerosis, *Acta Neuropathol.*, 93, 6, 537–550 [3](#)
- Deng, H. X., Chen, W., Hong, S. T., Boycott, K. M., Gorrie, G. H., Siddique, N., et al. (2011), Mutations in UBQLN2 cause dominant X-linked juvenile and adult-onset ALS and ALS/dementia, *Nature*, 477, 7363, 211–215 [11](#), [94](#), [95](#)

- Deng, H. X., Zhai, H., Fu, R., Shi, Y., Gorrie, G. H., Yang, Y., et al. (2007), Distal axonopathy in an alsin-deficient mouse model, *Hum. Mol. Genet.*, 16, 23, 2911–2920 [3](#)
- Devon, R. S., Orban, P. C., Gerrow, K., Barbieri, M. A., Schwab, C., Cao, L. P., et al. (2006), Als2-deficient mice exhibit disturbances in endosome trafficking associated with motor behavioral abnormalities, *Proc. Natl. Acad. Sci. U.S.A.*, 103, 25, 9595–9600 [3](#)
- Diaper, D. C., Adachi, Y., Sutcliffe, B., Humphrey, D. M., Elliott, C. J., Stepto, A., et al. (2013), Loss and gain of Drosophila TDP-43 impair synaptic efficacy and motor control leading to age-related neurodegeneration by loss-of-function phenotypes, *Hum. Mol. Genet.*, 22, 8, 1539–1557 [3](#)
- Doyon, Y., McCammon, J. M., Miller, J. C., Faraji, F., Ngo, C., Katibah, G. E., et al. (2008), Heritable targeted gene disruption in zebrafish using designed zinc-finger nucleases, *Nat. Biotechnol.*, 26, 6, 702–708 [89](#)
- Estes, P. S., Boehringer, A., Zwick, R., Tang, J. E., Grigsby, B., and Zarnescu, D. C. (2011), Wild-type and A315T mutant TDP-43 exert differential neurotoxicity in a Drosophila model of ALS, *Hum. Mol. Genet.*, 20, 12, 2308–2321 [3](#)
- Fecto, F., Yan, J., Vemula, S. P., Liu, E., Yang, Y., Chen, W., et al. (2011), SQSTM1 mutations in familial and sporadic amyotrophic lateral sclerosis, *Arch. Neurol.*, 68, 11, 1440–1446 [11](#)
- Feiguin, F., Godena, V. K., Romano, G., D’Ambrogio, A., Klima, R., and Baralle, F. E. (2009), Depletion of TDP-43 affects Drosophila motoneurons terminal synapsis and locomotive behavior, *FEBS Lett.*, 583, 10, 1586–1592 [3](#)
- Foley, J. E., Maeder, M. L., Pearlberg, J., Joung, J. K., Peterson, R. T., and Yeh, J. R. (2009), Targeted mutagenesis in zebrafish using customized zinc-finger nucleases, *Nat Protoc*, 4, 12, 1855–1867 [89](#)
- Frey, U. H., Bachmann, H. S., Peters, J., and Siffert, W. (2008), PCR-amplification of GC-rich regions: ‘slowdown PCR’, *Nat Protoc*, 3, 8, 1312–1317 [71](#)
- Gaj, T., Sirk, S. J., and Barbas, C. F. (2014), Expanding the scope of site-specific recombinases for genetic and metabolic engineering, *Biotechnol. Bioeng.*, 111, 1, 1–15 [89](#)

- Gidalevitz, T., Krupinski, T., Garcia, S., and Morimoto, R. I. (2009), Destabilizing protein polymorphisms in the genetic background direct phenotypic expression of mutant SOD1 toxicity, *PLoS Genet.*, 5, 3, e1000399 [3](#)
- Gong, Y. H., Parsadanian, A. S., Andreeva, A., Snider, W. D., and Elliott, J. L. (2000), Restricted expression of G86R Cu/Zn superoxide dismutase in astrocytes results in astrocytosis but does not cause motoneuron degeneration, *J. Neurosci.*, 20, 2, 660–665 [3](#)
- Gordon, P. H., Moore, D. H., Miller, R. G., Florence, J. M., Verheijde, J. L., Doorish, C., et al. (2007), Efficacy of minocycline in patients with amyotrophic lateral sclerosis: a phase III randomised trial, *Lancet Neurol*, 6, 12, 1045–1053 [4](#)
- Gosai, S. J., Kwak, J. H., Luke, C. J., Long, O. S., King, D. E., Kovatch, K. J., et al. (2010), Automated high-content live animal drug screening using *C. elegans* expressing the aggregation prone serpin 1-antitrypsin Z, *PLoS ONE*, 5, 11, e15460 [97](#)
- Gros-Louis, F., Kriz, J., Kabashi, E., McDearmid, J., Millecamps, S., Urushitani, M., et al. (2008), Als2 mRNA splicing variants detected in KO mice rescue severe motor dysfunction phenotype in Als2 knock-down zebrafish, *Hum. Mol. Genet.*, 17, 17, 2691–2702 [3](#)
- Groth, A. C., Fish, M., Nusse, R., and Calos, M. P. (2004), Construction of transgenic *Drosophila* by using the site-specific integrase from phage phiC31, *Genetics*, 166, 4, 1775–1782 [88](#)
- Gurney, M. E., Pu, H., Chiu, A. Y., Dal Canto, M. C., Polchow, C. Y., Alexander, D. D., et al. (1994), Motor neuron degeneration in mice that express a human Cu,Zn superoxide dismutase mutation, *Science*, 264, 5166, 1772–1775 [3](#), [73](#)
- Hadano, S., Benn, S. C., Kakuta, S., Otomo, A., Sudo, K., Kunita, R., et al. (2006), Mice deficient in the Rab5 guanine nucleotide exchange factor ALS2/alsin exhibit age-dependent neurological deficits and altered endosome trafficking, *Hum. Mol. Genet.*, 15, 2, 233–250 [3](#)
- Hanson, K. A., Kim, S. H., Wassarman, D. A., and Tibbetts, R. S. (2010), Ubiquilin modifies TDP-43 toxicity in a *Drosophila* model of amyotrophic lateral sclerosis (ALS), *J. Biol. Chem.*, 285, 15, 11068–11072 [3](#), [73](#)

- Hartley, J. L., Temple, G. F., and Brasch, M. A. (2000), DNA cloning using in vitro site-specific recombination, *Genome Res.*, 10, 11, 1788–1795 [93](#)
- Hatzipetros, T., Bogdanik, L. P., Tassinari, V. R., Kidd, J. D., Moreno, A. J., Davis, C., et al. (2013), C57BL/6J congenic Prp-TDP43A315T mice develop progressive neurodegeneration in the myenteric plexus of the colon without exhibiting key features of ALS, *Brain Res.* [4](#)
- Haubenberger, D., Bittner, R. E., Rauch-Shorny, S., Zimprich, F., Mannhalter, C., Wagner, L., et al. (2005), Inclusion body myopathy and Paget disease is linked to a novel mutation in the VCP gene, *Neurology*, 65, 8, 1304–1305 [69](#)
- Henke, W., Herdel, K., Jung, K., Schnorr, D., and Loening, S. A. (1997), Betaine improves the PCR amplification of GC-rich DNA sequences, *Nucleic Acids Res.*, 25, 19, 3957–3958 [71](#)
- Hochbaum, D., Ferguson, A. A., and Fisher, A. L. (2010), Generation of transgenic *C. elegans* by biolistic transformation, *J Vis Exp*, , 42 [76](#)
- Hollerer, I., Grund, K., Hentze, M. W., and Kulozik, A. E. (2014), mRNA 3'end processing: A tale of the tail reaches the clinic, *EMBO Mol Med*, 6, 1, 16–26 [70](#)
- Howe, K., Clark, M. D., Torroja, C. F., Torrance, J., Berthelot, C., Muffato, M., et al. (2013), The zebrafish reference genome sequence and its relationship to the human genome, *Nature*, 496, 7446, 498–503 [6](#)
- Howland, D. S., Liu, J., She, Y., Goad, B., Maragakis, N. J., Kim, B., et al. (2002), Focal loss of the glutamate transporter EAAT2 in a transgenic rat model of SOD1 mutant-mediated amyotrophic lateral sclerosis (ALS), *Proc. Natl. Acad. Sci. U.S.A.*, 99, 3, 1604–1609 [3](#)
- Huang, L., Pike, D., Sleat, D. E., Nanda, V., and Lobel, P. (2014), Potential pitfalls and solutions for use of fluorescent fusion proteins to study the lysosome, *PLoS ONE*, 9, 2, e88893 [76](#)
- Huang, P., Xiao, A., Zhou, M., Zhu, Z., Lin, S., and Zhang, B. (2011), Heritable gene targeting in zebrafish using customized TALENs, *Nat. Biotechnol.*, 29, 8, 699–700 [3, 89](#)

- Igaz, L. M., Kwong, L. K., Lee, E. B., Chen-Plotkin, A., Swanson, E., Unger, T., et al. (2011), Dysregulation of the ALS-associated gene TDP-43 leads to neuronal death and degeneration in mice, *J. Clin. Invest.*, 121, 2, 726–738 [3](#), [94](#)
- Iguchi, Y., Katsuno, M., Ikenaka, K., Ishigaki, S., and Sobue, G. (2013), Amyotrophic lateral sclerosis: an update on recent genetic insights, *J. Neurol.*, 260, 11, 2917–2927 [2](#)
- Isik, M. and Berezikov, E. (2013), Biolistic transformation of *Caenorhabditis elegans*, *Methods Mol. Biol.*, 940, 77–86 [76](#)
- Jaarsma, D., Teuling, E., Haasdijk, E. D., De Zeeuw, C. I., and Hoogenraad, C. C. (2008), Neuron-specific expression of mutant superoxide dismutase is sufficient to induce amyotrophic lateral sclerosis in transgenic mice, *J. Neurosci.*, 28, 9, 2075–2088 [3](#)
- Janssens, J., Wils, H., Kleinberger, G., Joris, G., Cuijt, I., Ceuterick-de Groote, C., et al. (2013), Overexpression of ALS-associated p.M337V human TDP-43 in mice worsens disease features compared to wild-type human TDP-43 mice, *Mol. Neurobiol.*, 48, 1, 22–35 [3](#)
- Jeong, J. Y., Kwon, H. B., Ahn, J. C., Kang, D., Kwon, S. H., Park, J. A., et al. (2008), Functional and developmental analysis of the blood-brain barrier in zebrafish, *Brain Res. Bull.*, 75, 5, 619–628 [97](#)
- Johnson, J. O., Mandrioli, J., Benatar, M., Abramzon, Y., Van Deerlin, V. M., Trojanowski, J. Q., et al. (2010), Exome sequencing reveals VCP mutations as a cause of familial ALS, *Neuron*, 68, 5, 857–864 [7](#), [11](#), [69](#)
- Jonsson, P. A., Ernhill, K., Andersen, P. M., Bergemalm, D., Brannstrom, T., Gredal, O., et al. (2004), Minute quantities of misfolded mutant superoxide dismutase-1 cause amyotrophic lateral sclerosis, *Brain*, 127, Pt 1, 73–88 [3](#)
- Jonsson, P. A., Graffmo, K. S., Andersen, P. M., Brannstrom, T., Lindberg, M., Oliveberg, M., et al. (2006), Disulphide-reduced superoxide dismutase-1 in CNS of transgenic amyotrophic lateral sclerosis models, *Brain*, 129, Pt 2, 451–464 [3](#)
- Ju, J. S. and Weihl, C. C. (2010), Inclusion body myopathy, Paget’s disease of the bone and fronto-temporal dementia: a disorder of autophagy, *Hum. Mol. Genet.*, 19, R1, 38–45 [7](#), [69](#)

- Jung, A., Ruckert, S., Frank, P., Brabletz, T., and Kirchner, T. (2002), 7-Deaza-2'-deoxyguanosine allows PCR and sequencing reactions from CpG islands, *MP, Mol. Pathol.*, 55, 1, 55–57 [72](#)
- Kabashi, E., Agar, J. N., Taylor, D. M., Minotti, S., and Durham, H. D. (2004), Focal dysfunction of the proteasome: a pathogenic factor in a mouse model of amyotrophic lateral sclerosis, *J. Neurochem.*, 89, 6, 1325–1335 [11](#), [95](#)
- Kabashi, E., Bercier, V., Lissouba, A., Liao, M., Brustein, E., Rouleau, G. A., et al. (2011a), FUS and TARDBP but not SOD1 interact in genetic models of amyotrophic lateral sclerosis, *PLoS Genet.*, 7, 8, e1002214 [3](#), [80](#)
- Kabashi, E., Brustein, E., Champagne, N., and Drapeau, P. (2011b), Zebrafish models for the functional genomics of neurogenetic disorders, *Biochim. Biophys. Acta*, 1812, 3, 335–345 [5](#)
- Kabashi, E., El Oussini, H., Bercier, V., Gros-Louis, F., Valdmanis, P. N., McDearmid, J., et al. (2013), Investigating the contribution of VAPB/ALS8 loss of function in amyotrophic lateral sclerosis, *Hum. Mol. Genet.*, 22, 12, 2350–2360 [3](#), [80](#)
- Kabashi, E., Lin, L., Tradewell, M. L., Dion, P. A., Bercier, V., Bourgouin, P., et al. (2010), Gain and loss of function of ALS-related mutations of TARDBP (TDP-43) cause motor deficits in vivo, *Hum. Mol. Genet.*, 19, 4, 671–683 [3](#), [80](#)
- Kawakami, K., Shima, A., and Kawakami, N. (2000), Identification of a functional transposase of the Tol2 element, an Ac-like element from the Japanese medaka fish, and its transposition in the zebrafish germ lineage, *Proc. Natl. Acad. Sci. U.S.A.*, 97, 21, 11403–11408 [88](#)
- Kearney, J. A. (2011), Genetic modifiers of neurological disease, *Curr. Opin. Genet. Dev.*, 21, 3, 349–353 [74](#)
- Kimonis, V. E., Fulchiero, E., Vesa, J., and Watts, G. (2008), VCP disease associated with myopathy, Paget disease of bone and frontotemporal dementia: review of a unique disorder, *Biochim. Biophys. Acta*, 1782, 12, 744–748 [69](#)
- Koppers, M., van Blitterswijk, M. M., Vlam, L., Rowicka, P. A., van Vught, P. W., Groen, E. J., et al. (2012), VCP mutations in familial and sporadic amyotrophic lateral sclerosis, *Neurobiol. Aging*, 33, 4, 7–13 [69](#)

- Kraemer, B. C., Schuck, T., Wheeler, J. M., Robinson, L. C., Trojanowski, J. Q., Lee, V. M., et al. (2010), Loss of murine TDP-43 disrupts motor function and plays an essential role in embryogenesis, *Acta Neuropathol.*, 119, 4, 409–419 [3](#)
- Kwan, K. M., Fujimoto, E., Grabher, C., Mangum, B. D., Hardy, M. E., Campbell, D. S., et al. (2007), The Tol2kit: a multisite gateway-based construction kit for Tol2 transposon transgenesis constructs, *Dev. Dyn.*, 236, 11, 3088–3099 [18](#), [19](#), [60](#), [88](#)
- Lagier-Tourenne, C., Baughn, M., Rigo, F., Sun, S., Liu, P., Li, H. R., et al. (2013), Targeted degradation of sense and antisense C9orf72 RNA foci as therapy for ALS and frontotemporal degeneration, *Proc. Natl. Acad. Sci. U.S.A.*, 110, 47, E4530–E4539 [3](#)
- Landgraf, D., Okumus, B., Chien, P., Baker, T. A., and Paulsson, J. (2012), Segregation of molecules at cell division reveals native protein localization, *Nat. Methods*, 9, 5, 480–482 [76](#)
- Lansbury, P. T. and Lashuel, H. A. (2006), A century-old debate on protein aggregation and neurodegeneration enters the clinic, *Nature*, 443, 7113, 774–779 [1](#)
- Lanson, N. A., Maltare, A., King, H., Smith, R., Kim, J. H., Taylor, J. P., et al. (2011), A Drosophila model of FUS-related neurodegeneration reveals genetic interaction between FUS and TDP-43, *Hum. Mol. Genet.*, 20, 13, 2510–2523 [3](#), [94](#)
- Lasiene, J. and Yamanaka, K. (2011), Glial cells in amyotrophic lateral sclerosis, *Neurol Res Int*, 2011, 718987 [95](#)
- Lee, Y. B., Chen, H. J., Peres, J. N., Gomez-Deza, J., Attig, J., Stalekar, M., et al. (2013), Hexanucleotide repeats in ALS/FTD form length-dependent RNA foci, sequester RNA binding proteins, and are neurotoxic, *Cell Rep*, 5, 5, 1178–1186 [3](#), [80](#)
- Lemmens, R., Van Hoecke, A., Hersmus, N., Geelen, V., D’Hollander, I., Thijs, V., et al. (2007), Overexpression of mutant superoxide dismutase 1 causes a motor axonopathy in the zebrafish, *Hum. Mol. Genet.*, 16, 19, 2359–2365 [3](#)
- Li, J., Huang, K. X., and Le, W. D. (2013), Establishing a novel C. elegans model to investigate the role of autophagy in amyotrophic lateral sclerosis, *Acta Pharmacol. Sin.*, 34, 5, 644–650 [75](#), [76](#)

- Li, J., Li, T., Zhang, X., Tang, Y., Yang, J., and Le, W. (2014), Human superoxide dismutase 1 overexpression in motor neurons of *Caenorhabditis elegans* causes axon guidance defect and neurodegeneration, *Neurobiol. Aging*, 35, 4, 837–846 [76](#)
- Li, Y., Ray, P., Rao, E. J., Shi, C., Guo, W., Chen, X., et al. (2010), A *Drosophila* model for TDP-43 proteinopathy, *Proc. Natl. Acad. Sci. U.S.A.*, 107, 7, 3169–3174 [3](#), [73](#)
- Liachko, N. F., Guthrie, C. R., and Kraemer, B. C. (2010), Phosphorylation promotes neurotoxicity in a *Caenorhabditis elegans* model of TDP-43 proteinopathy, *J. Neurosci.*, 30, 48, 16208–16219 [3](#), [73](#)
- Lieschke, G. J. and Currie, P. D. (2007), Animal models of human disease: zebrafish swim into view, *Nat. Rev. Genet.*, 8, 5, 353–367 [6](#), [97](#)
- Lin, M. J., Cheng, C. W., and Shen, C. K. (2011), Neuronal function and dysfunction of *Drosophila* dTDP, *PLoS ONE*, 6, 6, e20371 [3](#)
- Lin, S., Gaiano, N., Culp, P., Burns, J. C., Friedmann, T., Yee, J. K., et al. (1994), Integration and germ-line transmission of a pseudotyped retroviral vector in zebrafish, *Science*, 265, 5172, 666–669 [88](#)
- Ling, S. C., Polymenidou, M., and Cleveland, D. W. (2013), Converging mechanisms in ALS and FTD: disrupted RNA and protein homeostasis, *Neuron*, 79, 3, 416–438 [1](#), [2](#), [4](#), [96](#)
- Linton, M. F., Raabe, M., Pierotti, V., and Young, S. G. (1997), Reading-frame restoration by transcriptional slippage at long stretches of adenine residues in mammalian cells, *J. Biol. Chem.*, 272, 22, 14127–14132 [70](#)
- Lu, Y., Ferris, J., and Gao, F. B. (2009), Frontotemporal dementia and amyotrophic lateral sclerosis-associated disease protein TDP-43 promotes dendritic branching, *Mol Brain*, 2, 30 [3](#)
- Macarron, R., Banks, M. N., Bojanic, D., Burns, D. J., Cirovic, D. A., Garyantes, T., et al. (2011), Impact of high-throughput screening in biomedical research, *Nat Rev Drug Discov*, 10, 3, 188–195 [97](#)
- Meeker, N. D. and Trede, N. S. (2008), Immunology and zebrafish: spawning new models of human disease, *Dev. Comp. Immunol.*, 32, 7, 745–757 [96](#)

- Meng, X., Noyes, M. B., Zhu, L. J., Lawson, N. D., and Wolfe, S. A. (2008), Targeted gene inactivation in zebrafish using engineered zinc-finger nucleases, *Nat. Biotechnol.*, 26, 6, 695–701 [89](#)
- Miguel, L., Avequin, T., Delarue, M., Feuillette, S., Frebourg, T., Campion, D., et al. (2012), Accumulation of insoluble forms of FUS protein correlates with toxicity in *Drosophila*, *Neurobiol. Aging*, 33, 5, 1–15 [3](#)
- Miguel, L., Frebourg, T., Campion, D., and Lecourtois, M. (2011), Both cytoplasmic and nuclear accumulations of the protein are neurotoxic in *Drosophila* models of TDP-43 proteinopathies, *Neurobiol. Dis.*, 41, 2, 398–406 [3](#)
- Miller, R. G., Mitchell, J. D., Lyon, M., and Moore, D. H. (2003), Riluzole for amyotrophic lateral sclerosis (ALS)/motor neuron disease (MND), *Amyotroph. Lateral Scler. Other Motor Neuron Disord.*, 4, 3, 191–206 [97](#)
- Miller, T. M., Pestronk, A., David, W., Rothstein, J., Simpson, E., Appel, S. H., et al. (2013), An antisense oligonucleotide against SOD1 delivered intrathecally for patients with SOD1 familial amyotrophic lateral sclerosis: a phase 1, randomised, first-in-man study, *Lancet Neurol*, 12, 5, 435–442 [68](#)
- Mockett, R. J., Radyuk, S. N., Benes, J. J., Orr, W. C., and Sohal, R. S. (2003), Phenotypic effects of familial amyotrophic lateral sclerosis mutant Sod alleles in transgenic *Drosophila*, *Proc. Natl. Acad. Sci. U.S.A.*, 100, 1, 301–306 [3](#)
- Mosimann, C., Kaufman, C. K., Li, P., Pugach, E. K., Tamplin, O. J., and Zon, L. I. (2011), Ubiquitous transgene expression and Cre-based recombination driven by the ubiquitin promoter in zebrafish, *Development*, 138, 1, 169–177 [82](#)
- Mosimann, C., Puller, A. C., Lawson, K. L., Tschopp, P., Amsterdam, A., and Zon, L. I. (2013), Site-directed zebrafish transgenesis into single landing sites with the phiC31 integrase system, *Dev. Dyn.*, 242, 8, 949–963 [88](#)
- Munch, C., O’Brien, J., and Bertolotti, A. (2011), Prion-like propagation of mutant superoxide dismutase-1 misfolding in neuronal cells, *Proc. Natl. Acad. Sci. U.S.A.*, 108, 9, 3548–3553 [95](#)
- Nagai, M., Aoki, M., Miyoshi, I., Kato, M., Pasinelli, P., Kasai, N., et al. (2001), Rats expressing human cytosolic copper-zinc superoxide dismutase transgenes with amyotrophic lateral sclerosis: associated mutations develop motor neuron disease, *J. Neurosci.*, 21, 23, 9246–9254 [3](#)

- Nandi, D., Tahiliani, P., Kumar, A., and Chandu, D. (2006), The ubiquitin-proteasome system, *J. Biosci.*, 31, 1, 137–155 [9](#), [10](#)
- Neumann, M., Sampathu, D. M., Kwong, L. K., Truax, A. C., Micsenyi, M. C., Chou, T. T., et al. (2006), Ubiquitinated TDP-43 in frontotemporal lobar degeneration and amyotrophic lateral sclerosis, *Science*, 314, 5796, 130–133 [73](#)
- Nonaka, T., Masuda-Suzukake, M., Arai, T., Hasegawa, Y., Akatsu, H., Obi, T., et al. (2013), Prion-like properties of pathological TDP-43 aggregates from diseased brains, *Cell Rep*, 4, 1, 124–134 [95](#)
- Oeda, T., Shimohama, S., Kitagawa, N., Kohno, R., Imura, T., Shibasaki, H., et al. (2001), Oxidative stress causes abnormal accumulation of familial amyotrophic lateral sclerosis-related mutant SOD1 in transgenic *Caenorhabditis elegans*, *Hum. Mol. Genet.*, 10, 19, 2013–2023 [3](#)
- Oikonomou, G. and Shaham, S. (2011), The glia of *Caenorhabditis elegans*, *Glia*, 59, 9, 1253–1263 [96](#)
- Okamoto, K., Mizuno, Y., and Fujita, Y. (2008), Bunina bodies in amyotrophic lateral sclerosis, *Neuropathology*, 28, 2, 109–115 [1](#)
- Panula, P., Chen, Y. C., Priyadarshini, M., Kudo, H., Semenova, S., Sundvik, M., et al. (2010), The comparative neuroanatomy and neurochemistry of zebrafish CNS systems of relevance to human neuropsychiatric diseases, *Neurobiol. Dis.*, 40, 1, 46–57 [6](#)
- Papadakis, E. D., Nicklin, S. A., Baker, A. H., and White, S. J. (2004), Promoters and control elements: designing expression cassettes for gene therapy, *Curr Gene Ther*, 4, 1, 89–113 [81](#)
- Park, H. C., Kim, C. H., Bae, Y. K., Yeo, S. Y., Kim, S. H., Hong, S. K., et al. (2000), Analysis of upstream elements in the HuC promoter leads to the establishment of transgenic zebrafish with fluorescent neurons, *Dev. Biol.*, 227, 2, 279–293 [35](#)
- Parkes, T. L., Elia, A. J., Dickinson, D., Hilliker, A. J., Phillips, J. P., and Boulianne, G. L. (1998), Extension of *Drosophila* lifespan by overexpression of human SOD1 in motorneurons, *Nat. Genet.*, 19, 2, 171–174 [3](#)
- Phillips, J. P., Campbell, S. D., Michaud, D., Charbonneau, M., and Hilliker, A. J. (1989), Null mutation of copper/zinc superoxide dismutase in *Drosophila* confers

- hypersensitivity to paraquat and reduced longevity, *Proc. Natl. Acad. Sci. U.S.A.*, 86, 8, 2761–2765 [3](#)
- Pramatarova, A., Laganier, J., Roussel, J., Brisebois, K., and Rouleau, G. A. (2001), Neuron-specific expression of mutant superoxide dismutase 1 in transgenic mice does not lead to motor impairment, *J. Neurosci.*, 21, 10, 3369–3374 [3](#)
- Ramesh, T., Lyon, A. N., Pineda, R. H., Wang, C., Janssen, P. M., Canan, B. D., et al. (2010), A genetic model of amyotrophic lateral sclerosis in zebrafish displays phenotypic hallmarks of motoneuron disease, *Dis Model Mech*, 3, 9-10, 652–662 [3](#), [80](#), [93](#)
- Reaume, A. G., Elliott, J. L., Hoffman, E. K., Kowall, N. W., Ferrante, R. J., Siwek, D. F., et al. (1996), Motor neurons in Cu/Zn superoxide dismutase-deficient mice develop normally but exhibit enhanced cell death after axonal injury, *Nat. Genet.*, 13, 1, 43–47 [3](#)
- Ringholz, G. M., Appel, S. H., Bradshaw, M., Cooke, N. A., Mosnik, D. M., and Schulz, P. E. (2005), Prevalence and patterns of cognitive impairment in sporadic ALS, *Neurology*, 65, 4, 586–590 [2](#)
- Ripps, M. E., Huntley, G. W., Hof, P. R., Morrison, J. H., and Gordon, J. W. (1995), Transgenic mice expressing an altered murine superoxide dismutase gene provide an animal model of amyotrophic lateral sclerosis, *Proc. Natl. Acad. Sci. U.S.A.*, 92, 3, 689–693 [3](#)
- Robberecht, W. and Philips, T. (2013), The changing scene of amyotrophic lateral sclerosis, *Nat. Rev. Neurosci.*, 14, 4, 248–264 [2](#), [7](#), [11](#), [67](#), [95](#)
- Rowland, L. P. and Shneider, N. A. (2001), Amyotrophic lateral sclerosis, *N. Engl. J. Med.*, 344, 22, 1688–1700 [1](#)
- Sakowski, S. A., Lunn, J. S., Busta, A. S., Oh, S. S., Zamora-Berridi, G., Palmer, M., et al. (2012), Neuromuscular effects of G93A-SOD1 expression in zebrafish, *Mol Neurodegener*, 7, 44 [80](#)
- Sanhueza, M., Zechini, L., Gillespie, T., and Pennetta, G. (2014), Gain-of-function mutations in the ALS8 causative gene VAPB have detrimental effects on neurons and muscles, *Biol Open*, 3, 1, 59–71 [3](#)

- Sarkar, G., Kapelner, S., and Sommer, S. S. (1990), Formamide can dramatically improve the specificity of PCR, *Nucleic Acids Res.*, 18, 24, 7465 [71](#)
- Sasayama, H., Shimamura, M., Tokuda, T., Azuma, Y., Yoshida, T., Mizuno, T., et al. (2012), Knockdown of the Drosophila fused in sarcoma (FUS) homologue causes deficient locomotive behavior and shortening of motoneuron terminal branches, *PLoS ONE*, 7, 6, e39483 [3](#)
- Schmid, B., Hruscha, A., Hogl, S., Banzhaf-Strathmann, J., Strecker, K., van der Zee, J., et al. (2013), Loss of ALS-associated TDP-43 in zebrafish causes muscle degeneration, vascular dysfunction, and reduced motor neuron axon outgrowth, *Proc. Natl. Acad. Sci. U.S.A.*, 110, 13, 4986–4991 [3](#)
- Schnabel, J. (2008), Neuroscience: Standard model, *Nature*, 454, 7205, 682–685 [74](#)
- Schroder, R., Watts, G. D., Mehta, S. G., Evert, B. O., Broich, P., Fliessbach, K., et al. (2005), Mutant valosin-containing protein causes a novel type of frontotemporal dementia, *Ann. Neurol.*, 57, 3, 457–461 [39](#), [69](#)
- Scott, S., Kranz, J. E., Cole, J., Lincecum, J. M., Thompson, K., Kelly, N., et al. (2008), Design, power, and interpretation of studies in the standard murine model of ALS, *Amyotroph Lateral Scler*, 9, 1, 4–15 [98](#)
- Sephton, C. F., Good, S. K., Atkin, S., Dewey, C. M., Mayer, P., Herz, J., et al. (2010), TDP-43 is a developmentally regulated protein essential for early embryonic development, *J. Biol. Chem.*, 285, 9, 6826–6834 [3](#)
- Shan, X., Chiang, P. M., Price, D. L., and Wong, P. C. (2010), Altered distributions of Gemini of coiled bodies and mitochondria in motor neurons of TDP-43 transgenic mice, *Proc. Natl. Acad. Sci. U.S.A.*, 107, 37, 16325–16330 [3](#)
- Shaye, D. D. and Greenwald, I. (2011), OrthoList: a compendium of C. elegans genes with human orthologs, *PLoS ONE*, 6, 5, e20085 [6](#)
- Sonnhammer, E. L. and Durbin, R. (1997), Analysis of protein domain families in Caenorhabditis elegans, *Genomics*, 46, 2, 200–216 [6](#)
- Spina, S., Van Laar, A. D., Murrell, J. R., Hamilton, R. L., Kofler, J. K., Epperson, F., et al. (2013), Phenotypic variability in three families with valosin-containing protein mutation, *Eur. J. Neurol.*, 20, 2, 251–258 [69](#)

- Stadler, C., Rexhepaj, E., Singan, V. R., Murphy, R. F., Pepperkok, R., Uhlen, M., et al. (2013), Immunofluorescence and fluorescent-protein tagging show high correlation for protein localization in mammalian cells, *Nat. Methods*, 10, 4, 315–323 [77](#)
- Stallings, N. R., Puttaparthi, K., Luther, C. M., Burns, D. K., and Elliott, J. L. (2010), Progressive motor weakness in transgenic mice expressing human TDP-43, *Neurobiol. Dis.*, 40, 2, 404–414 [3](#)
- Stuart, G. W., McMurray, J. V., and Westerfield, M. (1988), Replication, integration and stable germ-line transmission of foreign sequences injected into early zebrafish embryos, *Development*, 103, 2, 403–412 [87](#), [88](#)
- Sun, Y., Yang, P., Zhang, Y., Bao, X., Li, J., Hou, W., et al. (2011), A genome-wide RNAi screen identifies genes regulating the formation of P bodies in *C. elegans* and their functions in NMD and RNAi, *Protein Cell*, 2, 11, 918–939 [95](#)
- Suster, M. L., Kikuta, H., Urasaki, A., Asakawa, K., and Kawakami, K. (2009), Transgenesis in zebrafish with the tol2 transposon system, *Methods Mol. Biol.*, 561, 41–63 [88](#)
- Swarup, V., Phaneuf, D., Bareil, C., Robertson, J., Rouleau, G. A., Kriz, J., et al. (2011), Pathological hallmarks of amyotrophic lateral sclerosis/frontotemporal lobar degeneration in transgenic mice produced with TDP-43 genomic fragments, *Brain*, 134, Pt 9, 2610–2626 [3](#), [73](#)
- Teschendorf, D. and Link, C. D. (2009), What have worm models told us about the mechanisms of neuronal dysfunction in human neurodegenerative diseases?, *Mol Neurodegener*, 4, 38 [4](#)
- Thermes, V., Grabher, C., Ristoratore, F., Bourrat, F., Choulika, A., Wittbrodt, J., et al. (2002), I-SceI meganuclease mediates highly efficient transgenesis in fish, *Mech. Dev.*, 118, 1-2, 91–98 [88](#)
- Therrien, M. and Parker, J. A. (2014), Worming forward: amyotrophic lateral sclerosis toxicity mechanisms and genetic interactions in *Caenorhabditis elegans*, *Front Genet*, 5, 85 [95](#), [97](#)
- Tsai, K. J., Yang, C. H., Fang, Y. H., Cho, K. H., Chien, W. L., Wang, W. T., et al. (2010), Elevated expression of TDP-43 in the forebrain of mice is sufficient to cause

- neurological and pathological phenotypes mimicking FTL-D-U, *J. Exp. Med.*, 207, 8, 1661–1673 [3](#)
- Tu, P. H., Raju, P., Robinson, K. A., Gurney, M. E., Trojanowski, J. Q., and Lee, V. M. (1996), Transgenic mice carrying a human mutant superoxide dismutase transgene develop neuronal cytoskeletal pathology resembling human amyotrophic lateral sclerosis lesions, *Proc. Natl. Acad. Sci. U.S.A.*, 93, 7, 3155–3160 [3](#)
- Turner, M. R., Bowser, R., Bruijn, L., Dupuis, L., Ludolph, A., McGrath, M., et al. (2013), Mechanisms, models and biomarkers in amyotrophic lateral sclerosis, *Amyotroph Lateral Scler Frontotemporal Degener*, 14 Suppl 1, 19–32 [4](#), [96](#)
- Turner, M. R., Cagnin, A., Turkheimer, F. E., Miller, C. C., Shaw, C. E., Brooks, D. J., et al. (2004), Evidence of widespread cerebral microglial activation in amyotrophic lateral sclerosis: an [11C](R)-PK11195 positron emission tomography study, *Neurobiol. Dis.*, 15, 3, 601–609 [1](#), [77](#)
- Uchida, A., Sasaguri, H., Kimura, N., Tajiri, M., Ohkubo, T., Ono, F., et al. (2012), Non-human primate model of amyotrophic lateral sclerosis with cytoplasmic mislocalization of TDP-43, *Brain*, 135, Pt 3, 833–846 [3](#), [74](#)
- Vaccaro, A., Tauffenberger, A., Aggad, D., Rouleau, G., Drapeau, P., and Parker, J. A. (2012), Mutant TDP-43 and FUS cause age-dependent paralysis and neurodegeneration in *C. elegans*, *PLoS ONE*, 7, 2, e31321 [3](#), [73](#), [75](#)
- Vance, C., Scotter, E. L., Nishimura, A. L., Troakes, C., Mitchell, J. C., Kathe, C., et al. (2013), ALS mutant FUS disrupts nuclear localization and sequesters wild-type FUS within cytoplasmic stress granules, *Hum. Mol. Genet.*, 22, 13, 2676–2688 [95](#)
- Varadaraj, K. and Skinner, D. M. (1994), Denaturants or cosolvents improve the specificity of PCR amplification of a G + C-rich DNA using genetically engineered DNA polymerases, *Gene*, 140, 1, 1–5 [71](#)
- Voigt, A., Herholz, D., Fiesel, F. C., Kaur, K., Muller, D., Karsten, P., et al. (2010), TDP-43-mediated neuron loss in vivo requires RNA-binding activity, *PLoS ONE*, 5, 8, e12247 [3](#)
- Wang, J., Farr, G. W., Hall, D. H., Li, F., Furtak, K., Dreier, L., et al. (2009), An ALS-linked mutant SOD1 produces a locomotor defect associated with aggregation and synaptic dysfunction when expressed in neurons of *Caenorhabditis elegans*, *PLoS Genet.*, 5, 1, e1000350 [3](#), [76](#)

- Wang, J., Slunt, H., Gonzales, V., Fromholt, D., Coonfield, M., Copeland, N. G., et al. (2003), Copper-binding-site-null SOD1 causes ALS in transgenic mice: aggregates of non-native SOD1 delineate a common feature, *Hum. Mol. Genet.*, 12, 21, 2753–2764 [3](#)
- Wang, J. W., Brent, J. R., Tomlinson, A., Shneider, N. A., and McCabe, B. D. (2011), The ALS-associated proteins FUS and TDP-43 function together to affect Drosophila locomotion and life span, *J. Clin. Invest.*, 121, 10, 4118–4126 [3](#)
- Wang, X. J., Yu, J., Wong, S. H., Cheng, A. S., Chan, F. K., Ng, S. S., et al. (2013), A novel crosstalk between two major protein degradation systems: regulation of proteasomal activity by autophagy, *Autophagy*, 9, 10, 1500–1508 [89](#)
- Watanabe, Y., Yasui, K., Nakano, T., Doi, K., Fukada, Y., Kitayama, M., et al. (2005), Mouse motor neuron disease caused by truncated SOD1 with or without C-terminal modification, *Brain Res. Mol. Brain Res.*, 135, 1-2, 12–20 [3](#)
- Watson, M. R., Lagow, R. D., Xu, K., Zhang, B., and Bonini, N. M. (2008), A drosophila model for amyotrophic lateral sclerosis reveals motor neuron damage by human SOD1, *J. Biol. Chem.*, 283, 36, 24972–24981 [3](#)
- Watts, G. D., Wymer, J., Kovach, M. J., Mehta, S. G., Mumm, S., Darvish, D., et al. (2004), Inclusion body myopathy associated with Paget disease of bone and frontotemporal dementia is caused by mutant valosin-containing protein, *Nat. Genet.*, 36, 4, 377–381 [39](#), [69](#)
- Wegorzewska, I., Bell, S., Cairns, N. J., Miller, T. M., and Baloh, R. H. (2009), TDP-43 mutant transgenic mice develop features of ALS and frontotemporal lobar degeneration, *Proc. Natl. Acad. Sci. U.S.A.*, 106, 44, 18809–18814 [3](#), [4](#)
- Westerfield, M. (2000), The zebrafish book: a guide for the laboratory use of zebrafish (Danio rerio) (University of Oregon Press) [35](#), [36](#), [37](#)
- White, R. M., Sessa, A., Burke, C., Bowman, T., LeBlanc, J., Ceol, C., et al. (2008), Transparent adult zebrafish as a tool for in vivo transplantation analysis, *Cell Stem Cell*, 2, 2, 183–189 [78](#)
- Wils, H., Kleinberger, G., Janssens, J., Pereson, S., Joris, G., Cuijt, I., et al. (2010), TDP-43 transgenic mice develop spastic paralysis and neuronal inclusions characteristic of ALS and frontotemporal lobar degeneration, *Proc. Natl. Acad. Sci. U.S.A.*, 107, 8, 3858–3863 [3](#)

- Wong, P. C., Pardo, C. A., Borchelt, D. R., Lee, M. K., Copeland, N. G., Jenkins, N. A., et al. (1995), An adverse property of a familial ALS-linked SOD1 mutation causes motor neuron disease characterized by vacuolar degeneration of mitochondria, *Neuron*, 14, 6, 1105–1116 [73](#)
- Wu, C. H., Fallini, C., Ticozzi, N., Keagle, P. J., Sapp, P. C., Piotrowska, K., et al. (2012), Mutations in the profilin 1 gene cause familial amyotrophic lateral sclerosis, *Nature*, 488, 7412, 499–503 [3](#)
- Wu, L. S., Cheng, W. C., Hou, S. C., Yan, Y. T., Jiang, S. T., and Shen, C. K. (2010), TDP-43, a neuro-pathosignature factor, is essential for early mouse embryogenesis, *Genesis*, 48, 1, 56–62 [3](#)
- Xi, Z., Yunusova, Y., van Blitterswijk, M., Dib, S., Ghani, M., Moreno, D., et al. (2014), Identical twins with the C9orf72 repeat expansion are discordant for ALS, *Neurology* [74](#)
- Xia, R., Liu, Y., Yang, L., Gal, J., Zhu, H., and Jia, J. (2012), Motor neuron apoptosis and neuromuscular junction perturbation are prominent features in a *Drosophila* model of Fus-mediated ALS, *Mol Neurodegener*, 7, 10 [3](#), [94](#)
- Xu, Y. F., Gendron, T. F., Zhang, Y. J., Lin, W. L., D’Alton, S., Sheng, H., et al. (2010), Wild-type human TDP-43 expression causes TDP-43 phosphorylation, mitochondrial aggregation, motor deficits, and early mortality in transgenic mice, *J. Neurosci.*, 30, 32, 10851–10859 [3](#)
- Xu, Z., Poidevin, M., Li, X., Li, Y., Shu, L., Nelson, D. L., et al. (2013), Expanded GGGGCC repeat RNA associated with amyotrophic lateral sclerosis and frontotemporal dementia causes neurodegeneration, *Proc. Natl. Acad. Sci. U.S.A.*, 110, 19, 7778–7783 [3](#)
- Yamanaka, K., Miller, T. M., McAlonis-Downes, M., Chun, S. J., and Cleveland, D. W. (2006), Progressive spinal axonal degeneration and slowness in ALS2-deficient mice, *Ann. Neurol.*, 60, 1, 95–104 [3](#)
- Yang, H., Wang, G., Sun, H., Shu, R., Liu, T., Wang, C. E., et al. (2014), Species-dependent neuropathology in transgenic SOD1 pigs, *Cell Res.*, 24, 4, 464–481 [3](#)

- Zang, D. W. and Cheema, S. S. (2002), Degeneration of corticospinal and bulbospinal systems in the superoxide dismutase 1(G93A G1H) transgenic mouse model of familial amyotrophic lateral sclerosis, *Neurosci. Lett.*, 332, 2, 99–102 [3](#)
- Zhang, T., Mullane, P. C., Periz, G., and Wang, J. (2011), TDP-43 neurotoxicity and protein aggregation modulated by heat shock factor and insulin/IGF-1 signaling, *Hum. Mol. Genet.*, 20, 10, 1952–1965 [76](#)
- Zhou, H., Huang, C., Chen, H., Wang, D., Landel, C. P., Xia, P. Y., et al. (2010), Transgenic rat model of neurodegeneration caused by mutation in the TDP gene, *PLoS Genet.*, 6, 3, e1000887 [3](#)
- Zu, Y., Tong, X., Wang, Z., Liu, D., Pan, R., Li, Z., et al. (2013), TALEN-mediated precise genome modification by homologous recombination in zebrafish, *Nat. Methods*, 10, 4, 329–331 [89](#)